Integrated Real-Time Control And Processing Systems For Multi-Channel Near-Infrared Spectroscopy Based Brain Computer Interfaces

Fiachra Matthews

Computer Science

National University of Ireland, Maynooth

A thesis submitted for the degree of

Doctor of Philosophy

February 2010

Head of Department: **Dr. Adam Winstanley**

Supervisors: **Prof. Barak A. Pearlmutter, Dr. Tomás E. Ward**

I would like to dedicate this thesis to my parents for their, ofttimes, unjustified faith in me.

Acknowledgements

This project left many of my friends uncontacted but would have been impossible without the help and support of many many people whom I can't all name here. A special thanks to all the residents, past and present, of S.P. Grove. You all know who you are.

Firstly thanks must go to my supervisors, Prof. Barak Pearlmutter and Dr. Tomas Ward, for giving me this opportunity in the first place and their eagerness to help in all things NIRS. Another person who is due immense praise is Dr. Charles Markham. Barak, Tomas and Charles deserve a tremendous amount of credit for this research as they all have shepherded it from beginning to end.

Thanks to all the staff and students of the Hamilton Institute who provided an unparalleled working environment that included support, academic and financial, and encouragement (badgering) during the write-up. Of the faculty who took an interest, thanks to Prof. Doug Leith, Prof. Robert Shorten, Prof. Peter Wellstead, Prof. Rick Middelton, Dr Ken Duffy, Dr Dave Malone, Dr Mark Readman and Dr Selim Solmaz. A special thank you to Doug for organizing fees during the project and to Rick for the Robocup work. Also, thanks must to go to the administrative staff Ms. Rosemary Hunt, Ms. Kate Moriarty and Mrs. Ruth Middelton for their help.

Anyone who knows me or this project will also know that this project would not be what it is today without the work of Dr. Christopher Soraghan. His work, ideas, enthusiasm and drive helped me immensely throughout the last four years. Thanks Chris.

To my entire family. Few people are as lucky to have such a close extended family who are there and ready to help during any situation. Two special mentions must go to Eibhlin and Aodhnait who went above and beyond

when my father was ill. Neither ever lacking in a smart (usually sarcastic) comment to keep things in perspective. Thanks guys.

Seamus, Caoilfhionn and Bla, have all been putting up with me for a while. Again it's hard to express how lucky I am with my family but between the three of them there is never a lack of conversation, support and stories to entertain.

To Meagan, I can't really find a good way to express what she's meant to me these last four years. She has listened to more whining from me over the last few months than most people hear in a lifetime. Despite that she's always been there for me. Thanks love.

To my parents, two people who are are as glad to see the back of this as I am. My mother, Olive, and my father, Jim, have supported me far beyond what I could have asked of them and I asked a lot. Their faith in me, especially in the last few months of this project, kept me on the right road.

Thanks Mam and Dad.

Abstract

This thesis outlines approaches to improve the signal processing and analysis of Near-infrared spectroscopy (NIRS) based brain-computer interfaces (BCI). These approaches were developed in conjunction with the implementation of a new customized flexible multi-channel NIRS based BCI hardware system (Soraghan, 2010). Using a comparable functional imaging modality the assumptions on which NIRS-BCI have been reassessed, with regard to cognitive task selection, active area locations and lateralized motor cortex activation separability. This dissertation will also present methods that have been implemented to allow reduced hardware requirements in future NIRS-BCI development. We will also examine the sources of homeostatic physiological interference and present new approaches for analysis and attenuation within a real-time NIRS-BCI paradigm.

Contents

Chapter 1

Introduction

Research in the area of brain computer interfaces promises significant rewards. To grant communication of any kind to someone who has lost this most basic and defining facet of the human condition is a goal of unparalleled importance. Similarly the ability to interrogate cerebral hemodynamics in a safe, non-invasive and convenient manner provides a valuable tool in the arsenal needed to achieve this goal.

Near-infrared spectroscopy first came to the fore in the nineteen seventies as a method of measuring cerebral and myocardial oxygen sufficiency (Jobsis, 1977). Using radiation in the near-infrared range an optical window of tissue transparency was discovered, thus allowing non-invasive optical interrogation of underlying biological structures.

Later, it became possible to expose a much higher detail of cerebral hemodynamics allowing the investigation of functional activity (Villringer *et al.*, 1993). Near-infrared spectroscopy as a brain-computer interface modality was pioneered by Coyle, Ward, Markham & McDarby (2004b) and has since become a well recognized approach to providing an alternative communication channel to those who have lost voluntary motor control.

1.1 Motivation

This document extends the work of Coyle *et al.* (2004b) by developing a custom-made flexible multichannel NIRS-BCI. Customized hardware was designed and built by Soraghan (2010) in conjunction with this research allowing many of the improvements outlined in further chapters. This work aims to address problems from a signals perspective along the entire processing chain which includes mental task choice, optical generation and acquisition, data processing systems, experimental control and feature classification.

There is no single solution to improving NIRS as a BCI modality. This dissertation outlines the background of and challenges in the NIRS signal processing chain (Matthews *et al.*, 2008a). We will then investigate approaches to modify and improve these techniques to make the more effective use of the signals detectable. Developments should also improve cost effectiveness so as to allow the modality to become more pervasive.

To achieve these goals this document will take a modular approach similar to that of the system implemented. Firstly we will examine the mental process and tasks available for implementing a computer control structure. Next we will revisit NIRS-BCI assumptions with a small study using a comparable functional mapping modality in conjunction with findings from the literature. We then define a custom NIRS-BCI hardware system which was designed in parallel with this work (Soraghan *et al.*, 2008a, 2009b; Soraghan, 2010). This hardware is specifically constructed to allow formulation and testing of alternative approaches to the challenges, e.g. non-stationary physiological noise removal.

A new software system is outlined to allow control of all aspects of an experiment or BCI application such as stimulus timing and biofeedback (Matthews *et al.*, 2008b). This allows versatility and enables rapid prototyping of new systems in a field demand-

ing further research. A novel approach to NIRS optical control and multiplexing is implemented that maintains system performance while reducing overhead in hardware. Finally, we will examine detected hemodynamic trends and implement novel approaches to optimize channel selection, hemodynamic analysis, and feature classification.

1.2 Contributions

The contributions of this thesis are as follows:

- Implementation of a robust and versatile software system to assist the research in terms of hardware control, signal acquisition, and user feedback.

- Development and implementation of a spread spectrum communications technique that maintains sufficient signal quality while reducing hardware requirements.

- Application of a signal decomposition method known as empirical mode decomposition to NIRS signals to reduce homeostatic physiological interference and also aid signal analysis.

- Adaptation of a model based analysis technique from functional magnetic resonance imaging to allow optimum channel selection and improve separation of right hand and left hand functional activity in motor cortex structures.

- The application of novel real-time feature classification methods to the selected optimum channels.

1.3 Dissertation Outline

Chapter 2 deals with the necessary scientific background behind this work. It includes information pertaining to functional areas of the brain, oxygen transportation in the

blood, and cranial circulation. Photon transportation in tissue is also discussed, as well as brain imaging modalities and an introduction to the physics and function of both functional magnetic resonance imaging (fMRI) and NIRS. Finally, Chapter 2 briefly outlines the area of brain-computer interfacing.

Chapter 3 details the current state of the art in NIRS-BCI and the current challenges in mental task selection, software, hardware, physiological interference reduction and feature classification. Chapter 4 presents a small fMRI study which is assessed in conjunction with current findings in the literature,with a discussion of functional activation in the motor cortex. It focuses on active area locations, separability, inter-subject variability, overt versus imagined motor actions, and the impact these findings have on NIRS.

Chapter 5 includes an outline of the hardware developed in parallel with this work and its versatility in allowing examination of different aspects of the NIRS-BCI paradigm. Chapter 6 discusses the implementation of a robust software platform for NIRS-BCI research. It further defines the specifications for such systems and details an implementation designed specifically for NIRS-BCI. In this platform, the optical multiplexing is moved entirely into software. In light of this, a novel spread spectrum approach to NIRS optical multiplexing is presented.

Chapter 7 implements novel homeostatic physiological noise removal and signal analysis techniques, model based methods of optimal source selection, and feature classification. Finally, Chapter 8 draws conclusions and presents future direction for NIRS-BCI signal processing and analysis.

1.4 Publications

1.4.1 Conference Publication

- <u>F. Matthews</u>, C. Soraghan, T.E. Ward, C. Markham, and B.A. Pearlmutter. Software platform for rapid prototyping of NIRS brain computer interfacing techniques. In *Conference proceedings:... Annual International Conference of the IEEE Engineering in Medicine and Biology Society. IEEE Engineering in Medicine and Biology Society. Conference*, volume 1, page 4840, 2008.

- C. Soraghan, C. Markham, <u>F. Matthews</u>, and T.E. Ward. Overview of Optical BCI Research at NUI Maynooth. In *The Association of Physical Scientists in Medicine Annual Scientific Meeting (APSM ASM) 2009.* NUIM, 2009.

- C. Soraghan, <u>F. Matthews</u>, C. Markham, BA Pearlmutter, R. ONeill, and TE Ward. A 12-Channel, real-time near-infrared spectroscopy instrument for brain-computer interface applications. In *Conference proceedings:... Annual International Conference of the IEEE Engineering in Medicine and Biology Society. IEEE Engineering in Medicine and Biology Society. Conference*, volume 1, page 5648, 2008.

- Christopher J. Soraghan, Tomas E. Ward, <u>Fiachra Matthews</u>, and Charles Markham. Optical safety assessment of a near-infrared brain-computer interface. In *Signals and Systems Conference, 208. (ISSC 2008). IET Irish*, pages 174–179, June 2008.

- C Soraghan, <u>F Matthews</u>, D Kelly, T Ward, C Markham, B Pearlmutter, and R O'Neill. A dual-channel optical brain-computer interface in a gaming envrioment. In *Proceedings of the 9th International Conference on Computer Games: AI, Animation, Mobile, Educational and Serious Games*, Dublin Institute of Technology, Ireland, November 2006.

1.4.2   Journal Publication

- <u>F. Matthews</u>, B.A. Pearlmutter, T.E. Ward, C. Soraghan, and C. Markham. Hemodynamics for brain-computer interfaces. *Signal Processing Magazine, IEEE*, 25(1):87–94, 2008.

- C.J. Soraghan, C. Markham, <u>F. Matthews</u>, and T.E. Ward. Triple wavelength led driver for optical brain–computer interfaces. *Electronics Letters*, 45(8):392–394, 2009.

- Tomas E Ward, Christopher J Soraghan, <u>Fiachra Matthews</u>, and Charles M Markham. A concept for extending the applicability of constraint induced movement therapy through motor cortex activity feedback using a neural prosthesis. *Computational Intelligence and Neuroscience*, 2007.

Chapter 2

Background

Neuronal activity produces distinct changes in regional cerebral blood flow (rCBF) which is the basis for many functional imaging modalities (Villringer & Dirnagl, 1995). Near-infrared spectroscopy (NIRS) takes advantage of trends in blood-oxygen levels related to this shift in rCBF to identify localized functional activity in the brain (Villringer *et al.*, 1993). Using cognitive tasks it is possible to record repeatable, volitional and detectable mental activity using NIRS. This activity forms the basis of a brain computer interface. The developments presented in this dissertation, analysis of functional activity and advances in NIRS-BCI techniques, are all based on these premises.

The purpose of this chapter is to act as a primer to anatomical and biological processes pertinent to this thesis, describe modalities used in the non-invasive measurement of functional brain activity, and introduce the paradigms of brain-computer interfacing.

2.1 Physiological Processes & Structures

This section will explain the physiological process and structures important in the development of a NIRS-BCI.

2.1.1 Brain Anatomy

The adult brain weighs on average about 1.5kg and is made up of four physical sections; Cerebellum, Cerebrum, brain stem and Diencephalon or lymbic system. In its early embryonic form it is made up of three membrane enclosed sacs or vesicles (Gray, 1918). These vesicles, called the mid-brain (mesencephalon), the fore-brain (prosencephalon) and the hind-brain(rhombencephalon), go on to form the structures familiar in the adult brain (Figure 2.1).
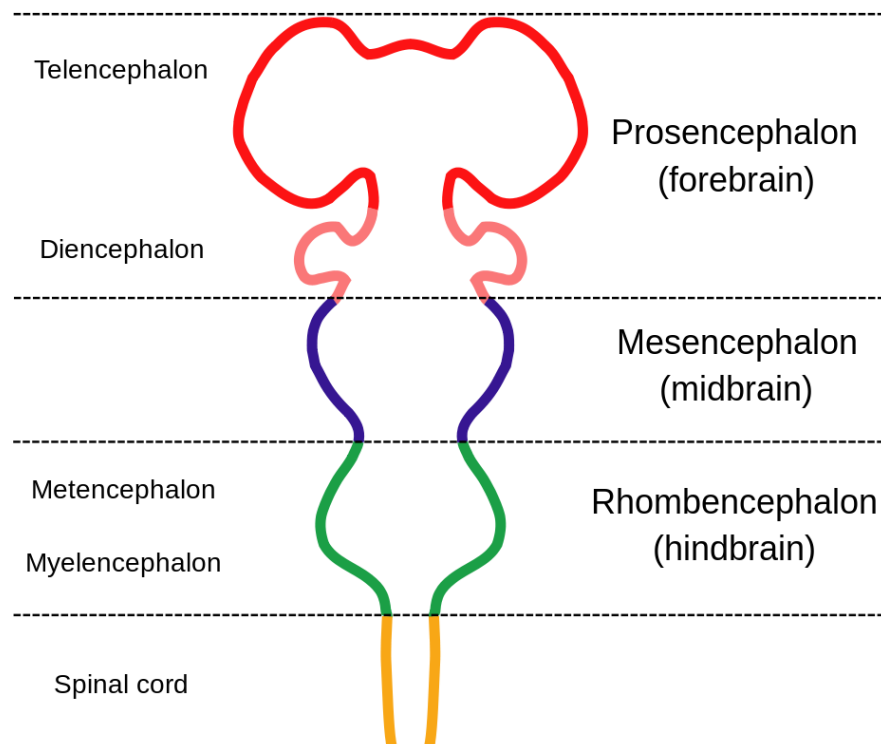
Figure 2.1: The Basic structure of the embryonic brain.

The embryonic hind brain forms the medulla-oblongata, pons and the cerebellum and continues to expand to form a fourth ventricle. The mid-brain becomes the cerebral aqueduct that serves as a communication hub for motor function, eye movement and auditory control. The mid-brain in conjunction with the medulla-oblongata and pons make up the brain-stem in an adult brain as seen in Figure 2.2.
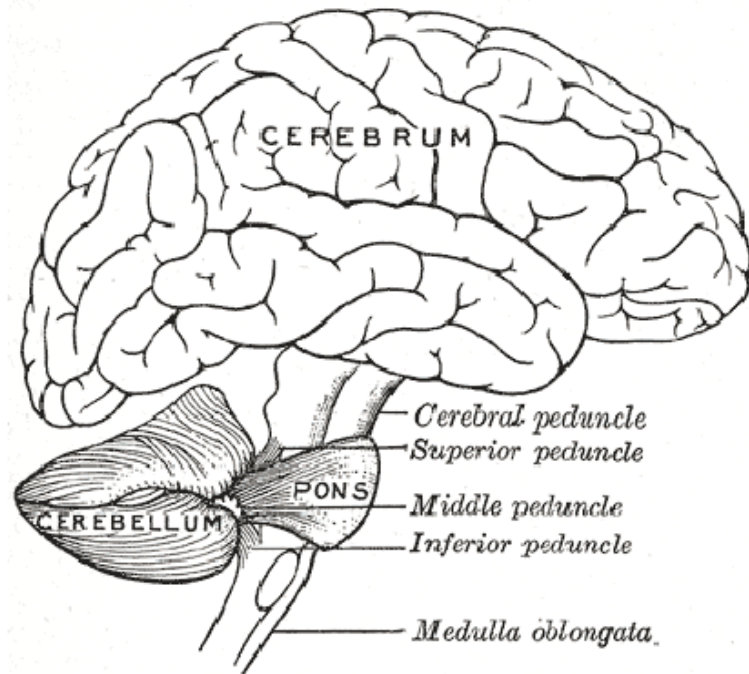
Figure 2.2: Connections between the cerebrum and brain stem and associated parts. (From Gray, 1918)

The fore-brain undergoes the greatest change from the embryonic stage. It expands laterally to form two more hollow vesicles which become the lateral ventricles and the walls of the fore-brain form the cerebral hemispheres. The posterior part of the embryonic fore-brain forms also forms part of the lymbic system. In the search for detectable, volitional, repeatable functional activation this work will mainly concentrate on the cerebrum.

The cerebrum consists of two hemispheres generally with contralateral control responsibilities. The surface area is maximized due to its folded nature. These folds or gyri allow for a much larger area to form inside the cranium than would otherwise be possible. The cerebrum is believed to be mainly responsible for movement control, sensory processing, olfaction, learning, memory, language and communication.

For functional analysis purposes the cerebrum is classified into four lobes: frontal,

occipital, parietal and temporal as shown in Figure 2.3. These areas were originally defined by which bone of the cranium they are under. In Section 2.1.2 we will discuss in greater detail the functions of each lobe.
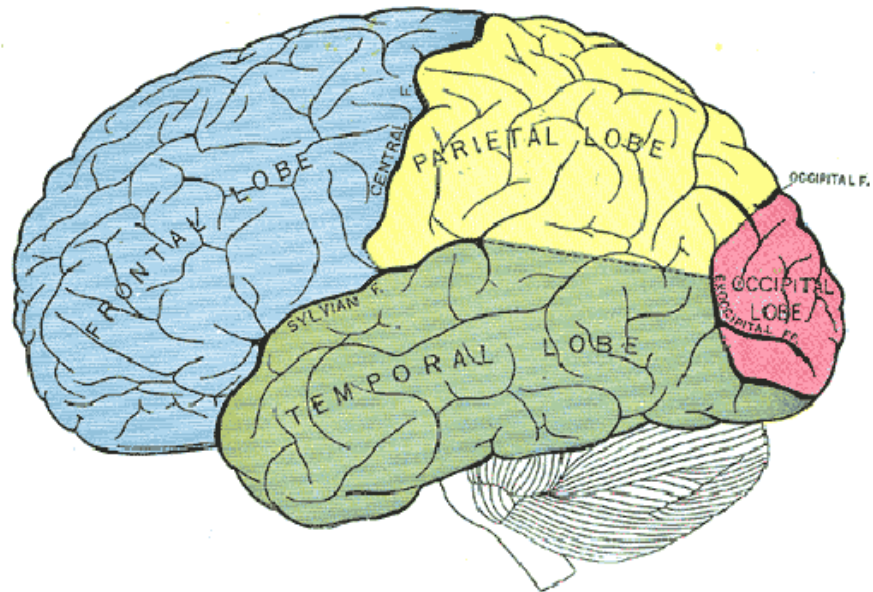
Figure 2.3: The Cerebral Lobes are highlighted above. (From Gray, 1918)

2.1.2 Functional Areas

2.1.2.1 Frontal Lobe

The frontal lobe is considered to be responsible for higher reasoning, mathematical ability, and verbal fluency (Kandel *et al.*, 2000).

The frontal lobe is involved in motor skills, including speech, and cognitive functions. The motor cortex, located anterior to the parietal lobe receives connections from the somatosensory cortex, processes and initiates motor functions. The frontal lobes are also important for language skills. Broca's area, a region on the left side of the frontal lobe, is involved in processing language and controlling the muscles responsible for speech (Martin, 2006). Other functions of the frontal lobes include learning, thought and memory.

2.1.2.2 Parietal Lobe

The parietal lobes contain the primary and association cortices for somatosensory functions that receive and process all somatosensory input from the body, such as touch and pain. A region called Wernicke's area, distal to the temporal lobe, is important for understanding the sensory (auditory and visual) information associated with language.

2.1.2.3 Occipital Lobe

The occipital lobe contains the primary visual cortex and is responsible for processing visual signals. Raw signals from the retina pass through the lateral geniculate nucleus of the thalamus before continuing on to the visual cortex. Peristriate regions of the occipital lobe are responsible for colour and movement discrimination as well as visuospatial processing (Kandel *et al.*, 1991).

2.1.2.4 Temporal Lobe

The temporal lobe processes auditory information from the ears and relates it to Wernicke's area of the parietal lobe and the motor cortex of the frontal lobe.

2.1.3 Neuronal Structures

The fundamental component of the brain and nervous system is the neuron. Neurons are responsible for the transmitting of nerve impulses throughout the nervous system. The brain itself consists of approximately 10^{11} neurons (Stevens, 1979).

Neuronal cells consist of three main parts, the soma, dendrites and the axon. The soma is the main cell body containing the nucleus and controls protein synthesis, genomic expression and metabolism. The dendrites branch into the soma and are the receiver pathways for signaling from other neurons. The axon emerges as a single structure from the soma and branches to other neurons, constituting the output signaling pathway of the cell (Marieb, 2003). The point of contact that neurons share is

referred to as the synapse.
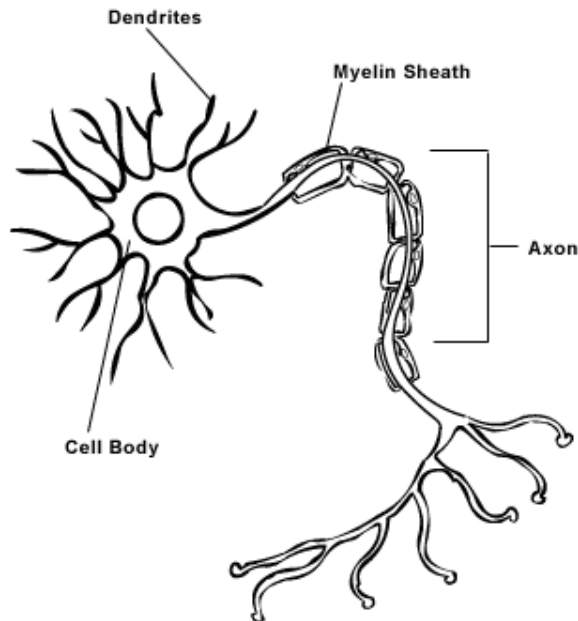
Figure 2.4: A Neuron. The inputs (Dendrites), the cell body (soma), and the output (axon). The myelin sheet insulates the axon on some neurons heightening the speed of nerve impulses along its length.

The synapse consists of a small gap called the cleft bracketed by the pre and post-synaptic endings. Signals between neurons flow from the pre-synaptic to the post synaptic ending via the cleft. These synapse are membrane to membrane junctions that allow the chemically mediated transmission of electrical signals. The electrical signals, or action potentials, are a result of changes in the potentials of the cell membrane in relation to the movement of charged ions (Nicholls *et al.*, 1992). Neuronal excitation increases the membranes permeability to sodium ions which causes a decrease in membrane potential referred to as depolarization. Hyperpolarization is the inverse process, creating an increase in the membrane potential. At a certain threshold depolarization causes the neuron to transmit an action potential along the length of its axon. Hyperpolarization causes a reduction in the transmission of action potentials.

As soon as the potential has been transmitted the sodium permeability is dramatically decreased, potassium permeability increases and the resting state balance is restored (Nicholls *et al.*, 1992).

When the action potential reaches the pre-synaptic ending it releases molecules that traverse the cleft and bind to the post-synaptic ending. These molecules are called neurotransmitters and cause shifts in the permeability of the post-synaptic membrane which in turn feeds the same process in the connected neuron (Kandel *et al.*, 1991).

2.1.4   Oxygen Transportation

Oxygen is required to maintain most forms of animal and plant life on the planet acting as the oxidizing agent in cellular respiration. Aerobic (as opposed to anaerobic) respiration involves a set of metabolic processes that combines nutrients with oxygen to produce energy.

Oxygen acts as a terminal electron receptor in the electron transport chain that makes up certain parts of cellular respiration. This process creates Adenosine triphosphate (ATP) which is the cellular energy source.

In humans, oxygen is drawn in from the air through the mechanical action of the lungs. From there it passes through the walls of the alveoli where it enriches oxygen depleted blood from the veins and enters the arteries and is pumped back around the body by the heart.

The blood in vertebrates is made up of plasma, platelets, red and white blood cells. The plasma is 90% water and carries hormones, glucose and dissolved CO_2 for excretion. The plasma is the main carrier for excretory substances for the body (Jalonen, 1981). Platelets, which are formed in the bone marrow, are pivotal to homeostasis which leads to the formation of blood clots. White blood cells or *leukocytes* contain the ability to fend off infectious disease and are the mainstay of the immune system.

Red blood cells contain the oxygen carrying molecule hemoglobin and are the most

abundant cells of the blood. The ability of hemoglobin to carry blood around the body to feed the necessities of cellular respiration shall be a highly important theme within this dissertaion. The next section deals briefly with the chemical and mechanical processes of oxygen-hemoglobin interactions.

2.1.4.1 Functions of Hemoglobin

Over 95% of oxygen carried in the body's arteries is bonded to hemoglobin. The amount of the gas that can be dissolved in the plasma is dependent on the gas's partial pressure and only makes up 1.5% of oxygen demand throughout the body. Oxygen supplied by this method alone would never be sufficient to maintain the cells of the entire body.
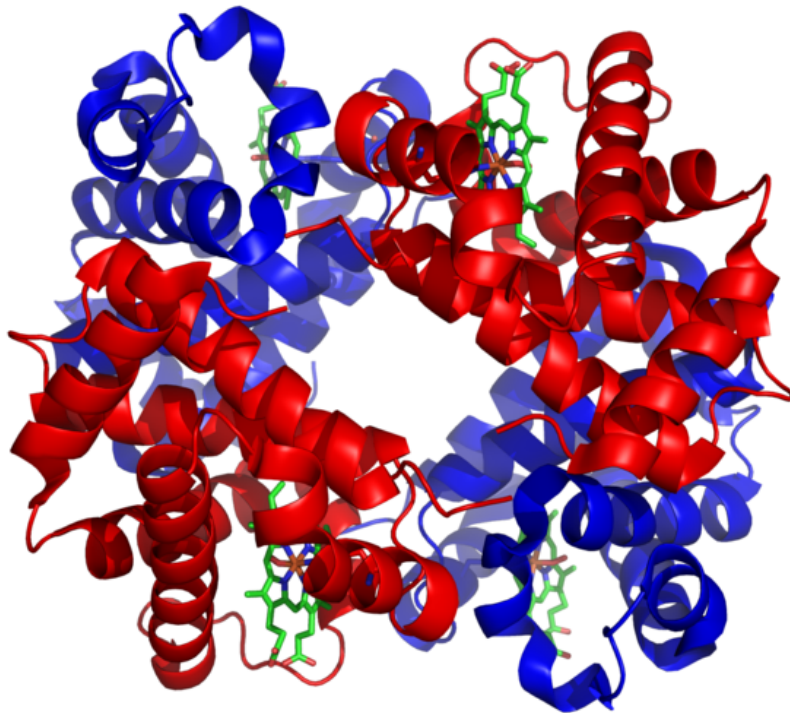
Figure 2.5: Structure of the human hemoglobin molecule.(From Wikipedia Commons)

Hemoglobin is an iron containing metalloprotein that is the main carrier of oxygen around the body (Dickerson & Geis, 1983). A red blood cell contains about 250 million hemoglobin molecules. Excluding water, hemoglobin makes up about 97% of the red blood cell's composition. Each molecule can bind to four oxygen molecules (Curtis & Barnes, 1989). This binding allows the blood to carry about 65 times more oxygen (Clark, 1997) than could be allowed according to Henry's Law which states:

At a constant temperature, the amount of a given gas dissolved in a given type and volume of liquid is directly proportional to the partial pressure of that gas in equilibrium with that liquid.

The process whereby oxygen attaches and detaches to the hemoglobin molecule is dependent on the partial pressure of oxygen in the lungs versus the tissues requiring supply (De Villota *et al.*, 1981). When de-oxygenated hemoglobin acquires a single oxygen molecule it becomes easier for more oxygen to attach to the group until the molecule is saturated. This property presents a sigmoidal response of oxygen saturation dependent on oxygen pressure (Chappell, 1985). In Figure 2.6 we see this sigmoidal response, known as the dissociation curve.

Hemoglobin can take other forms and also bind with molecules other than oxygen. These variants can change the properties of the oxygen transportation process as well as interfere, to different degrees, with the process of in-vivo oxygen saturation measurement.

2.1.5   Cerebral Blood Flow

The cerebral arteries supply the brain with blood carrying oxygen and nutrients both of which are vital to its function. Figure 2.7 displays the three main arteries that supply the cerebrum, anterior cerebral artery, middle cerebral artery and posterior cerebral artery. The circular form of these interconnected arteries is referred to as the circle
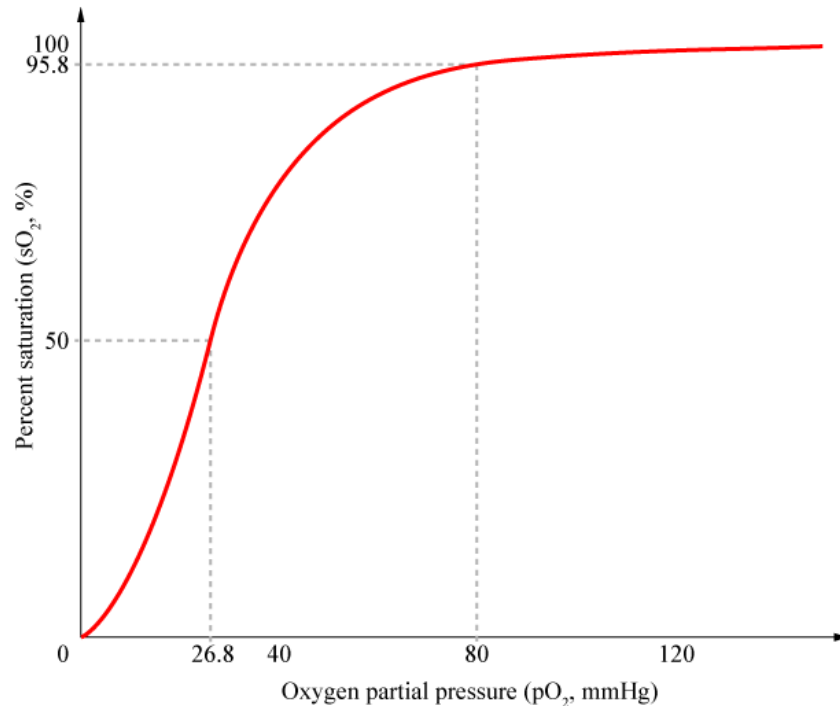
Figure 2.6: Hemoglobin-Oxygen dissociation curve. The curve shows the oxygen saturation in the blood at a given partial oxygen pressure. (Wikipedia Commons, released under GNU Free Documentation License. A copy of this license is available in appendix C)

of Willis. This arrangement allows consistent and continuous supply of blood to the structures of the brain (Berne & Levy, 1996).

The continuous supply of blood to the brain is vital. Even a short interruption to this supply induces subject blackout within seconds and permanent damage within a few minutes (Berne & Levy, 1996). Due to this nearly 15% of the total cardiac resting output is dedicated to the blood supply to the brain. The direct supply of blood to the neurons of the brain is mediated using small branches from the arteries called arterioles. These arterioles enter the cortex at right angles and branch out to all areas requiring supply. Figure 2.8a shows an arteriole penetrating the cortex from the sub-arachnoid space through all levels of the cerebral cortex. Figure 2.8b is an image from a rat cortex
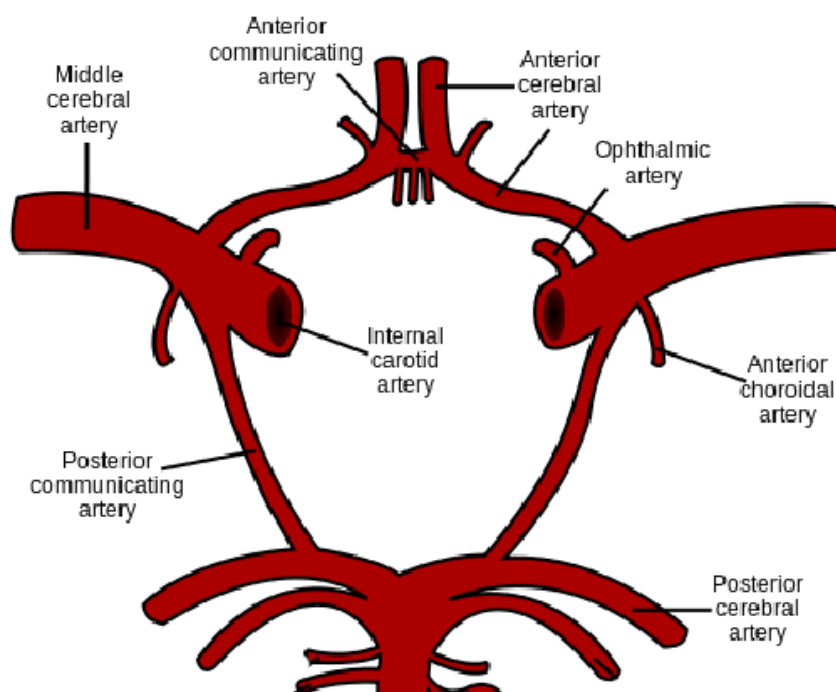
Figure 2.7: Image of the main cerebral arteries forming the Circle of Willis.

demonstrating the density and organization of the cortical microvasculature.

2.1.6 Neuro-vascular Coupling

2.1.6.1 Neuro-vascular Correlates to Mental Activity

During neuronal activities, like the neurotransmitter recycling and the post action potential restoration of ionic gradients, energy is required in the form of adenosine triphosphate (ATP). Activity within neurons enacts a set of processes to maintain the necessary supply of ATP. Figure 2.9 is illustrative of the following process. Initially, upon activation, the necessary ATP is synthesized with anaerobic glycolysis. This produces small quantities of ATP but not enough to maintain activation and the ATP production quickly transfers to aerobic glycolsis, or oxidative glucose metabolism. This latter process is dependent on a continuous supply of both glucose and oxygen from

17
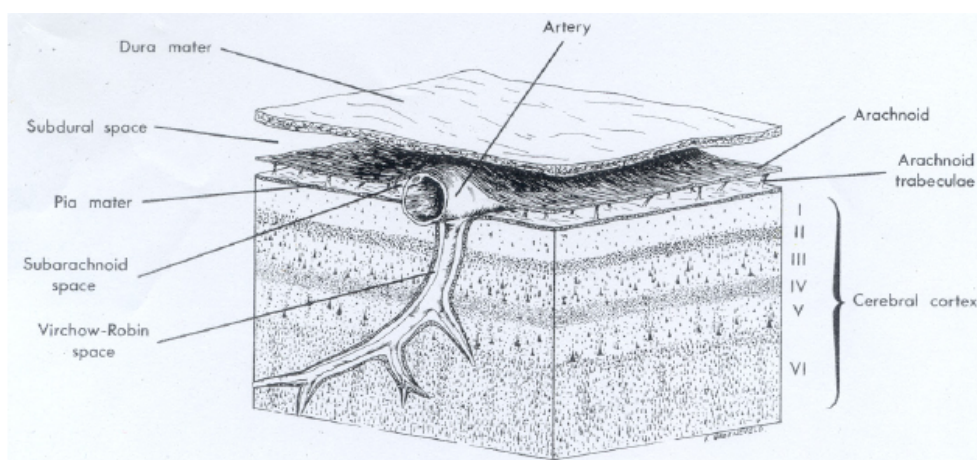
(a) Diagram of the arteriole entering the cortex

(b) Arteriole organization in the cortex of a rat

Figure 2.8: Images of arteriole structures for blood supply to the cortex. Images reproduced from Berne & Levy (1996)

hemoglobin as discussed earlier. The supply of both these substances is controlled by the regional cerebral blood flow (rCBF). The blood vessels of the brain respond accordingly to the increased requirements. The mechanism by which the blood vessels respond is still a matter of debate and will be discussed later. The increase in demand
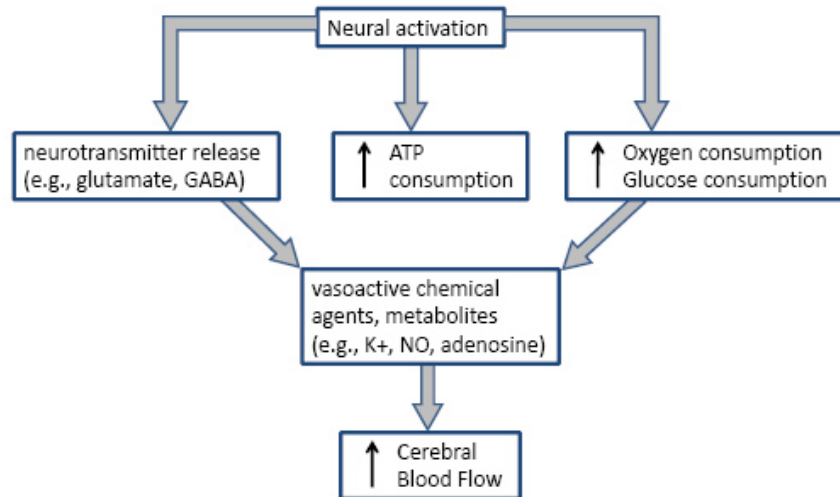
Figure 2.9: Physiological changes associated with neuronal activation. Reproduced from Pasley & Freeman (2008)

for glucose and oxygen initiates an increase in rCBF. The magnitude of this increase is matched by that of the glucose consumption but not that of oxygen consumption. This leads to an oversupply of oxygen (over saturation of HbO_2) which is detectable using NIRS and fMRI (Pasley & Freeman, 2008).

As discussed, there is a causal link between neuronal activation and changes in rCBF but the mechanism of this correlation is not well understood. An initial hypothesis on this mechanism came from Roy & Sherrington (1890).

> "We conclude then, that the chemical products of cerebral metabolism contained in the lymph which bathes the walls of the arterioles of the brain can cause variations of the calibre of the cerebral vessels: that in this reaction the brain possesses an intrinsic mechanism by which its vascular supply can be varied locally in correspondence with local variations of functional activity."

This work suggests the changes in rCBF are mediated directly by energy demand

implying feedback systems relating to ionic and molecular by-products. In this theory, vasodilation is triggered by these glycolic by-products altering the blood flow to the region. A re-examination of this work shows that the link between neural activity and rCBF was correctly identified but the coupling mechanisms suggested are believed to be over-simplified and unverified in subsequent studies (Friedland & Iadecola, 1991).

A number of alternate theories are under investigation. One theory suggests that there is evidence linking neuronal innervation to smooth muscle cells that mediates rCBF (Hamel, 2004). Another theory proposes that neuronal signaling occurs via neurotransmitters in a feed-forward fashion (Attwell & Iadecola, 2002). This theory relies on the concept of the importance of astrocytes linking these neurotransmitters to vasodilation (Harder *et al.*, 1998; Takano *et al.*, 2006).

In the next sections we proceed to examine the functional imaging techniques that take advantage of the oxygenation changes caused by neurovascular coupling.

2.2 Magnetic Resonance Imaging

Magnetic resonance imaging (MRI), originally termed Nuclear Magnetic Resonance (NMR), was first developed in the early seventies. Using the magnetic spin of hydrogen molecules it became possible to image certain substances, including human tissue, far beyond what x-ray was capable of. The first image from an NMR scanner was published in 1973 (Lauterbur, 1973). Human trials were published only four years later in 1977 (Damadian *et al.*, 1977). Currently MRI is used world wide in medical diagnostics and research. Figure 2.10 is an example of a high resolution structural scan of a human brain.

The next section will briefly cover the basic theory behind MRI and extend it to the detection of functional activity concentrating on activity in the motor cortex.
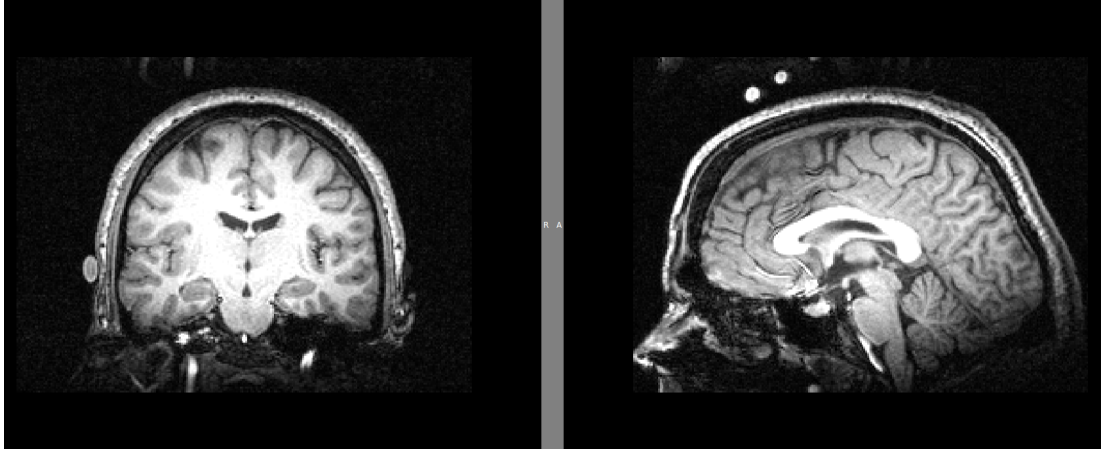
Figure 2.10: Structural Image from an MRI scan. This example shows how MRI allowed non-invasive detailed imaging of structures

2.2.1 Physics of MRI

Using strong magnetic fields, radio transmitters and an assortment of detectors for both radio frequency (RF) and magnetic signals it is possible to build 2 and 3D images which are detailed enough for clinical diagnostics or physiological assessment of functional activity. Before we can fully understand the ramifications of this technology we must first understand the background of magnetic and resonance.

2.2.1.1 Magnetism

Magnetism, when applied to materials is descriptive of how the material's components behave when in a magnetic field. Magnetic fields arise generally from a number of sources and in certain types. Electric currents passed through a conductor generates magnetic fields and is the basis for large electro-magnets and electric motors. Certain materials have specific magnetic properties. These magnetic properties exist due to orbiting electrons generating an angular momentum also referred to a magnetic moment (Bushberg *et al.*, 2002). Although there are numerous type of magnetism, we will only explain those necessary to the understanding of MRI.

The strongest naturally occurring source of magnetism is ferromagnatisim. It is common in metals iron, nickel or cobalt. These materials have clusters of atoms in which the directionality of the poles within the substance is uniform. These clusters are referred to as domains. When these domains do not all have uniform direction, the material is considered un-magnetized. Introducing a magnetic field near an un-magnatized ferromagnetic material will cause the domains to line up and the material becomes "traditionally" magnetic. Ferromagnetic materials are also the only magnetic materials that retain their properties after the removal of the field.
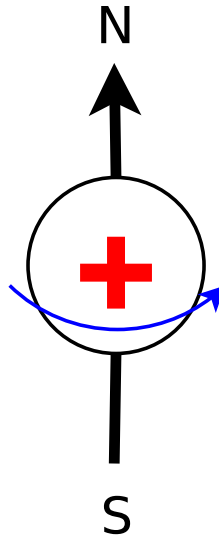
Figure 2.11: The positive charge of a proton in the nuclei of a hydrogen atom exhibits magnetic properties and allows it to align with an external magnetic field.

Paramagnetism is when a material has an unpaired electron that induces a positive magnetic moment. Outside an external magnetic field there is a net magnetic moment of zero due to the random directionality of these spins. Hence the properties of paramagnetic materials can only be fully observed within an externally applied field.

Diamagnatisim is the weakest form of magnetism and similarly to paramagnetism its effects are only visible within an externally applied field. Diamagnetic materials

exhibit a weak repulsion of magnetic field flux. All materials can be shown to have diamagnetic properties in a strong enough magnetic field. Conversely the force is so weak a material with any other magnetic properties will overpower its effects nearly instantly.
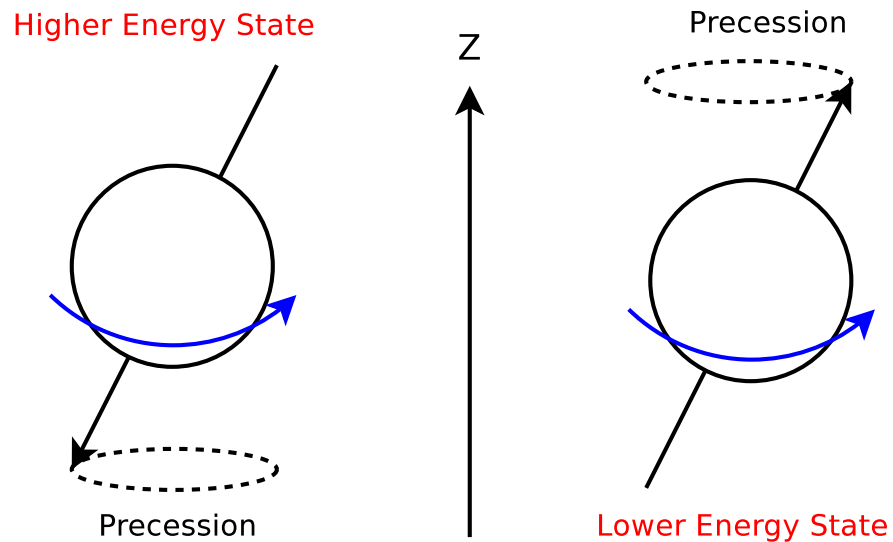
Figure 2.12: Inside a strong magnetic field protons will align parallel with the field direction Z. The directions are slightly imbalanced toward the positive field direction due to it being at a lower energy state for the protons. There protons will precess around the Z axis at the Lamour frequency.

MRI uses the magnetic properties of hydrogen atoms in fat and water molecules to image biological tissue. The positively charged proton in the nucleus of a hydrogen atom spins about its axis. This effect, called nuclear magnetism causes the hydrogen proton, shown in figure 2.11, to act like a very small magnet.

When an external magnetic field, of field direction Z, is applied to these protons they align either toward or directly opposite the direction of the field. Referred to as the Zeeman effect either direction of alignment is a specific energy state for that proton. The energy state reached in aligning toward Z is slightly lower hence there is a net detectable increase of the magnetic field strength in the Z direction. Without this MR imaging would be impossible. These protons, within the field, precess around the

Z axis. This is called resonance.

2.2.2 Resonance

Resonance occurs when a proton is aligned in a magnetic field. Shown in figure 2.12 the protons precess around the axis of direction of the main magnetic field B_0. As before we will refer to this as the Z axis. The frequency at which a particle resonates is called the Lamor Frequency. This frequency is derived from the gyromagnetic ratio of the particle multiplied by the magnetic field strength.

$$\omega_0 = \gamma B_0$$

Where ω_0 is the Lamour frequency, γ is the gyromagnetic ration and B_0 is the magnetic field strength. The gyroscopic ration is a constant and is unique to the nucleic structure.
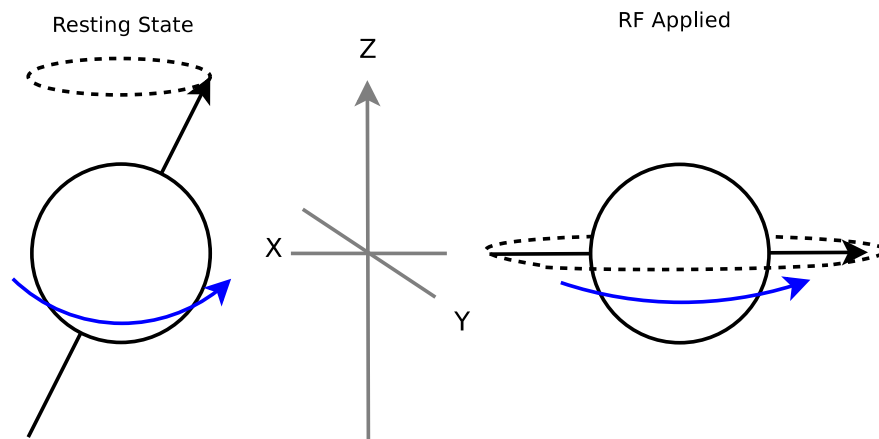
Figure 2.13: The application of an RF pulse at the Lamour frequency causes the proton to spiral away from the longitudinal Z axis to the traversal XY plane.

If an RF pulse, generated at the Lamor frequency, is applied at $90°$ to the precessing protons they begin to tip away from the Z axis to the XY plane as seen in figure 2.13. Macroscopically, the net detectable magnetization of the aligned protons spirals away

from the Z axis. When the RF pulse is removed the protons return to their original state over time. The time it takes to return to baseline is variable for different tissue types. It is this time discrepancy that allows differentiation of internal detail after the imaging process.

2.2.3 Relaxation Times

There are a number of measured relaxation times that can supply different information for imaging.

2.2.3.1 T1 Relaxation

The T1 is the measured time relating to a return to the net magnetization in the Z direction. The energy absorbed by the protons from the RF is released after the signal is stopped. This energy is released as a retransmission of the original RF frequency and as heat to surrounding tissues or lattice. This is referred to as spin lattice relaxation. There is an exponential rate of return and the T1 time is specifically the time taken for the net magnetization in the Z direction to reach 63% its original length. For imaging purposes it is known that white matter in the brain has a short T1 time, gray matter has a slightly longer time and cerebrospinal fluid is longer again (Pooley, 2005).An image generated from these timing contrasts is referred to as a T1 weighted image. Figure 2.14a and figure 2.10 are examples.

2.2.3.2 T2 Relaxation

When the RF pulse is applied the spins of all the protons become phase aligned creating a net magnetic effect in the XY plane. Once this RF is removed the protons start to dephase due to a number of effects. For a pure T2 time the interaction of the individual protons magnetic fields is the only cause of dephasing. This is referred to as spin-spin relaxation. Where as T1 relaxation times are in the region of seconds, T2 times are in

the millisecond region. Figure 2.14b is an example of a T2 weighted image.
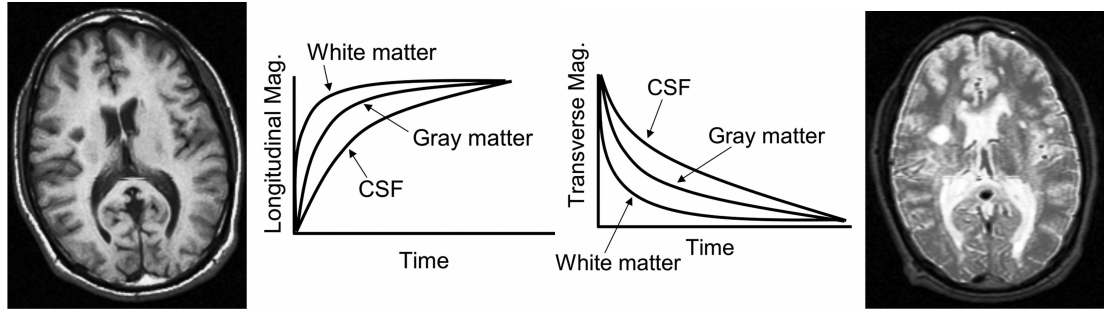
(a) T1 Weighted image and the comparative graph (b) T2 Weighted image and the comparative graph of T1 times for tissue types of T2 times for tissue types

Figure 2.14: Examples of T1 and T2 weighted images with associated timing graphs

2.2.3.3   T2* Relaxation

T2* (pronounced T2 star) relaxation times are related to the reality that Spin-spin interactions are not the only influence on the dephasing. The other causes are the presence of other magnetically susceptible materials, magnetic field inhomogeneities and chemical changes in the tissues. These have the effect of significantly shortening the measured T2 times.

2.2.4   Functional Imaging

In the early nineties it became possible, using high magnetic field and fast T2* relaxation times, to image functional activity (Ogawa & Lee, 1990; Ogawa *et al.*, 1990). Hemoglobin, after it has been de-oxygenated becomes paramagnetic, as opposed to the diamagnetic oxy-hemoglobin, displaying a contrast on MRI images. As discussed in Chapter 2 hemodynamic activity is thought to be linked to neural activity due to increased aerobic glycolisis in the neuronal cells.

At the onset of neural activation, there is an increase in cerebral blood flow (CBF), cerebral blood volume (CBV), and oxygen delivery. As discussed in chapter 2 the area is

supplied with more oxygen than it needs so there is an increase of the ratio of oxygenated to deoxygenated hemoglobin. The increase in the quantity of the diamagnetic oxy-hemoglobin increased the T2* time for a particular area hence an increase in contrast on a T2* weighted image.

Although the hemoglobin quantities are quite small the effect of the magnetic susceptibility in the paramagnetic deoxy-hemoglobin has a significant effect. This induces a $1\% - 10\%$ intensity change of the T2* data during an activation task (Thulborn *et al.*, 1982).

2.3 Near-infrared Spectroscopy

Near-infrared spectroscopy (NIRS) is an analysis method which uses electromagnetic radiation in the near-infrared spectrum (around 650–950 nm). Radiation at these wavelengths is passed through a substance and the collected light intensities are used to determine the properties of the substance. NIRS has been used in the areas of quality control, pharmaceuticals and medical diagnostics (Cope, 1991) to name but a few applications. In the context of this thesis, discussion is confined to the ability of NIRS to interrogate cerebral tissue to determine functional brain activity.

Studies performed by Jobsis (1977) discovered an optical window of tissue transparency in the near-infrared spectrum allowing light, within this range, to penetrate the skull and interrogate the surface of the cerebral cortex. When interrogating a smaller substances it is possible to use trans-illumination methods. Trans-illumination records ballistic photons traversing the entire substance. This has been applied in a clinical setting for infants (Cope, 1991).

When using NIRS to investigate the adult cortex it is necessary to use reflectance mode spectroscopy. Optical sources are placed at right angles to the scalp over particular areas. The photons enter the scalp, skull and cortex tissue and undergo multiple

scattering events. A small percentage of the transmitted photons are back reflected and emerge within a few centimeters of the injection point. During the scattering they may reach up to a centimeters into the cortex (Okada & Delpy, 2003). Monte-Carlo photonic modeling has been used to show the scattering photons that exit at the detector locations follow a banana shaped path to reemerge from the scalp (Okada *et al.*, 1997). Figure 2.15 shows the results of a Monte-Carlo model of tissue scattering (Humphreys, 2007). It is possible to see this banana shaped path the photons follow.
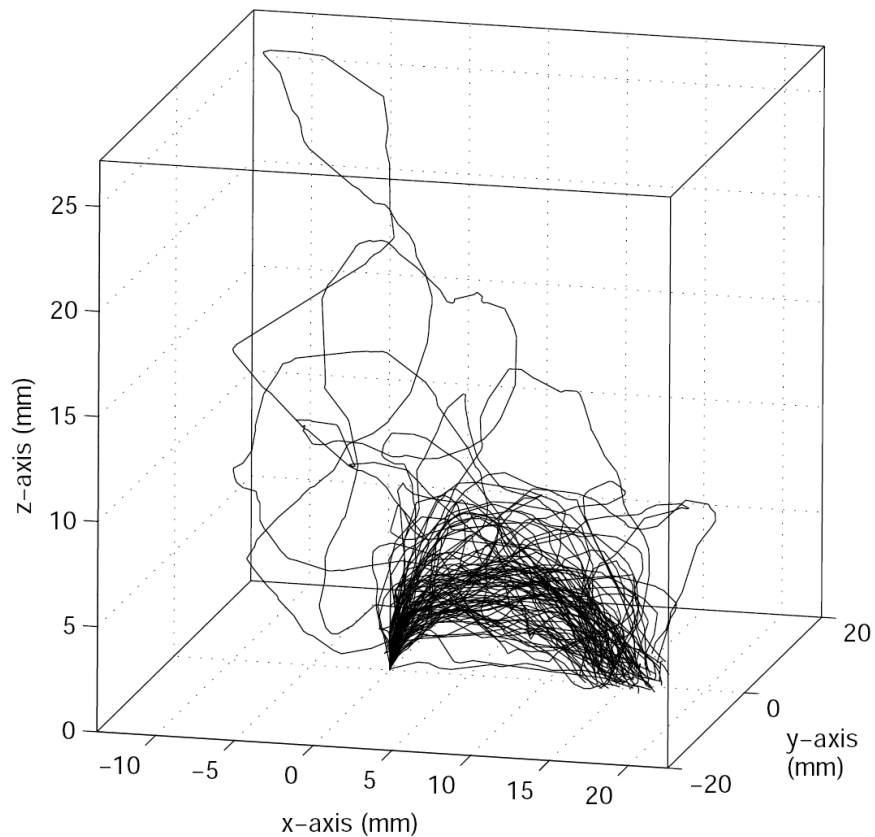
Figure 2.15: 3 Dimensional plot of the paths of detected photons in tissue generated with a Monte-Carlo model. Figure reproduced from Humphreys (2007)

The changes in oxygenation in the tissue caused by the neuronal activity covered earlier alters the tissue opacity to NIR light. This, in turn, alters the number of reflected detectable photons.

2.3.1 Photon Tissue Interactions

The substances in the blood that induce changes in tissue opacity are referred to as chromophores. Two chromophores of particular interest in fNRIS are HbO_2 and HbR. The concentrations of these chromophores change in specific manners during cerebral activation. These chromophores also have wavelength dependent optical absorption properties that allows NIRS to monitor changes in their concentration.
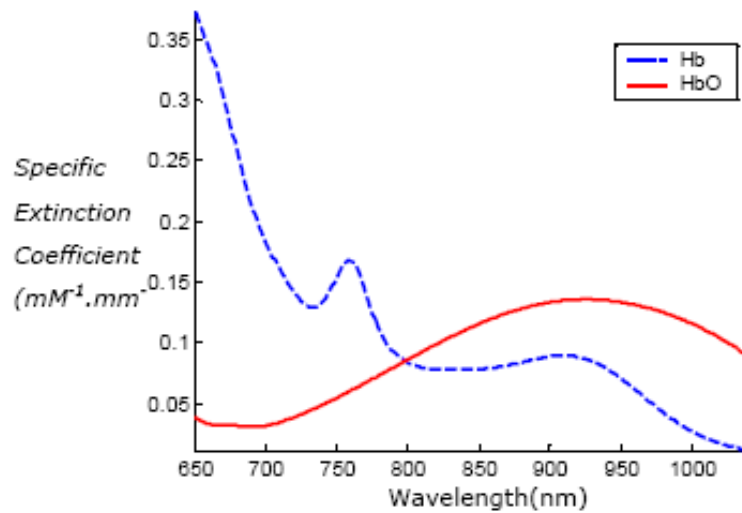
Figure 2.16: Wavelength dependent changes in the absorption properties of HbO_2 and HbR. Figure reproduced from Coyle (2005)

Figure 2.16 shows the changes in the extinction coefficients of HbO_2 and HbR versus the wavelength of interrogatory light (Cope, 1991). To adequately differentiate both chromophores, two wavelengths must be chosen either side of the point where the extinction coefficients cross, also referred to as the isosbestic point. This point is defined as a specific wavelength at which two chemical species have the same molar absorptivity. A review of the specific factors of wavelength is available from Uludag *et al.* (2004).

With the correct choices made it is possible to calculate relative changes in chromophores concentration using the Beer-Lambert law.

2.3.1.1 Beer-Lambert Law

The Beer-Lambert law states that the attenuation in light intensity is proportional to the concentration of an absorbing compound in a non-absorbing medium and the path-length of the photons.

If we let A be the attenuation in dB; I_0, the intensity of the incident light; I_1, the intensity of the detected light; l, the distance that the light travels through the material (the path-length); c, the concentration of chromophores; α, the absorption coefficient of the chromophore; λ, the wavelength of the light; and k, the extinction coefficient then:

$$A = \alpha l c = \log_{10} \frac{I_0}{I_1}, \qquad\qquad \alpha = \frac{4\pi k}{\lambda} \qquad\qquad (2.1)$$

Equation 2.1 provides a simple means to relate light absorption to underlying chemical concentration.

2.3.1.2 Modified Beer-Lambert Law

When considering the interrogation of brain tissue it is necessary to modify this equation to account for the highly scattering nature of the medium. The modification must include an additive term to account for scattering losses and a term for the change in the optical path-length.

$$A = \log_{10} \frac{I_0}{I_1} = \alpha \, l \, c \, \mathrm{DPF} + G \qquad\qquad (2.2)$$

The Differential Path-length Factor (DPF) is a scaling term to account for the increased path-length due to scattering while G is an additive scalar term incorporating the scattering losses. The DPF can be determined from experimentally derived studies Duncan *et al.* (1995) making the key measurement the change in transmitted light intensity. It is this change that constitutes a signal correlated with neural activity. An

fNIRS-BCI utilizes this measurement principle along with instrumentation capable of measuring A accurately to determine optical correlates of hemodynamics.

2.3.2   Detectable Activation Trends

During localized neuronal activation it is possible, using NIRS, to identify the specific chromophore trends. The work of Edvinsson *et al.* (2002) identified three main factors that influence these trends. The first is an increase in Cerebral Blood Flow (CBF) the second is an increase in oxygen consumption and the third is an increase in Cerebral Blood Volume (CBV). Figure 2.17 illustrates the effect these three trends have on ΔHbR and ΔHbO_2. During functional activation these three trends occur simultaneously, with the detected NIRS signal highlighting the dominant influence of the above trends (Coyle, 2005).

These detectable trends are descussed in detail in Chapter 3.
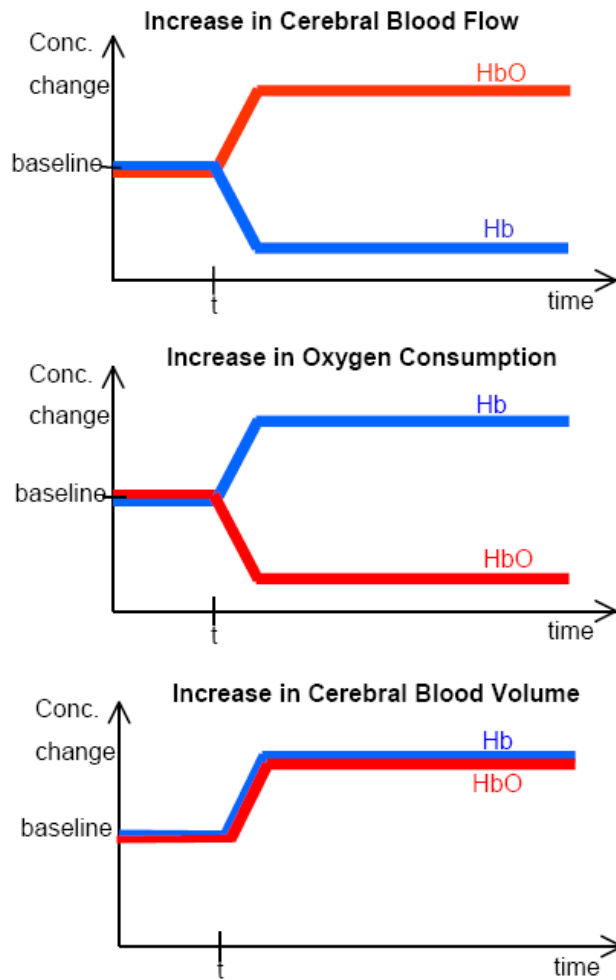
Figure 2.17: Changes occurring in cerebral oxygenation during stimulus. Stimulus occurs at time t. Reproduced from Coyle (2005)

2.4 Brain Computer Interfacing (BCI)

This dissertation deals with the signal and systems issues surrounding optical Brain Computer Interfaces (OBCI). This section outlines the background of BCI research including a discussion of generic BCI models, non-invasive brain activity monitoring modalities and common cognative tasks asscoiated with BCI control.

This section aims to outline the basic, pertinent information necessary for further chapters in this dissertation. Comprehensive reviews of the field of BCI research can be found in the work of Wolpaw *et al.* (2000), Mason *et al.* (2007) and Allison *et al.* (2007).

2.4.1 Generic BCI Models

A device can be described as a BCI if it provides a subject with a communication channel to an external environment independently of voluntary muscle control (Soraghan, 2010; Vallabhaneni *et al.*, 2005). These systems are employed in cases of severe motor disability with the aim of returning the control of certain functions that have been lost.

BCIs can be characterized in a number of ways based on the different modalities of physiological measurement (Electroencephalography (EEG) (Guger *et al.*, 2001; Pfurtscheller *et al.*, 2006), Electrocorticography (ECoG) (Hill *et al.*, 2006), Magneto-encephalography (MEG), Magnetic Resonance Imaging (MRI) (Weiskopf *et al.*, 2004; Yoo *et al.*, 2004)), mental activation strategies (dependent versus independent), degree of invasiveness and so on (Mason *et al.*, 2007).

Figure 2.18 is an illustration of a generic BCI model. A functional brain scanning modality is used to detect signal relating to brain activity. This signal is digitized and passed on for further processing. The next stage filters and analyses this signal for predefined activity templates. If detected, these templates are classified and used to control a device and possibly fed back to the user.
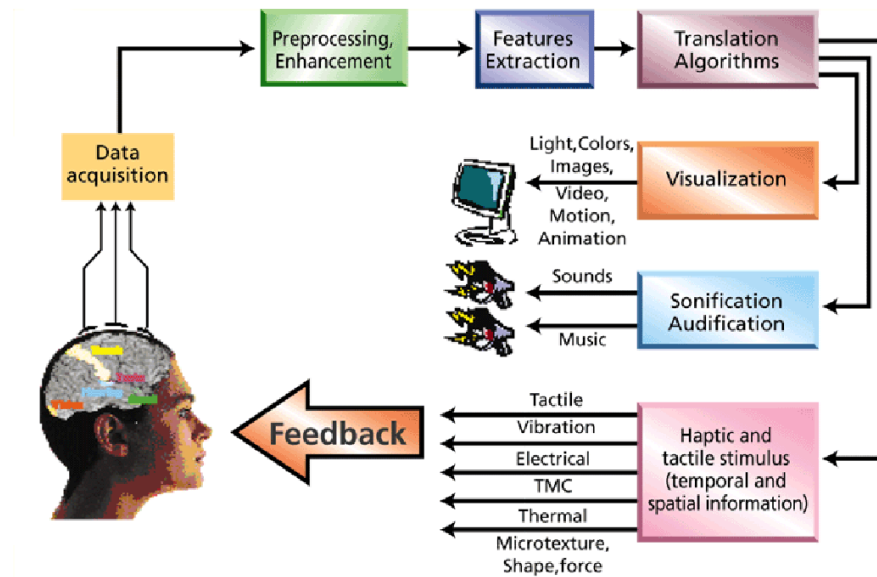
Figure 2.18: Generalized concept of a Brain-computer Interface

2.4.2 BCI Suitable Non-invasive Modalities

2.4.2.1 Electroencephalography (EEG)

Electroencephalography (EEG) measures electrical activity of the brain non-invasively via electrodes placed on a subjects scalp. Berger (1929) demonstrated it was possible to measure these electrical signals in humans creating a modality which is now used widely in clinical diagnosis and functional activity studies. EEGs are performed by attaching electrodes to the scalp of a subject over particular areas believed to be associated with certain brain activities. This placement is defined by the 10-20 electrode system of the international federation (Jasper, 1983). The measured activity is related to the activity of millions of nerve cells under the electrode. These signals are characterized in both the frequency and time domains and both domains have been used in BCI research.

2.4.2.2 Functional Magnetic Resonance Imaging (fMRI)

As previously discussed in Section 2.2 fMRI tracks changes in the blood oxygen level dependent (BOLD) signal. Studies have shown this signal to be closely linked with the

electrical signals measured using EEG (Logothetis, 2003). This signal is also closely linked to the measurements of fNIRS (Strangman *et al.*, 2002b) modality discussed in Section 2.3.

2.4.3 Cognitive Responses used in BCI

2.4.3.1 Neural Rhythms

EEG signals are often analyzed in the frequency domain, and can be classed by their spectral peak into different bands or rhythms. Abnormalities in EEG rhythms may result from injury, disease, infection or surgery and is therefore an important tool in neuropsychological testing (Martin 1997). In functional analysis the EEG rhythms may be affected by different thoughts, actions or state of mind, e.g., planning to perform a movement can attenuate the Mu band.

2.4.3.2 Evoked Potentials

Evoked potentials (EP) are a subset of detectable mental activity used in EEG based BCIs. They are described as electrical potentials recorded from the nervous system using EEG. EPs mesured in the occipital region during external stimuli of the visual system are referred to as Visual Evoked Potentials (VEP)

The P300 or oddball response is a positive peak in potential that occurs after the presentation of unusual stimulus which is prominent in the Parietal lobe. This stimulus might be characterized by a familiar name in a list of unfamiliar names or similarly with images and faces.

An EP associated with movement is the readiness potential (RP). Prior to a performed movement a slow negative potential shift can be detected in the motor cortex region (Misulis & Spehlmann, 1994).

Evoked potentials resulting from visual stimulation (VEP), oddball paradigms (P300) or preparation for movement (readiness potential) have been used in a number of BCI

applications. These signals are endogenous responses, which minimize training periods. The implementations of these signals by various BCI research groups are discussed in the following sections.

2.4.3.3 Slow Cortical Potentials

Electrical signals from the brain that vary in amplitude slowly are known as slow cortical potentials (SCPs). These are DC shifts in the EEG signal lasting from a few hundred milliseconds up to several seconds or minutes. Negative SCPs are typically associated with movement and other functions involving cortical activation, while positive SCPs are usually associated with reduced cortical activation. Subjects can learn to control their SCPs by means of visual or auditory feedback.

2.4.3.4 Neuro-vascular correlates

Neuro-vascular correlates describe the hemodynamic response detectable by fNRIS and fMRI. By monitoring specific regions of the cortex it is possible for a subject to volitionally induce this response using targeted mental tasks such as imagined or overt motor movement or mental arithmetic.

2.5 Chapter Conclusion

The background knowledge required to produce a NIRS is extensive and spans a number of fields including physics, biology, physiology, psychology and computer science. This chapter has attempted to present the necessary information to understand the processes and mechanics of NIRS-BCI.

Chapter 3

Current Challenges in NIRS-BCI

This thesis postulates the importance of a broad view of NIRS-BCI to enable improvements in all areas of system design and signal processing. To achieve any improvements it is first necessary to examine the current research in the area and assess the challenges that remain there. To this end this chapter will examine the processes behind NIRS and review the work of other groups involved in NIRS-BCI. We start with an analysis of the cognitive strategies used to produce volitionally driven physiological measurement changes. This is followed by a review of hardware and software systems and concludes with an outlining of issues introduced by physiological noise in NIRS-BCI research and current solutions therein.

3.1   Mental Activation Tasks in NIRS

Chapter 2 outlines the basic process behind neuro-vascular coupling. This process is the basis for functional NIRS (fNIRS) investigation. For an effective NIRS-BCI it is necessary to define a set of volitional mental tasks that produce repeatable and detectable hemodynamic changes. In NIRS BCI research there are two main functional areas that are generally interrogated. The first is the motor cortex where movement,

both actual and imagined, are triggers for activation (Porro *et al.*, 1996). The second is the frontal cortex where activities such as mental calculations (Inouye *et al.*, 1993), object visualization and certain imagined verbal activity (singing)(Boso *et al.*, 2006) are triggers. Firstly, we must assess how functional activation manifests itself in NIRS signals.

3.1.1 Functional Activation Characteristics

3.1.1.1 Cerebral Blood Volume

Certain groups use only the shifts in measured regional cerebral blood volume (rCBV) as the trigger for experiments (Naito *et al.*, 2007). Due to the influx of blood to an activated area an increase in rCBV is indicative of possible activation in the interrogated region. Using fNIRS this increase in rCBV is characterized by a decrease in detected light intensity because of higher absorption in the tissue. Classifying these trends requires the use of recorded raw light intensities and can be done with a single wavelength. This makes it a simple mechanism though unreliable due to constant and widespread shifts in rCBV unrelated to activations. In cases of stroke it has been shown that meausres of CBF perform better at identifying and characterizing brain injury than CBV (Sorensen *et al.*, 1999). A more reliable method for assessing functional activation is the measurment of changes in blood oxygen levels.

3.1.1.2 Blood Oxygenation

Using the modified Beer-Lambert law outlined in Chapter 2 it is possible to calculate the concentration changes in both oxy-hemoglobin (ΔHbO_2) and deoxy-hemoglobin (ΔHbR) (Villringer *et al.*, 1993). Many fNIRS-BCI implementations have used ΔHbO_2 alone as the classification signal (Coyle, 2005; Ranganatha *et al.*, 2007). ΔHbO_2 trends during activation have a much higher amplitude than that of ΔHbR . During an activation ΔHbO_2 rises sharply in the first 3–5 seconds. This is due to the "watering-

the-garden" effect where the brain over saturates an active area to supply neurons with oxygen (Mayhew, 2003). However ΔHbR has been shown to be be a better indicator of localized activation(Mayhew, 2003). This feature is demonstrated during data analysis performed in Chapter 7.
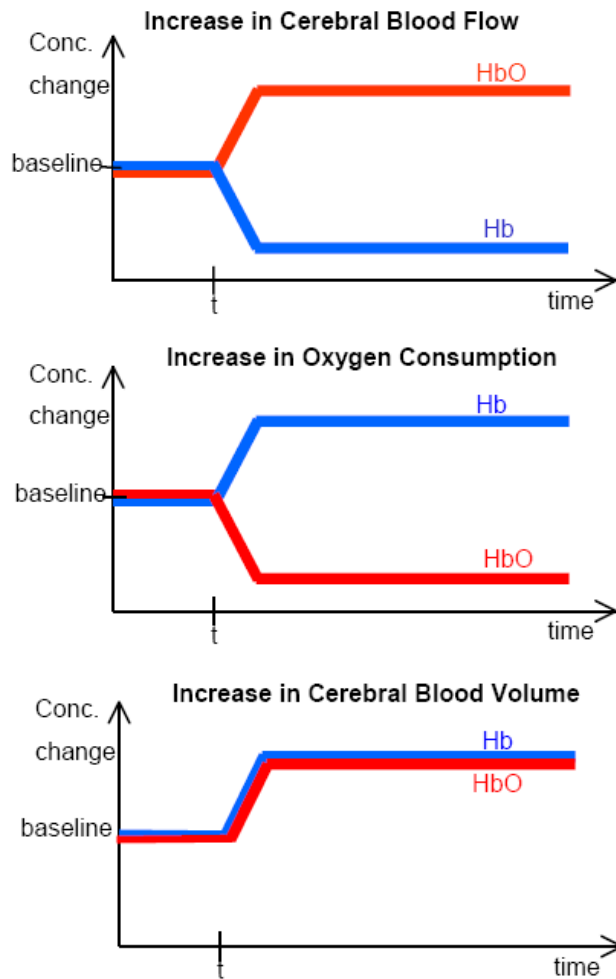
Figure 3.1: Changes occurring in cerebral oxygenation during stimulus. Stimulus occurs at time t. Reproduced from Coyle (2005)

Figure 3.1 shows examples of trends visible in ΔHbR and ΔHbO_2 during stimulus. Certain frontal activations have been shown to exhibit the decrease in ΔHbO_2 and increase ΔHbR seen in the second example in Figure 3.1 (Soraghan, 2010). A recent study has attributed this trend to neuronal hyperpolarization in the area leading to arteriolar vasoconstriction (Devor *et al.*, 2007). Another recent study has been carried out with reference to the Fast Oxygen Response in Capillary Event (FORCE) (Kato, 2004). This study stated that there was an oxygen exchange event occurring in capillaries in the activated region. Should these results be adequately replicated this effect holds promise for improving the throughput in an fNIRS-BCI.

3.1.2   Locating Activity

Before describing specific mental tasks used in BCIs it is important to outline a standard for locating these activities versus scalp markers. The standard adopted here and in other NIRS research is that of the EEG 10-20 system (Coyle, 2005; Ranganatha *et al.*, 2007; Ward *et al.*, 2007).

Figure 3.2 shows the 10-20 system. Each point is defined as a distance from a center line running from the nasion (bridge of the nose) to the inion (back of the skull) on the surface of the scalp (Jasper, 1983). Studies have been performed to show that each point is related to some underlying cortical structure (Homan *et al.*, 1987).

3.1.3   Motor Cortex

Motor cortex activation is used in all BCI modalities. The advantage of motor cortex activation is it generally requires little or no user training although motor imagery training has been shown to improve detection rates (Hwang *et al.*, 2009). Mental strategies that require training can over time become frustrating for subjects and lead to abandonment (Spinney, 2003). Another advantage to using motor based activation is the areas of the brain where this action is attributed is in the cerebral cortex making
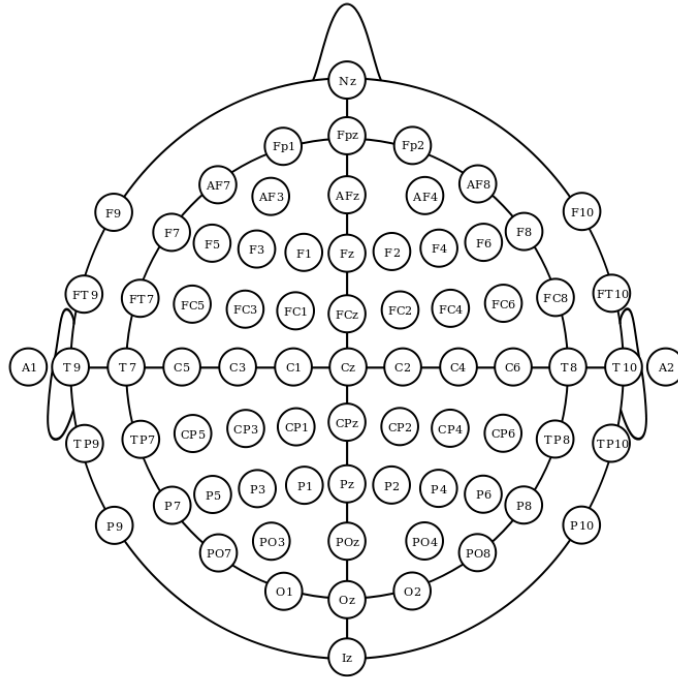
Figure 3.2: The EEG 10-20 system for electrode placement. The line from the nasion to the inion defines the zero line. Then even numbered points are on the right and odd numbered points are on the left.

is accessible to NIRS imaging.

Figure 3.3 is a representation of the motor cortex. We can see that large areas of the motor strip are responsible for the hands and tongue due to the need for precise movement. The size of the area associated with hands and fingers lead many BCI modalities to use fist clenching or finger opposition, both actual and imagined, as cognitive tasks including NIRS-BCI (Coyle, 2005; Ranganatha *et al.*, 2007; Soraghan, 2010; Ward *et al.*, 2007).

Activity in the primary motor cortex is shown to be correlated to most motor actions (Allison *et al.*, 2000). To consider the entire process of movement, the supplementary motor area (SMA) must also be included. The SMA is believed to be where motor
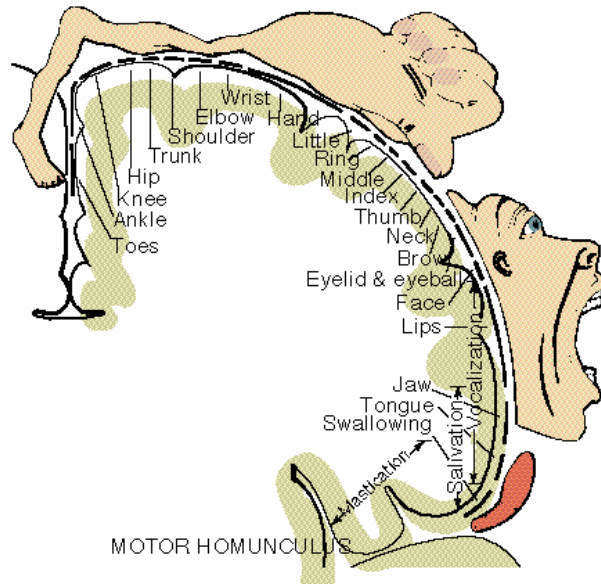
Figure 3.3: Representation of the distibution of motor control throughout the cortex.

planning is achieved (Shibasaki *et al.*, 1993; Tanji & Shima, 1994). Motor activity for the hands manifests itself under C3 and C4 according to the 10-20 system (Homan *et al.*, 1987). The specific hemodynamic activity is characterized as an increase in ΔHbO_2 and a decrease in ΔHbR as shown in Figure 3.4.

In Chapter 4 we will investigate the validity of motor activity in NIRS-BCI paradigms and examine inter-subject variability of activation locations using a small fMRI study.

3.1.3.1 Lateralized Activations

During a single handed activation it is widely assumed that only the contra-lateral hemisphere of the brain demonstrates a response (Cramer *et al.*, 1999). It has been shown experimentally that both hemispheres can respond similarly (Coyle *et al.*, 2004a). It is therefore necessary to develop systems to correctly classify differences between left hand and right hand activations. Two methods that have improved classification rates are Hidden Markov Models (HMMs) and Support Vector Machines (SVMs). Using finger tapping and motor imagery experiments on five subjects these systems were
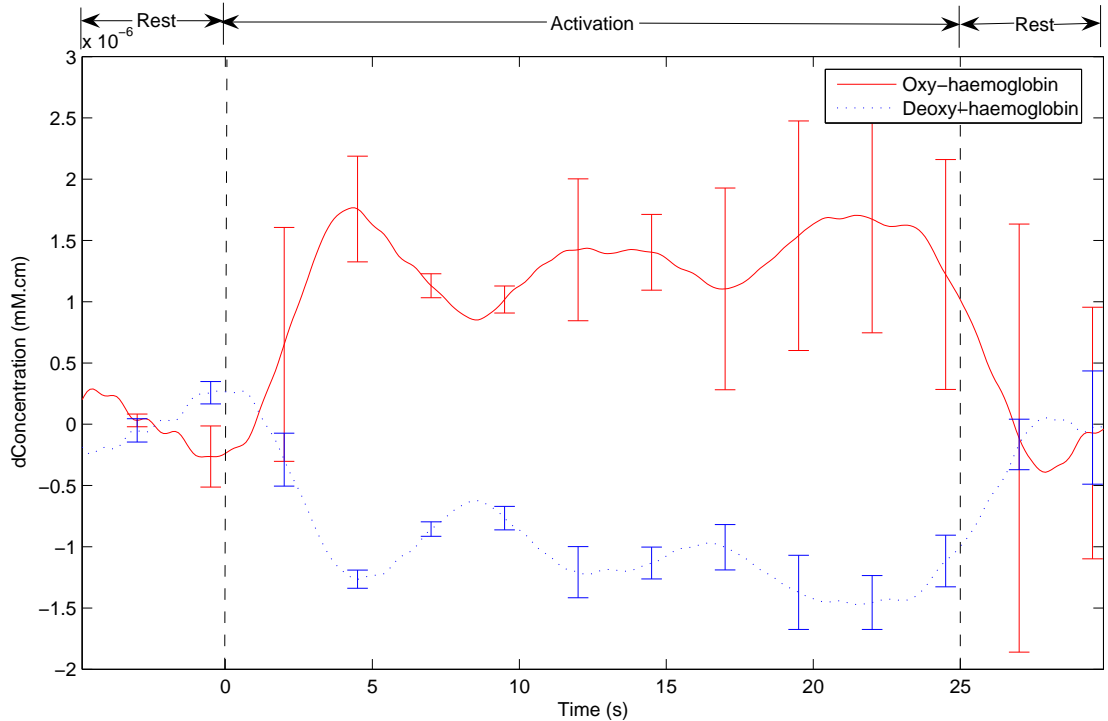
Figure 3.4: Hemodynamic during a motor activity task. Characterized by an increase in ΔHbO_2 and a decrease in ΔHbR

able to achieve accuracy above 80% for overt finger tapping and above 70% for motor imagery (Ranganatha *et al.*, 2007). HMM performed best overall, bettering SVM by 16% in motor imagery classification.

Feature extraction and classification represent the final step in an optical BCI design process. Ultimately the overall performance is determined through careful consideration of every stage in the signal processing schema.

3.1.3.2 Overt vs Imagined Motor Action

Motor imagery for mental activation has proven effective in a wide range of BCI modalities. The first NIRS motor imagery studies for BCI, done by Coyle (2005), showed detectable and repeatable activations but with lower classification rates than overt movement. This approach is common among other BCI groups (Ranganatha *et al.*,

2007; Soraghan, 2010).

Motor imagery can be induced by the imagination of first-person activation or observation of the same third-person activity (Jeannerod, 1995). It has been shown that motor imagery retains many of the recorded neural correlates induced by overt motor activity. Many functional neuroimaging studies have shown that motor imagery activates the areas involves in early motor control and planning (Decety *et al.*, 1994; Roth *et al.*, 1996).

Motor imagery has been encouraged within the BCI community due to the ability to detect activation in an able bodied person that could be replicated by a disabled person. An argument that remains open for further investigation is that an instruction to a disabled person to imagine moving, for example, a limb that they have no control over is redundant. In order to get the best response the subject should attempt to move said limb. Recent studies have shown overt movement to be more effective, more comfortable and keeps subjects more alert during experiments in able bodied subject experiments (van de Laar, 2009). Without further study the reliance of imagined movement for able bodied subjects may be an unnecessary constraint.

Throughout this thesis the experiments (Chapter 4 & 7) analyzed use both overt and imagined motor tasks. They are compared and the differences are highlighted.

3.1.4   Frontal Cortex Activity

The frontal lobe is believed to be responsible for reasoning, reward processes, long term planning and a number of other higher level functions. Placing NIRS optodes in the region of FP_z on the 10-20 system, it is possible to detect activity using a number of volitional tasks. Instructing the user to imagine a known 3D shape and then rotate it has been shown to elicit cortical activity in MRI studies (Cohen *et al.*, 1996).

In NIRS, studies have been performed using two types of tasks to elicit a hemodynamic change. Instructing a subject to sing a song fast in their head has been used

effectively for locked in patients by Naito *et al.* (2007). Another common task instructs subjects to perform mental arithmatic calculations (Bauernfeind *et al.*, 2008; Soraghan, 2010).

Mental calculation studies were performed in parallel with this work by Soraghan (2010) and show that an inverted response relative to activity in the motor cortex. That is an increase in ΔHbR and a decrease in ΔHbO_2 as shown in Figure 3.5.
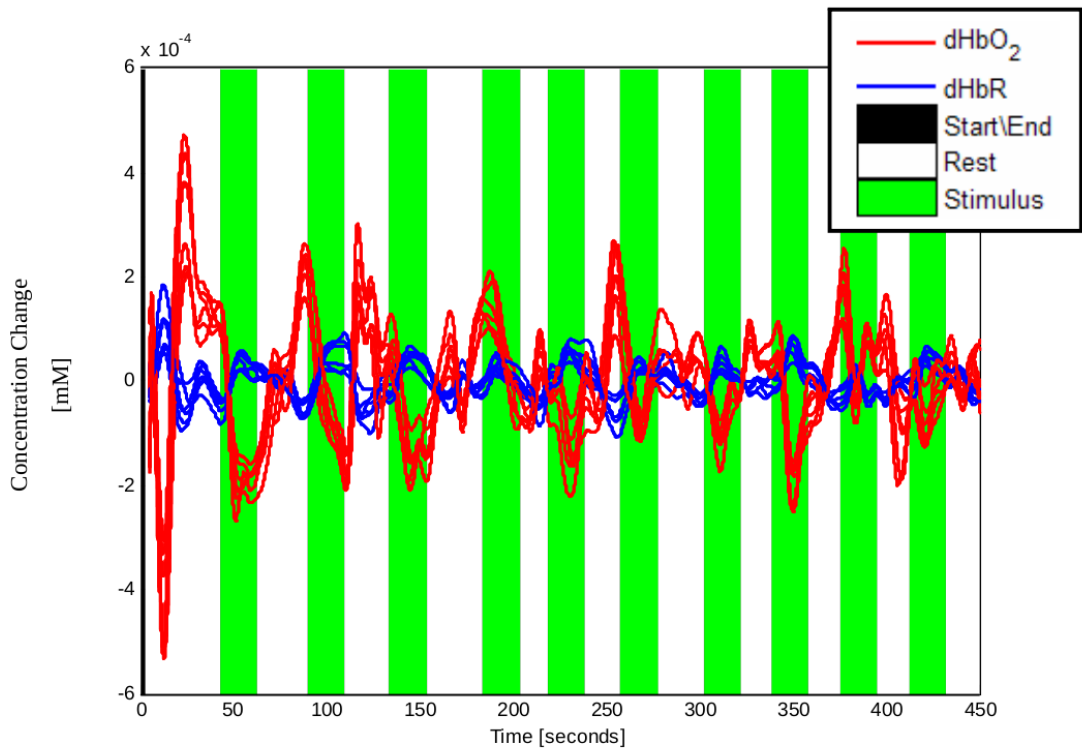
Figure 3.5: Hemodynamic during a mental calculation task. Characterized by a decrease in ΔHbO_2 and an increase in ΔHbR

3.1.5 Discussion

Within the NIRS-BCI experimental paradigm, the mental tasks chosen to ellicit mental activity have mainly focused on the motor and frontal cortex activation. In Chapter 4 and 7 we will examine experiments from both, with the aim of highlighting the possi-

bilities for improvement in efficiency by using different locations and task instruction within the same experiment.

3.2 Hardware Systems

In Chapter 5 a bespoke NIRS-BCI designs is outlined. The system described there was created in parallel with this research with the aim of creating an entire system versatile enough to address problems throughout the signal processing chain. In this section we outline the challanges imposed by NIRS-BCI on hardware systems and review the systems common to other groups involved in this area.

3.2.1 Interrogatory Signal Synthesis Problem

NIRS requires the generation of optical signals which then must then be detected reliably and consistently post tissue interrogation. We refer to this as the interrogatory signal synthesis problem.When discussing the hardware / software chain of a NIRS system it is necessary to consider the problem in different terms than that of EEG. Firstly optical source wavelengths must be correctly chosen (Uludag *et al.*, 2004) and in some way modulated so that different wavelength information can be extracted at acquisition time. Multiple source per detector (multi-channel) setups add another level of complexity to the signal multiplexing. Optical acquisition systems must be sensitive enough to detect and demodulate wavelength and channel data. To maximize the results for any NIRS-BCI system, Chapter 5 and 6 demonstrate the advantage of fully customizable systems.

3.2.2 Commercial Systems

There are a number of commercial multi-channel devices in existence for NIRS studies. Each takes a number of different approaches to the interrogatory signal synthesis prob-

lem. The OMM-1000 (Shimadzu Corporation) is a 20 channel device that uses three wavelengths (780nm, 805nm, 830nm) per source (Miyai *et al.*, 2001; Ranganatha *et al.*, 2007). Sources are laser diodes and optical detection is done using photon multiplier tubes. Multi-channel multiplexing is achieved by cycling through all the source-detector parings using a time division approach. The entire sampling cycle can be performed at 14Hz and is digitized using a 16-bit analog to digital converter.

The TechEN CW systems can be specified with up to 32 sources and detectors (The CW6 version). Laser diodes are modulated using carrier frequencies and the detectors are Hamamatsu avalanche photo-diodes (Huppert *et al.*, 2006). Demodulation is performed in hardware using Texas Instruments DSP processors. Effective sampling rates can be set up to 25Hz depending on the number of source detector pairings. Recently an API was provided by TechEN that allow signals to be monitored and processed in real-time and TechEN. The system is designed to integrate with the HomER NIR data analysis software for offline and statistical processing.

3.2.3 Custom Designs

Customs system have been designed by a number of research groups. Single/dual channel systems using LED and laser diodes have been implemented specifically aimed at NIRS-BCI applications (Bauernfeind *et al.*, 2008; Coyle, 2005). These systems concentrate on hemodynamic changes and attempt to classify activations in real-time.

3.2.4 Discussion

We have seen above an example of the NIRS equipment available to the general research community. The difficulties presented by most of these systems exist in the signal processing realm. Users tend to have no control over raw optical data and the options provided for implementing processing systems on the hemodynamic data in real-time are unsuitable. As stated earlier, it is necessary to create fully customizable system to

achieve improvments along the entire data processing chain.

The work presented in this document address these problems using the first custom-built multi-channel NIRS system designed specifically for BCI applications (Soraghan *et al.*, 2008a, 2010). It allows examination of all approches including optical sources, signal generation, modulation, acquisition, processing and classification.

3.3 Software Systems

Currently there is no software package designed specifically for NIRS-BCI analysis. NIRS-BCI research groups have developed systems independently to suit particular purposes. Here we will examine two systems to build a set of best requirements for such systems. The first, BCI 2000, is a general purpose BCI software platform used predominately with EEG-BCIs (Krusienski *et al.*, 2007; Wilson *et al.*, 2009; Yamawaki *et al.*, 2005) but also with EcOG (Leuthardt *et al.*, 2006) and EEG-fMRI combinations (Hinterberger *et al.*, 2004). The second is an offline NIRS data analysis system, HomER (Huppert, 2006).

3.3.1 BCI2000

The BCI2000 system is one of the most prominent BCI software systems (Schalk *et al.*, June 2004). It was designed as a general purpose BCI interface. The BCI2000 consists mainly of four modules. The source module handles data acquisition while the signal processing module handles data processing. The user application module handles user feedback during experiments and the operator module is the control system for the researcher preforming various studies. These modules are all controlled via a graphical user interface.

The entire system is open source and written in Borland C++. The source module can be re-configured for different acquisition systems and any supplementary devel-

opment is done in C++. The processing module has easily configurable filter sets. Extending modules for processing can be written in C++ and it is also possible to include Matlab MEX files.

3.3.2 HOMER

HomER is a Matlab based NIR data analysis package developed by The Center for Functional Neuroimaging Technologies (Huppert, 2006). It requires the input of the demodulated optical intensities and calculates hemodynamic concentrations. HomER can preform noise removal and generate statistics associated with averaged activations. Finally, this software also allows topographic mapping of activations according to optode placement maps.

3.3.3 Discussion

These examples possess all the components required in versatile and robust software systems for NIRS-BCIs. While it might be possible to adapt current platforms to provide the functionality necessary for such systems, the relative novelty of nearly all NRIS-BCI research demands new approaches to accomodate new advances in the field.

In Chapter 6 we will outline a NIRS-BCI software system created for the hardware described in Chapter 5. This software will provide the functionality to control all aspects of the systems including experimental setup, user feedback, hardware interaction and timing, data processing and recoding and signal processing. Developed using National Instruments Labview it also allows rapid prototyping of new processing methods that can be implemented both offline and online and provides data replay systems for simulated real-time testing (Matthews *et al.*, 2008b).

3.4 Physiological Interference

A substantial quantity of the energy in fNIRS signals is composed of physiological signals other that the hemodynamic response of interest. This physiological interference is caused mainly by heartbeat, respiratory influences and a number of low frequency oscillations attributed to blood-pressure changes and other factors.

Due to the spectral overlap these signals collectively make functional activation difficult to detect without substantial post-processing. Figure 3.6 shows the frequency spectrum of a single wavelength fNIRS time series during an experiment. The physiological noise sources are particularly apparent in this domain.

Many approaches to fNIRS noise removal evolved from methods used in other brain scanning modalities. Experiences with EEG and fMRI serve as good examples for extension to fNIRS. Several of these methods have been implemented in clinical fNIRS research but have yet to be incorporated into an fNIRS-BCI system. There are still numerous avenues available to improve the SNR prior to feature extraction in an fNIRS-BCI. This section explores the major sources of noise and examines the methods that have been implemented to deal with these artifacts in all areas of fNIRS research. We will discuss these methods and highlight those that prove most useful to fNIRS-BCIs.

3.4.1 Pulse Artifact

During NIRS measurement the influence of the cardiac cycle is a significant source of noise. The systolic increase in blood pressure during a cycle traverses the body and manifests in pressure and volume changes in the cerebral arterioles as a result of cardiac pumping. This periodic increase in blood pressure and volume reduces the opacity of the tissue which manifests in the variation of detected optical intensities of NIR equipment. This periodicity generally exists in the 0.8–1.2 Hz.

Another challenge of the influence of the cardiac cycle on the NIR signal is the beat
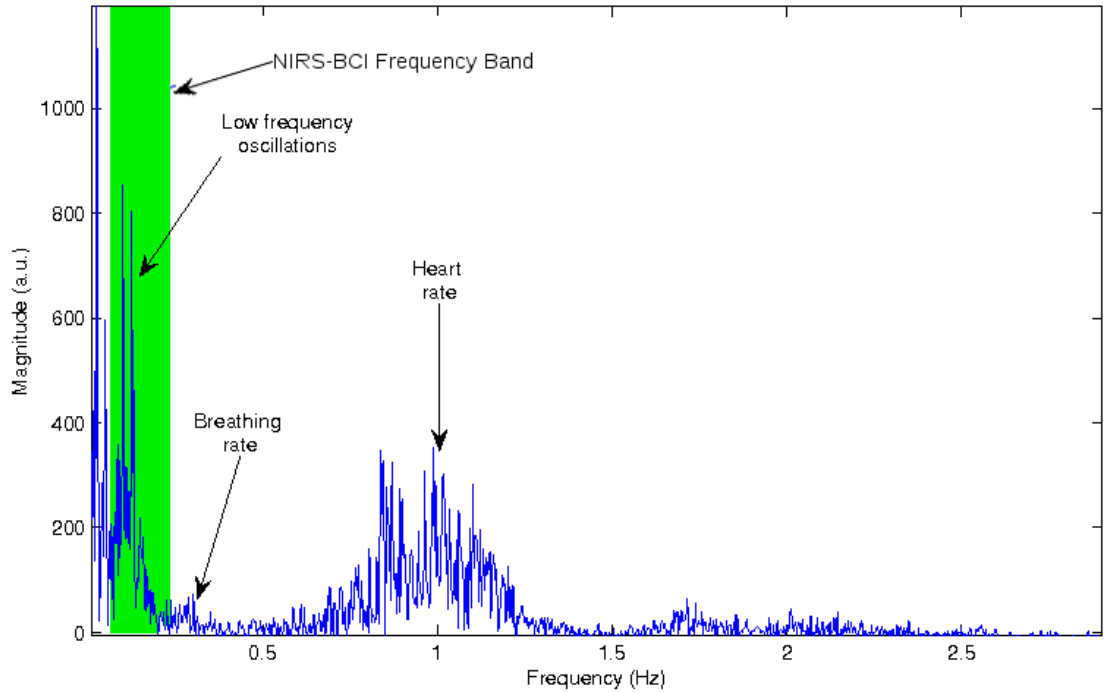
Figure 3.6: Sources of noise in fNIRS signal

to beat variation in frequency and amplitude. Due to these characteristics, it must be classed as non-linear and non-stationary process. Stationarity in a signal implies that its statistical characteristics do not change over time (Shiryaev, 1996) whereas a non-linear system is described as system whose outputs are not a linear combination of its inputs. Both these properties pose difficulties in using standard signal processing methods. This variability in the signal has proven useful in clinical scenarios as certain types of variation can be indicative of ill health (Bigger *et al.*, 1992). In NIRS measurement however these inhibit the filtering of this interference to clearly detect hemodynamic sifts.

Given the cardiac cycle's spectral distance for the signal of interest it is possible to define low-pass filter stopbands wide enough to attenuate the interference with little disruption of the desired signal (Bauernfeind *et al.*, 2008; Soraghan *et al.*, 2009a; Ward *et al.*, 2007). Online fNIRS-BCIs have used simple moving average filters to reduce

the effect of the signal prior to the thresholding for feature extraction (Soraghan *et al.*, 2006).

The previously mentioned analysis software HomER (Huppert, 2006) uses a Type II Chebyshev low-pass filter by default to smooth out the heart rate (Ranganatha *et al.*, 2007). Other approaches have also calculated a mean value between cardiac peaks and troughs. Next an interpolation is performed through those mean points to produce a smoothed signal (Coyle *et al.*, 2007). Another approach is to use a system where all the beats are averaged. This average waveform is then matched against each individual beat using a linear regression algorithm and the resulting waveform is subtracted from the signal (Gratton & Corballis, 1995).

A recent study used narrower source detector spacings to collect information on global interference patterns and train adaptive filters to cancel them. This proved effective when the near and far sources correlated well during rest periods. Results were generally poorer when this correlation was not as strong (Zhang *et al.*, 2009).

3.4.2 Low Frequency Interference Sources

There exists a set of low frequency interference sources within the NIRS signal which present challenges to activation detection. These can be grouped as follows:

- Influence of respiratory function $\sim$0.3Hz

- Low frequency changes ($\sim$0.1Hz) possibly related to blood pressure regulation (Cooley *et al.*, 1998).

- Very low frequency changes ($\sim$0.04Hz) believed connected to thermal or bodily fluid regulation (Seydnejad & Kitney, 2001).

The final two components have been generally termed the Mayer Waves (Cooley *et al.*, 1998), or vasomotion, V-signal and spontaneous oscillations (Elwell *et al.*, 1999). Similarly to the arterial heart beat these are non-linear and non-stationary signals. The
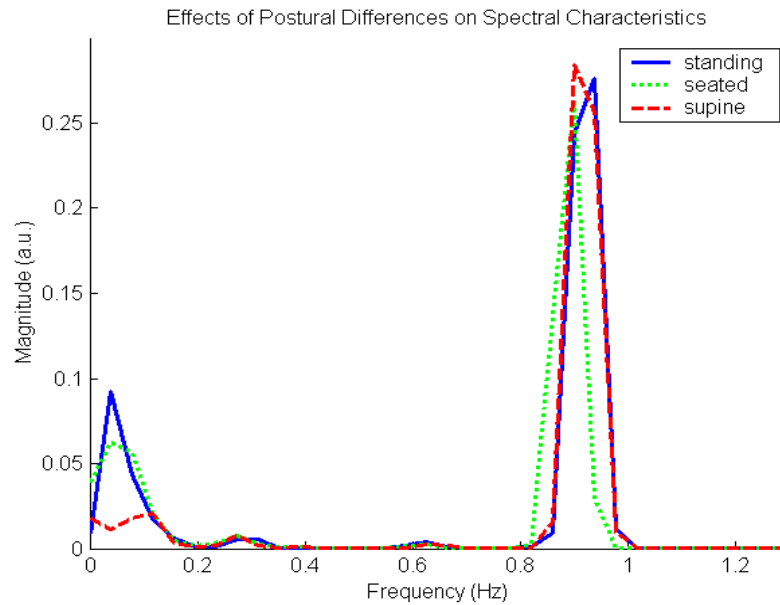
Figure 3.7: Effect of subject position on Mayer wave (Coyle *et al.*, 2004a)

causes are not well understood but there are many non-linear mathematical models published attempting to ascertain their underlying causes (Seydnejad & Kitney, 2001). Placing a subject in a near-supine position reduces the amplitude of the oscillation (Figure 3.7) but does not entirely eliminate it. Mayer Waves are particularly problematic at 0.1Hz given its spectral overlap with volitionally induced hemodynamic changes.

Common signal processing approaches include standard band-pass filtering but given the spectral overlap with the activations it cannot be guaranteed that signals of interest are attenuated in the process. Another approach to removal is to use an algorithm from the IEEE 1057 standard to fit a sine wave to the data (Coyle *et al.*, 2007). This sine wave is then subtracted leaving a denoised signal. Difficulties arise when attempting to implement this approach in a real-time setting.

3.5 Motion Artifact

Subject motion is a source of significant disruption in the fNIRS signal and is termed motion artifact. Motion artifact disruption is caused by many different factors. Movement of the optodes and detectors can change the angle of incidence of the transmitted and detected light, increasing the affect of the reflectance of the skin surface. Motion can cause an increase in blood flow through the scalp or, more rarely, an increase in blood pressure in the interrogated cerebral regions. The orientation of the head can affect the signal due to gravity's influence on the blood (Izzetoglu *et al.*, 2005). These compounded effects are a significant source of noise if the head is not physically restricted. Implementing fNIRS in a completely mobile scenario increases these effects. The ambulatory interference of walking and totally free head motion would further increase the amplitude and change the nature of the artifact.

A common approach to motion artifact removal in many brain scanning modalities is that of adaptive finite impulse response (FIR) filtering. This requires collection of additional information about the noise in order to alter the filter coefficients. Such information can be collected through accelerometers attached to the head to record movement. The advantage of this approach is that it makes real-time filtering possible. Weiner filtering functions effectively for offline cleaning of data in both stationary and ambulatory scenarios but has yet to be implemented in a fNIRS-BCI (Izzetoglu *et al.*, 2005).

As motion artifact causes the largest statistical variance within the data set it is possible to implement a Principal Component Analysis filter to remove it. This method is used in the NIRS analysis software HomER (Huppert, 2006) and has performed well in offline BCI analysis (Ranganatha *et al.*, 2007).

3.6   Chapter Conclusion

Although many groups are currently working in NIRS BCI development many difficulties still remain. The concepts to be presented in this thesis will detail the choices of mental activation strategies and help confirm, with the aid of the literature and independent fMRI experiments, the validity of these choices. We will provide evidence in support of our contention: that robust multi-channel hardware and versatile software is required in order to improve signal detection. These customizable systems will, in turn, enable the next generation of NIRS system to be lower in cost and complexity. We will also outline new approaches of signal analysis for future study as well as improvements to physiological noise removal techniques.

Chapter 4

Revisiting NIRS-BCI Assumptions

In the previous chapters, we have established that fNIRS is capable of detecting consistent and volitional patterns of hemodynamic activity associated with different mental tasks. The measurement of brain activity, as related to hemodynamic trends, has stemmed from insights gained from functional magnetic resonance imaging (fMRI) (Bandettini *et al.*, 1992; Ogawa & Lee, 1990). Previous research in fMRI has proven invaluable in the establishment of experimental protocols in fNIRS-BCI development. This chapter will outline this research and will examine shortcomings and avenues for improvement within these established protocols. To this end a small fMRI study is presented, along with reviews of associated literature, to assess the validity of the assumptions in task selection and protocol design. Specifically we will focus on motor cortex tasks and ascertain their effectiveness within an fNIRS-BCI paradigm.

Many NIRS-BCI research groups focus on the use of motor activity as mental tasks (Coyle, 2005; Ranganatha *et al.*, 2007; Soraghan, 2010; Ward *et al.*, 2007). As described in Chapter 2 the motor cortex, posterior to the frontal lobe, is responsible for motor control. Motor tasks are common in most BCI research due to the intuitive nature

of task instructions and because detected responses are repeatable and consistent in both character and location (Allison *et al.*, 2000). Motor activity is still considered an applicable mental activity even when the motor cortex has been damaged (Cao *et al.*, 1998). This following experiment allows the investigation of cerebral locations of activation, activation separability and the effect of using imagined versus overt motor movement on the response intensity (Ersland *et al.*, 1996).

4.1 Experimental Design

4.1.1 Motivation

There have been a number of concurrent NIRS fMRI studies performed to establish the correlation between the two modalities (Strangman *et al.*, 2002b; Toronov *et al.*, 2001). Using this correlation a small study was conducted to examine the assumptions established regarding motor tasks in NIRS-BCI paradigms. These assumptions encompass the location of activities, the particular motor task detectable using NIRS and the validity of overt versus imagined movement. We also make direct measurements of inter-subject variability (ISV) of activity locations on the subjects within this study.

4.1.2 Protocol

The protocol for the MRI experiment was designed to elicit separable activations from different areas along the motor strip. With this in mind four motor tasks were chosen.

- Left Hand

- Right Hand

- Both Feet

- Tongue

Each task was to be performed both overtly and imagined. This will allow the examination of the difference between overt and imagined paradigms.

These experiments were performed in a Siemens Allegra scanner with a magnetic field strength of 3T. Behind the chamber a projector displayed the cues which can be observed by the subject via a mirror mounted on the head transmit coil. To ensure adequate time separation of each activation, each cue was displayed for 16s followed by rest periods of 30 seconds (Soraghan, 2010). The protocol was created and displayed using PyEPL (Geller *et al.*, 2007), a python based experiment design software. Each task was repeated eight times and tasks were presented in a random order.

Following the functional scans a T1-weighted 32 slice axial and a T1-weighted MP-RAGE structural scans were performed. These scans are performed to provide anatomical structure images upon which the functional scans are overlaid. In post processing the functional images are registered to the 32 slice axial scan which share similar spatial resolution. This represents a intermediate step to allow accuracy when the functional images are finally overlaid on the high resolution MP-RAGE.

The full experimental protocol was as follows:

- **Subjects**: Two healthy male subjects with an average age of 25. Both subjects were right handed according to the Edinburgh Handedness Inventory (Oldfield, 1971).

- **Preparation**: Subjects were placed in the scanner in a supine position. The head transmit coil was placed over their heads and the mirror was positioned so they could best see the cues being projected behind them.

- **Guidance**: Each subject was briefed on the cues they would receive prior to the experiment. The experiment began when the subject was placed in the chamber and could see the screen. The cues started with "The experiment begins shortly..." then after a short time a "Get Ready..." instruction was supplied. The stimulus

instructions were:

1. Overt Right Hand

2. Overt Left Hand

3. Overt Both Feet

4. Overt Tongue

5. Imagery Right Hand

6. Imagery Left Hand

7. Imagery Both Feet

8. Imagery Tongue

Between each stimulus a rest period was signaled using " +" symbol on the screen. Within an fMRI experiment these stimulus instructions are referred to as experimental variables (EVs).

Figure 4.1: fMRI protocol Diagram

- **Timing**: Each stimulus was presented in 8 blocks, each block consisting of 16 seconds for the cue and the rest period for 30 seconds. The order of the presented stimulus was randomized to avoid habituation (Dale, 1999).
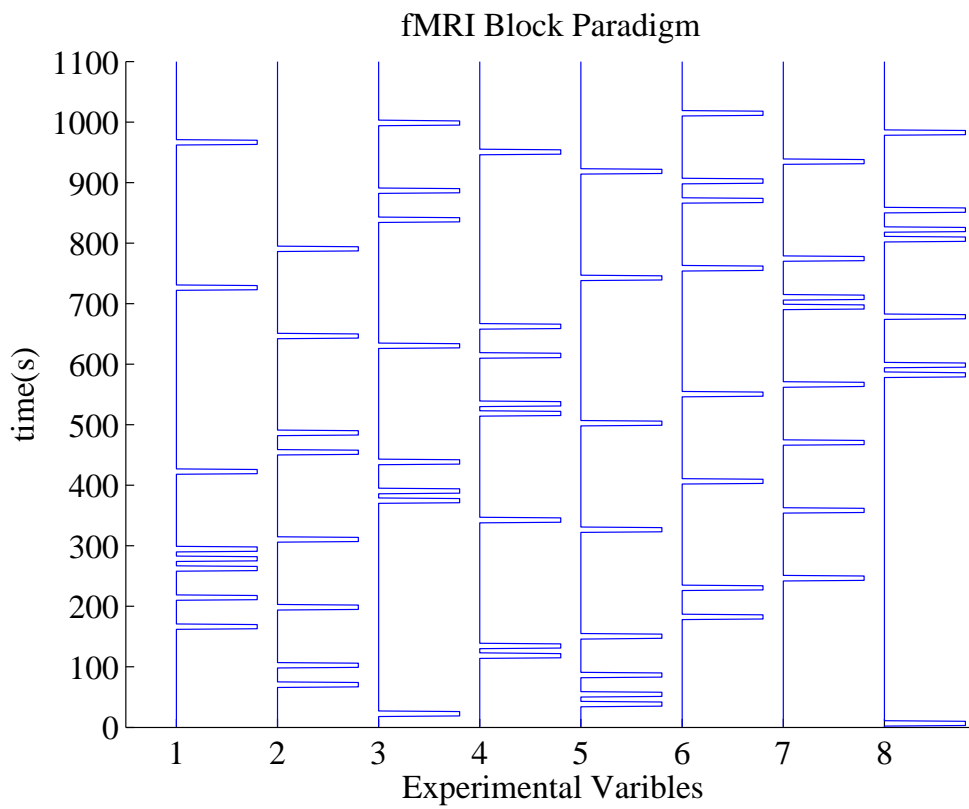
Figure 4.2: fMRI protocol Diagram.Each column displays the block onsets of an EV. The numbers assigned to each column correspond to the EV listed in the experimental protocol (Section 4.1.2)

4.2 fMRI Post-Processing

Upon completion of these trials, the functional data was processed using the software FSL (Smith *et al.*, 2004; Woolrich *et al.*, 2009). To ascertain which areas of the brain were most active during the course of each stimulus, the design of the experimental protocol was used to generate a general linear model (GLM) of the data. In further discussion of this analysis the smallest three dimensional area the scanner can distinguish is referred to a volumetric pixel or a voxel. The results are analyzed using a general linear model.

4.2.1 General Lineal Models

A general linear model (GLM) is a statistical analysis method for univariate data (Mardia *et al.*, 1979). They facilitate a series statistical tests and hypothesis testing according to pre-defined models of data variation. They are formulated as follows

$$Y = XA + E \tag{4.1}$$

where Y is the recorded data, X is a design matrix describing the expected results, A is the parameters to be estimated and E is the error or noise in the system. The model parameters A are estimated using linear regression and the resultant model XA is statistically compared to Y.

4.2.2 GLM applied to fMRI

Applying this analysis to fMRI data allows the statistical analysis of functional activation. The analysis is often referred to as statistical parametric mapping (SPM) (Friston *et al.*, 1995).

To perform this analysis, firstly, the timings of the stimulus onsets are gathered from the experimental control system. Each EV has a stimulus train generated from

these timings. To adequately model the expected responses of the data a representative hemodynamic response function (HRF) is chosen. This analysis uses the probability density function from a gamma distribution as descriptive of an HRF (Ciuciu *et al.*, 2003; Rajapakse *et al.*, 1998). The point processes associated with each EV's onset timings are convolved with this HRF to produce the GLM design matrix. Figure 4.3 shows the design matrix of the model where each column is representative of an EV. The column numbers match the numbered EVs listed in Section 4.1.2.
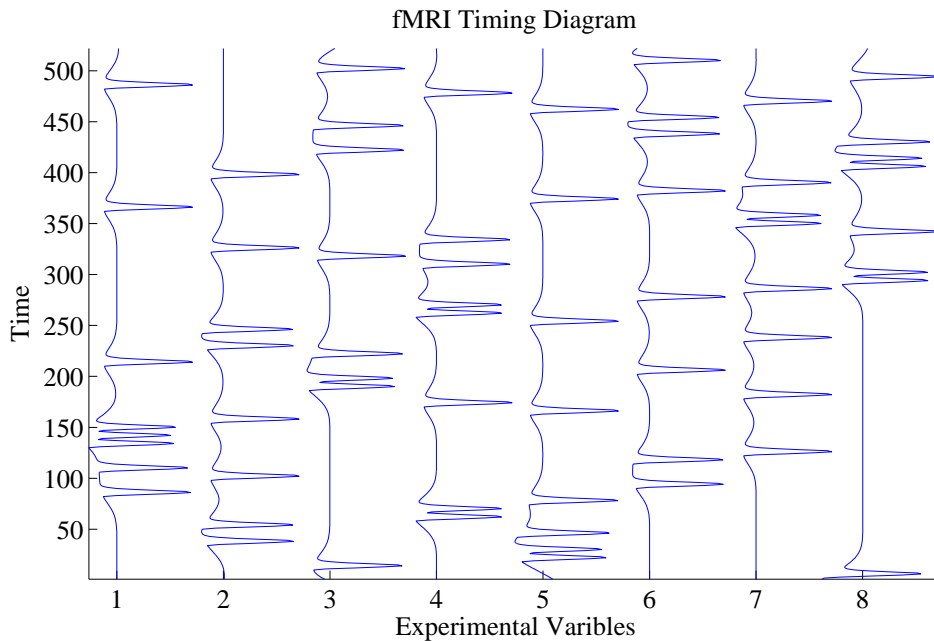
Figure 4.3: GLM Design Matrix. The numbers assigned to each column correspond to the EV listed in the experimental protocol (Section 4.1.2)

A linear regression is performed between the design matrix and the recorded data. For every voxel a parameter estimate (PE) value is returned relating to every EV indicating the 'goodness' of the fit along with an error measure.

4.2.3 Statistical Mapping

To create statistical maps on fMRI image data, it is first necessary to apply a set of statistical measures onto the PE from the GLM. The PE is divided by the error to give a t value indicating the significance of the the fit for that voxel. The t value along with PE and the error are then used to calculate a Z statistic for each EV against each voxel. A Z-test is a statistical test that compares sample and population means to determine if there is a significant difference. The Z-test only requires that the population have a normal distribution which we can assume in this case using the central limit theorem (Billingsley, 2008) and that the mean of the population is known.

The Z-test unit is the number of standard deviations the particular sample is from the mean of the population. Applying this analysis on the PEs and errors across all voxels it is possible to generate a statistical measure of the location of activations. To generate images of these statistical maps a lower bound is set on the Z-statistic for a particular EV. Voxels with values above this threshold are marked as active.

When analyzing information from time-series data the figures in further sections overlay a partial model of the response data. These partial models represent only the predicted response of a single EV and are useful for the purposes of visually highlighting correlations in time-series data.

4.3 Experimental Results

The results obtained from this statistical processing of the experimental data are presented here. Z-statistics are thresholded and adjacent active voxels are clustered for analysis.

4.3.1 Functional Activations

From the processed data there is discernible activation in particular regions along the cortex. The data from the post statistical processing generates clusters of active voxels. These are listed in order of size. The largest cluster is the area of greatest activation during a particular EV.

In both subjects, the cluster locations are mapped to the standard brain map supplied by FSL. These active regions lie generally along a region posterior to the frontal lobe or Brodmann's Area 4. This area is generally believed to hold the primary motor cortex (Brodmann, 1994; Macdonell *et al.*, 1999; Mazziotta *et al.*, 1995).

EV	Vox. per Cluster	Z-Max	Z-Max Location (Voxel Space)		
			X	Y	Z
Overt Feet	370	20.1	33	36	28
Overt Left Hand	412	12.2	46	37	21
Overt Right Hand	303	19.2	42	37	23
Overt Tongue	278	18.1	45	32	17
Imagined Feet	336	15.1	33	35	28
Imagined Left Hand	3827	20.1	33	36	28
Imagined Right Hand	283	10.8	37	37	28
Imagined Tongue	54	8.42	33	35	28

Table 4.1: List of largest clusters for each EV. Z-Max is the largest Z value in the cluster. The last three are the XYZ location of the voxel with the largest Z value.

Table 4.1, shows an example of the data from the largest clusters of voxels associated with each EV for Subject One. Table 4.1 also shows the largest Z statistic within the voxel cluster and the 3D coordinates location of that voxel.

Figure 4.4 shows two time series plots of the fMRI data from Subject 1. The first is
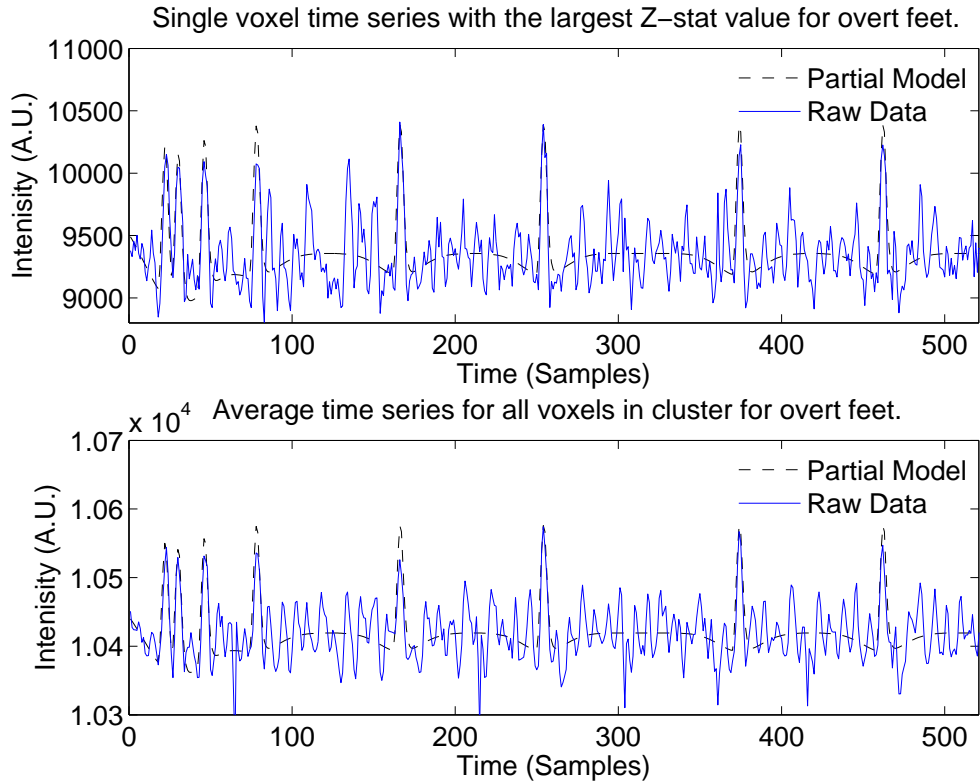
Figure 4.4: fMRI time-series data associated with overt both feet activation from Subject 1 with a partial model overlayed

the time series recorded from a single voxel with the highest Z statistic in the cluster. The second is the averaged time series from all the voxels in the cluster. Both series are overlayed with a an activation model for a single EV (Overt Both Feet) which is referred to as a partial model.

4.3.2 Activation Locations

As discussed in the last section, functional activation is statistically derived in voxel clusters for each EV. These voxel clusters are registered to the structural brain images and then rendered into viewable images. Figures 4.5 and 4.6 show the registered images in slices for the four overt activation types for subject one. From left to right the images

are presented from the coronal, transverse and sagittal planes respectively. From a first viewing these areas seem to align with the motor strip (Rao *et al.*, 1993).

(a) Overt Both Feet   (b) Overt Left Hand
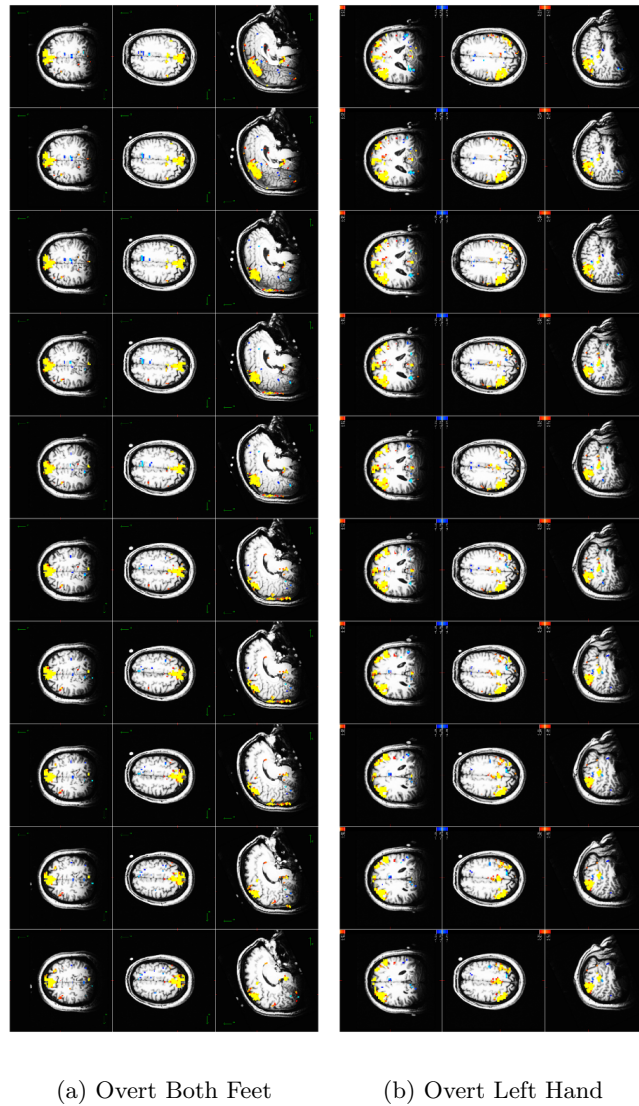
Figure 4.5: fMRI activation clusters for four stimulus types

As can be seen from figure 4.5b and 4.6b both the left hand and the tongue have elicited bi-lateral activation. While non-problematic for the tongue, this bi-lateral activation make separation and differentiation of left and right hand activation difficult
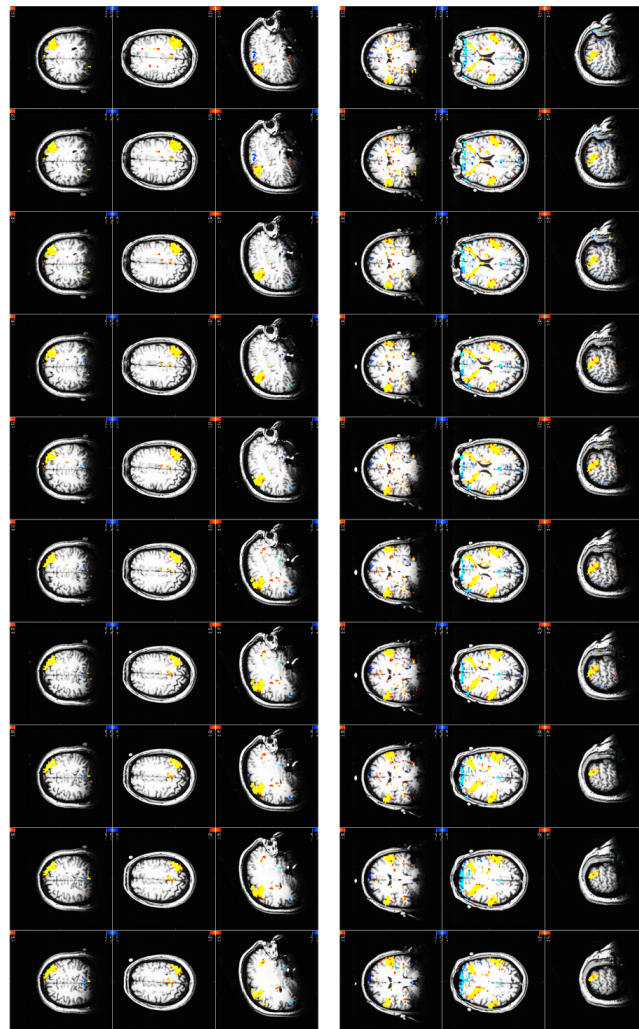
(a) Overt Right Hand   (b) Overt Tongue

Figure 4.6: fMRI activation clusters for four stimulus types

(Kim *et al.*, 1993). There is a clear intensity difference between hemispheres for left hand activation. The more intense cluster on the right hemisphere is the left hand control area in accordance with the literature (Strick & Preston, 1982).

Next we will examine in detail the locations of each activation

4.3.2.1 Activation Area: Feet

Using a registration of a standard brain image it is possible to accurately map the functional areas to documented locations. Figure 4.7 is a 3D mapping of the functional voxel clusters for the feet activation. From the image it is possible to see the activation centered to the top of the brain in the pre-frontal area. The activation itself spreads out in both hemispheres and there is a quantity of activity on the surface.However, both subjects showed that the largest concentration of hemodynamic activity during feet activation was deeper in the cortex than in hand activation.
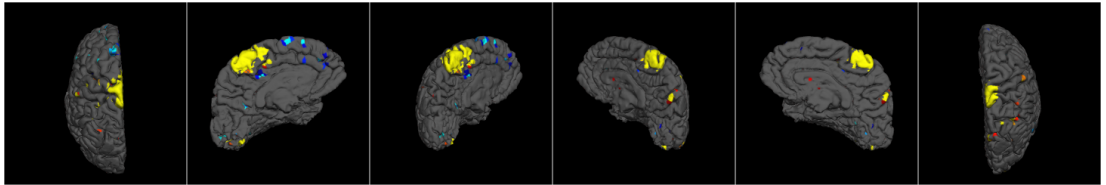
Figure 4.7: 3D mapping of images for surface correlation: feet overt

4.3.2.2 Activation Area: Left Hand

The left hand activation seen in Figure 4.8 is strongest in the right hemisphere in accordance with the contralateral nature of brain activity. There is however quite a significant activation of the left hemisphere. This is indicative of the occasional bilateral activation mentioned in Chapter 2 (Cramer *et al.*, 1999). This activation also occurs quite close to the surface of the cortex.
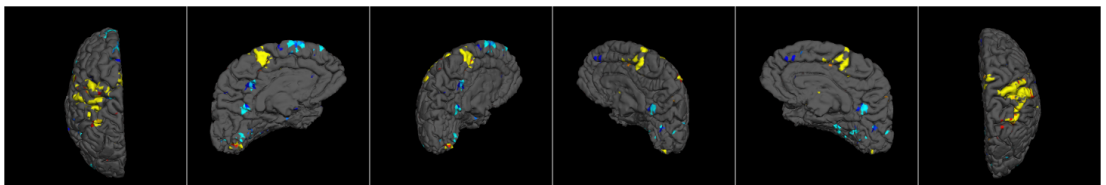
Figure 4.8: 3D mapping of images for surface correlation: left hand overt

4.3.2.3   Activation Area: Right Hand

Figure 4.9 is an example of the mapping for the right hand activation. The right hand activation is more substantial for both subject's than the left, perhaps due to it being the subjects dominant hand. The right hand activation, unlike the left, elicits almost no bilateral activation for both subjects which correlates with studies of hemispheric asymmetry (Kim *et al.*, 1993).
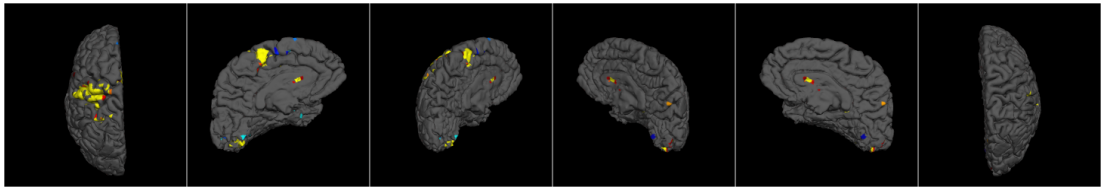
Figure 4.9: 3D mapping of images for surface correlation: right hand overt

4.3.2.4   Activation Area: Tongue

In figure 4.10 the activation of the tongue activation is mapped onto the white matter. Unlike the previous images which showed the surface pial matter the tongue is generally much deeper and bilateral. This presents difficulty in using the tongue within a NIRS paradigm due to the depth of the activation.
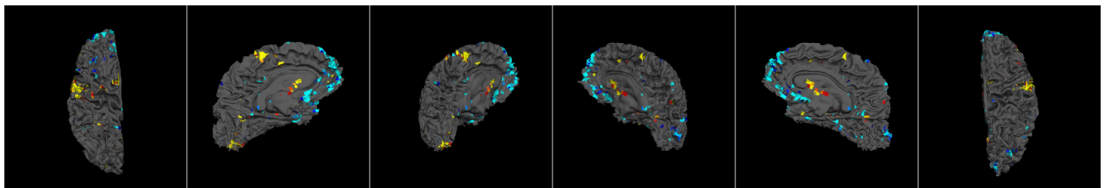
Figure 4.10: 3D mapping of images for surface correlation: tongue overt

4.3.3   Cortex Depth

To ascertain the depth at which these activations occur within the cortex we use Figure 4.11 which is an activation map rendered with skin and scalp components. The feet

activation (Figure 4.11a) can be seen as a wide cluster spread just against the skull in the central region of the cortex although the most active regions within the feet clusters are a few cm below the surface of the cortex.

(a) Overt Both Feet   (b) Overt Left Hand

(c) Overt Right Hand   (d) Overt Tongue
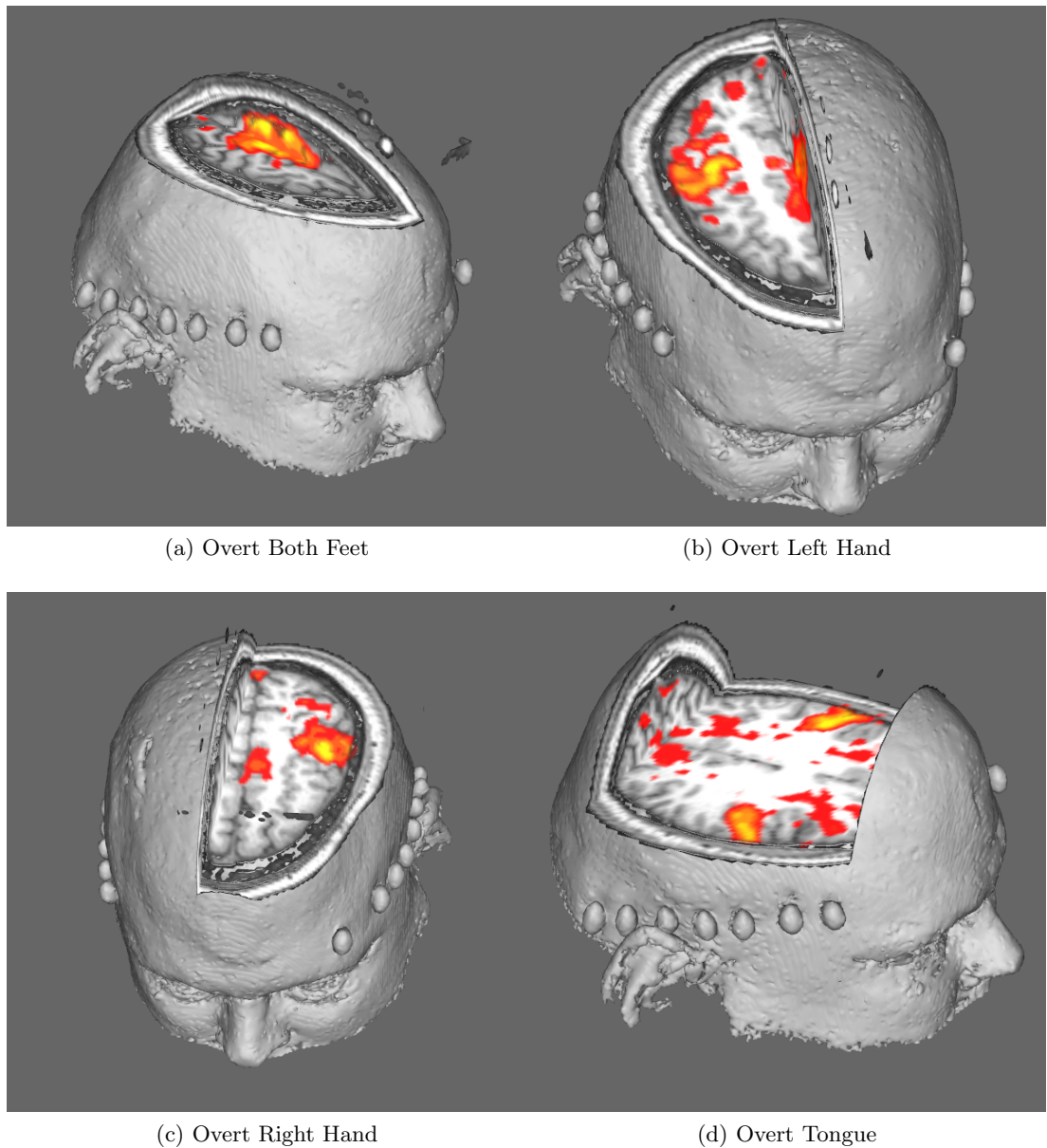
Figure 4.11: 3D mapping of images for surface correlation

Both hand activations, seen in Figure 4.11b & 4.11c, also spread out across the skull.

These wide activation patterns are indicative of a signal reachable and detectable using NIRS (Okada & Delpy, 2003). The tongue activation, seen in Figure 4.11d, however has a much narrower skull contact indicating it may be more difficult to detect reliably.

4.3.4 Locational Impact for NIRS

As mentioned in the previous section this location information is valuable for the creation of NIRS-BCI experimental protocols. First, the choice of optode locations can be challenging without some other measure like fMRI data. Second, it is possible now to make distinctions into which activation types are applicable to NIRS studies.

As we showed in Section 4.3.3 the tongue activation, while significant, has quite a narrow point of contact with the skull. The peak of the tongue activation also occurs much deeper into the cortex than other activation types. This makes it undesirable as part of a NIRS-BCI.

4.3.5 Inter-subject Variability

With this fMRI data it is possible to analyze the differences in the locations of activation between the two subjects. This allows a clearer idea of how optode positions may change on a subject-by-subject basis.

When positioning fNIRS sources and detectors the locations C3 and C4 from the 10–20 electrode placement system are used as a guide for the hands area of the primary motor cortex (Coyle, 2005). Hand activations for both subjects produced responces in the vicinity of these locations though the differences between the locations of strongest activation could differ by up to 2cm. The areas most active during hand movement in subject one was slightly posterior to C3 and C4, where as, it was slightly anterior in subject two.

Although this small difference is unlikely to cause an issue within fMRI studies it presents serious issues in single-channel fNRIS systems. The only option avail-

able to maximize signal strength of such a system is a trial and error approach to source/decetor placement (Coyle, 2005). This alone highlights the necessity of multi-channel approaches for fNIRS.

4.3.6 Overt & Imagined Motor Movement

Using imagined movement paradigms are common in the BCI community. It is therefore worth investigating the differences in the activation strengths and locations during both overt and imagined trials.

Activations	Num voxels	mean	median	max	Voxel X	Voxel Y	Voxel Z
IBF	802	2.64	2.46	14.11	33	36	28
OBF	802	6.76	5.71	20.14	33	36	28
ILH	1258	2.57	2.26	10.28	31	32	27
OLH	1258	6.91	6.03	19.86	21	36	25
IRH	797	3.38	3.2	10.77	37	37	28
ILH	797	6.34	5.51	19.22	42	37	23
IT	1625	1.6	1.39	8.42	33	35	28
OT	1625	6.06	5.42	18.13	45	32	17

Table 4.2: Comparison of overt and imagined activations. Largest voxel cluster for each activation along with the number of voxels in the cluster, mean, median, and max Z value and the location of the voxel with the largest Z within the cluster.

Table 4.2 is a collection of statistics comparing the overt and imagined activations over specific areas. The areas chosen were masks of the entire region of voxels that are thresholded as active areas for these EVs. The table reports the max, mean and median of the averaged Z-statistics across that area for each EV.

The table clearly demonstrates that in all cases the imagined activations are weaker than the overt. For further comparison, Figure 4.12 shows the same time series as Figure 4.4 but in this image the partial model for the imagined activations has been overlayed also. This location was the source of the largest activation for overt feet movement.

The imagined activity, although present, is clearly of a lower intensity than the overt.
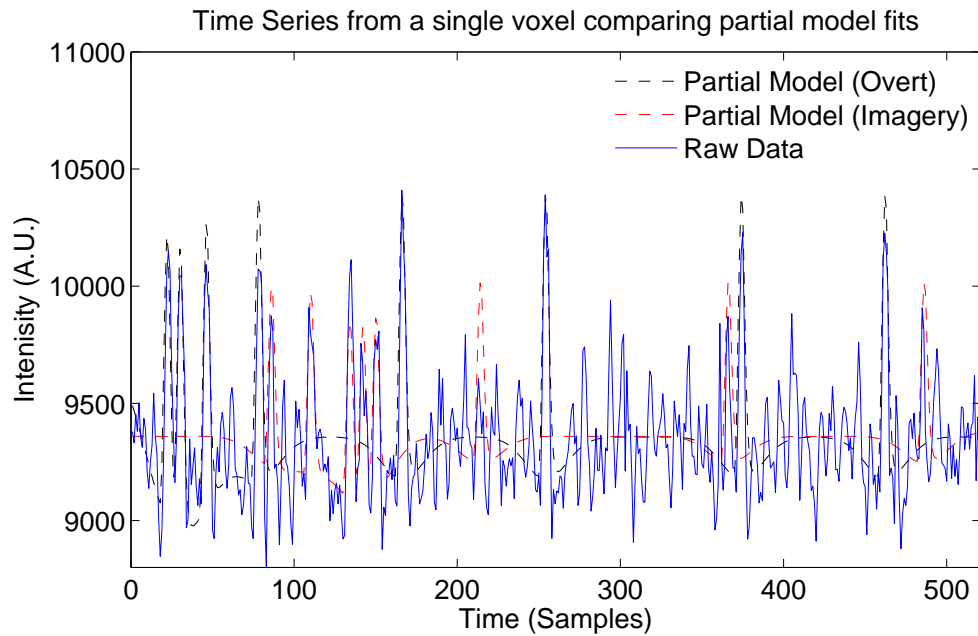
Figure 4.12: Raw Time Series Data overlayed with the cope models for overt and imagined foot movement

This will allow us to compare the similar recordings with NIRS and overt movement can be used as a testing and validation for able bodied subjects. Imagined movement will prove difficult to extract in a single-trial paradigm but methods of consistant detection via NIRS would be a significant achievement of any bespoke NIRS-BCI.

4.4 Conclusions

We have seen that a hemodynamic distinction is possible between different types of motor activity, namely left and right hands but there is symmetric hemispheric activity which make the distinction difficult. This is reflected in Haihong & Cuntai (2006) and Ranganatha *et al.* (2007). Although, consistent discrimination of these activations will allow an increase in bit rates in a NIRS-BCI by increasing the number of experimental cues or creating multi-selection options for users. Both tongue and feet present some difficulties due to their activation location and depth on the cortex.

This study indicates that for long-term fNIRS study of a single subject a preliminary fMRI study is advantageous. If this is unfeasible, multi-channel fNIRS is shown to be a necessity to locate the areas of highest activity.

In the following chapters we outline the development of a customizable multi-channel fNIRS system specifically directed at BCI applications. Chapter 7 outline systems similar to the GLM for detecting the most active channels for single trial experiments.

Chapter 5

Customized, Versatile Multi-channel Real-time CWNIRS Hardware Design

To achieve the aim of improving fNIRS-BCI approaches and implementations we first outline a new custom-built hardware system capable of facilitating these improvements. Chapter 3 highlights the importance of customizable systems while Chapter 4 exposes the necessity of multi-channel systems to realize the best results from fNIRS as a BCI modality. This chapter will detail the work done in parallel with this research by Soraghan, Matthews, Markham, Pearlmutter & Ward (2010). We will outline the design and creation of a highly customizable, multi-channel CWNIRS system for BCI applications.

5.1 Introduction

The first fNIRS-BCI implementation was designed by Coyle (2005). It was a custom-made, continuous wave fNIRS-BCI. The system is composed of two lock-in amplifiers

(Ametek 7265), two avalanche photodiodes (APD, Hamamatsu C5460-01), two fiber optic bundles, an LED driver driving four, single wavelength LEDs (760 nm*2, and 880 nm*2, Opto Diode Corp.), and function generators. Coyle *et al.* (2004a) used a 16-bit Keithley digital-to-analog converter PCMCIA card as a data acquisition module, sampling four output channels from the lock-in amplifiers (which demodulated the detectors). An illustration of that system is shown in Figure 5.1.
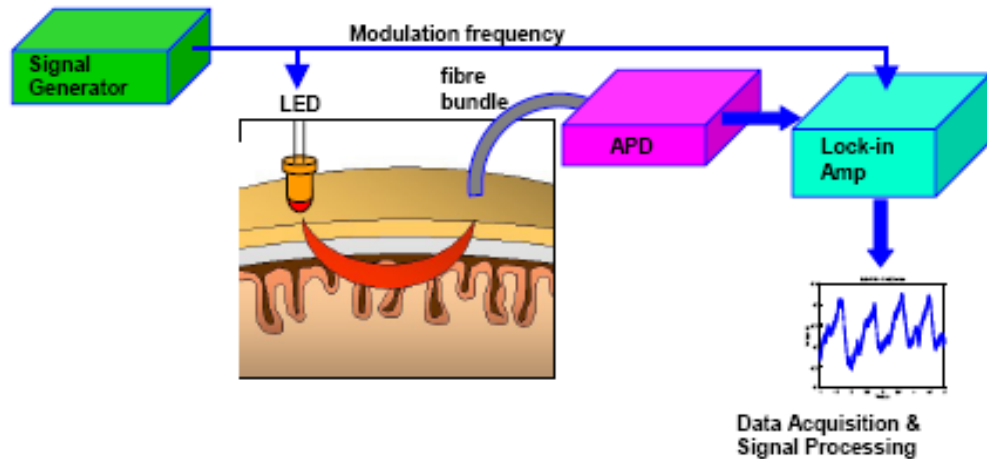
Figure 5.1: Components of the NIRS-BCI developed by Coyle (2005)

This system was expanded upon by Soraghan *et al.* (2006) who added two further acquisition systems for applications in simple gaming and for conceptualizing a novel NIRS-BCI application in stroke rehabilitation (Ward *et al.*, 2007). These extra acquisition systems allowed the interfacing of external devices to provide subject feedback and interaction. Published descriptions of fNIRS-BCI provide an exposition of the systems and their applications (Coyle *et al.*, 2004a,b, 2007; Soraghan *et al.*, 2006).

In extending this work it became necessary to design a new hardware system that can incorporate new approaches at every point in the data processing chain. With the advances in semi-conductor production the facilities exist to customize and optimize NIRS systems for particular applications (Wolf *et al.*, 2007). It is possible to charac-

terize different NIRS hardware systems using criteria like light source type, wavelength selection, light detection systems and processing/feedback systems (Strangman *et al.*, 2002a).

The system described here was designed as a modular and versatile platform to quickly prototype and test solutions to many different aspects of NIRS-BCI. These include signal conditioning, acquisition and generation, physiological noise analysis, and classification. For a detailed exposition of the hardware specifications and design please refer to Soraghan (2010). What follows is a concise description of the instrument as it pertains to the rest of the dissertation.

5.2 Hardware Summary

Initially, the hardware necessary perform fNIRS must be specified. Figure 5.2 shows a block diagram of the major components.
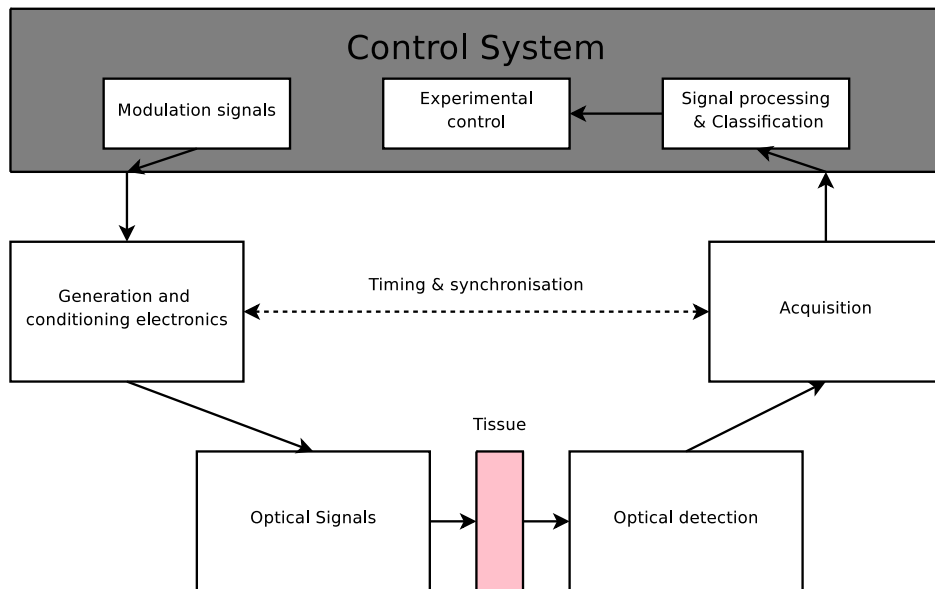
Figure 5.2: Block diagram of General NIRS system design

The initial advancement from the design of Coyle *et al.* (2004a) was to develop

a scalable, multi-channel NIRS platform. Whereas, the original system was a dual channel system using hardware-based lock-in amplifiers for demodulation of detector outputs, this new design was based on a more flexible software-based modulation-demodulation system, inspired by the work of Everdell *et al.* (2005). Thus, the new system was initially designed to use multiple carrier frequencies to modulate the optical sources. This required equipment with generation and acquisition rates as well and a powerful central processing unit to coordinate data timing, synchronization, and triggering.

In the following sections, the system components illustrated in Figure 5.2 are described, including the optical light source and detection equipment, specified to maximize the detection of oxy-hemoglobin (ΔHbO_2) and deoxy-hemoglobin (ΔHbR) concentration changes.

5.3 Generation and Acquisition Systems

5.3.1 Specification

In order to maximize the number of sources and detectors that could be implemented in a frequency based modulation strategy, the acquisition and generation hardware has a number of constraints. The modulation system envisioned would be capable of generating carrier signals (sinusoidal). The previous implementation of Coyle *et al.* (2004a) used modulation frequencies up to 20kHz and demodulation via lock-in amplifiers. This upper limit was deemed to be appropriate for further advancement. For the acquisition, The Nyquist-Shannon sampling theorm would require acquisition rates of at least twice that of the highest generated frequency (Shannon, 1949). To ensure as little noise be introduced due to poor signal acquisition resolution the requirement for acquisition was set at ten times the highest frequency. Thus, a 200kHz acquisition rate system was desired to allow sufficient reconstruction of these sinusoidal signals.

5.3.1.1 Generation Requirements

- Sine wave generation.

- Generation frequencies up to 20kHz.

- Multiple generation channels.

5.3.1.2 Acquisition Requirements

- Acquisition rates of 200kHz;

- Multiple input channels.

- Simultaneous sampling on all channels without reduction of acquisition rates.

- On-board analog anti-aliasing filters and amplifiers.

5.3.2 Design Choices

A National Instruments (NI) solution for data processing was chosen. The selection ensured simplified, robust timing interactions between generation and acquisition cards and allowed central control of both, through a single workstation running Labview.

The generation and acquisition cards chosen are housed in a proprietary NI interface chassis (PXI-1033). This chassis connects to a Workstation via a PCI-express card in the Workstation. Timing and synchronization is ensured by having a 10MHz clock shared between the cards on the chassis backpane, with communication via the real-time system integration (RTSI) bus.

5.3.2.1 Generation Card

The PXI-6723 is a multi-function digital-to-analog converter (DAC). It provides 32 analog output (AO) channels (13-bit), with signal generation up to 800kS/s. For the 24 AO channels needed to drive the LEDs, a 60kS/s rate is achievable. The generation

card is coupled to the LED driver (for optical sources power and stability) via BNC cables, and two breakout boxes. The high power required for the LED sources are provided by axillary power supplies, rather than by the DAC card.

5.3.2.2   Acquisition Card

Acquisition is handled using two PXI-4462 cards. Each unit has four channels, capable of simultaneously sampling at 204.8kHz. This is a key feature of the CWNIRS system to ensure scalability without a reduction in sampling rate as the number of channels increase. The modules have analog filters for anti-aliasing, along with analog amplifiers to maximize the use of the 24-bits available .

5.4 Optical sources and Signal Conditioning

Optical source selection was governed by a number of factors. Optical sources for NIRS applications can include laser diodes or light emitting diodes (LEDs) (Strangman *et al.*, 2002a). Laser diodes have the advantage of producing energy that is effectively monochromatic and spatially coherent. This allows much higher powers and translates to higher signal-to-noise for NIRS applications. Nevertheless, the main drawback of laser diodes is that of safety (Sliney & Wolbarsht, 1980). The power and coherence of the energy produced is capable of causing damage, especially to the eye. This issue has moved a number of NIRS research away from lasers, especially in the area of neonatal investigation (Bozkurt & Onaral, 2004).

LEDs do not suffer from the same safety issues as laser diodes and are cheaper to produce (Soraghan *et al.*, 2008b). LEDs are lower in power though and the wavelengths produced are spread around the central wavelength (broadband). Given the cost and safety issues it was decided to use LEDs in this design. Moreover, LEDs can be placed in direct contact with the scalp and multiple wavelengths can be housed within the same package (Soraghan *et al.*, 2009b).

Another factor, wavelength selection, is crucial to the correct conversion of the recorded light levels to changes in HbR and HbO (Uludag *et al.*, 2004). As mentioned in Chapter 3 wavelength of light chosen to best resolve both chromophores are either side of the isosbestic point (Figure 5.3).

In the case of ΔHbO_2 & ΔHbR wavelengths should be chosen either side of 800nm in order to allow for spectroscopic determination of both. The choice of wavelength is bounded to between a large optical absorption of hemoglobin around 650nm and that of water at 950nm. The wavelengths chosen in this system were 760nm and 880nm. A more detailed discussion of wavelength selection can be found in Sato *et al.* (2004) and Okui & Okada (2005).
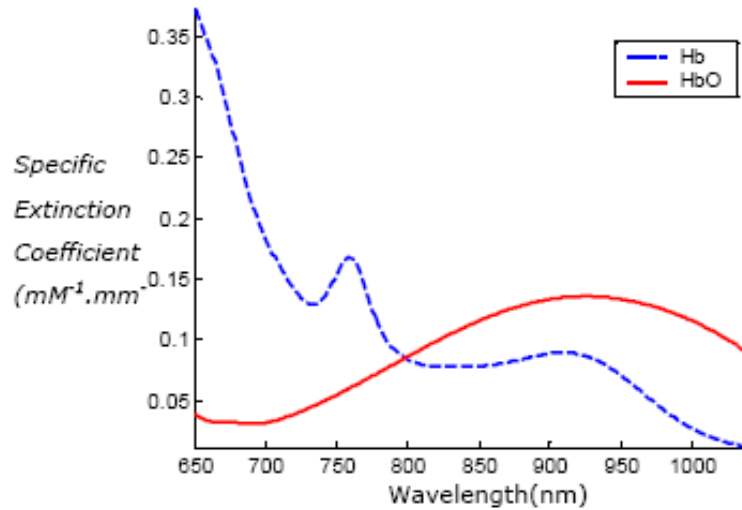
Figure 5.3: Wavelength dependent changes in the absorption properties of HbO_2 and HbR. Figure reproduced from Coyle (2005)

5.4.1   Optical Current-Driving Circuitry

The light sources specified above are current driven devices and the current is proportional to their optical output power. The system must be able to control and modulate these LEDs at specific frequencies. Given that the signal generation cards generate varying voltages, a linear relationship between the potentials generated and the current supplied to the LEDs must be ensured.

Although this is a common problem in electronics containing LEDs it is made increasingly complex in this case because of a number of factors. These additional constraints are that the system must allow modulation from DC (for time-division multiplexing) to several kHz, and that the LED packages contain numerous dies all on a common anode.

Hence, a new driver was designed to cater for these constraints. This driver uses PNP transistors for current amplification, and uses differential operational amplifiers (op-amps) to detect the voltage drop across the current-limiting resistors for the LEDs. Negative feedback of these signals ensures stability and linearity in the optical output
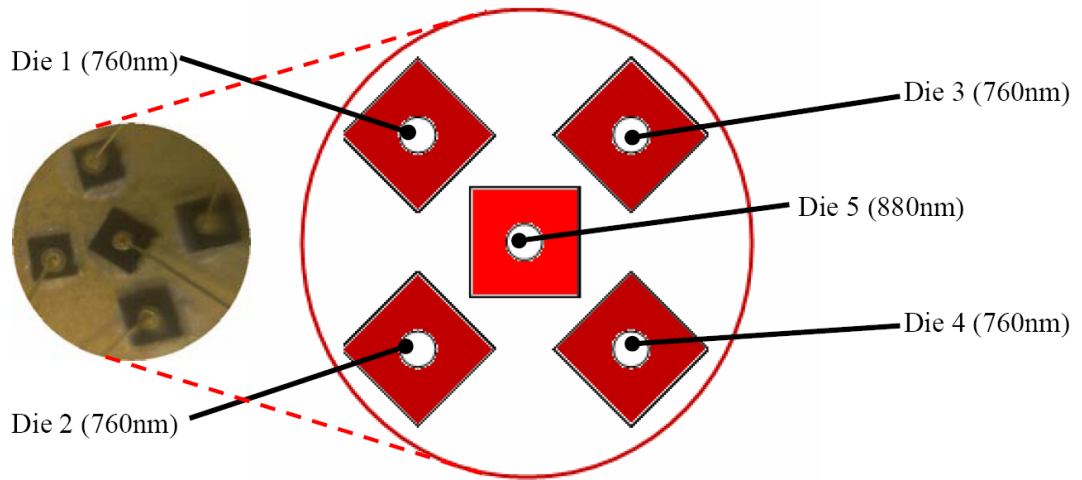
Figure 5.4: LED Die configuration. (Image courtesy of Soraghan (2010))

of the LEDs (Soraghan *et al.*, 2009b).

5.4.2 Customized Optical Sources

Optical sources were custom design for this project to ensure the correct specification. Previous prototypes used separate LEDs for each wavelength but this proved difficult in coupling to the subject (Coyle, 2005) and introduced some potential error. A specification for dual wavelength LEDs was submitted to Opto Diode Corporation. The resulting design was a single LED package containing five dies. In practice, 760nm dies have lower output powers and are more highly absorbed in the tissue than 880nm. To solve this problem four of the five dies in the LED package are at 760nm (see Figure 5.4). This is especially important as 760nm is pivotal in the detection of concentration changes of ΔHbR (more sensitive) which is a better localizer for metabolically active tissue (compared to ΔHbO_2) (Hirth *et al.*, 1996).

The final LED design (OD-1894) is contained in a TO-39 header with a lensed cap. It has five leads (4 + 1) with a common anode for all dies. The lens cap ensures a 10° beam angle. The output of the 760nm dies are ±10nm with a 30nm full width
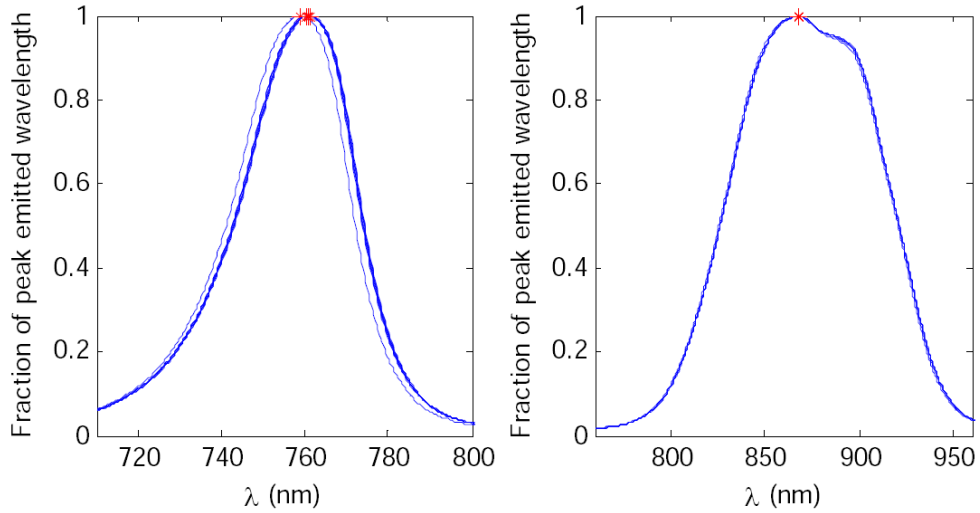
Figure 5.5: Spectrometer recording for LEDs wavelength spread. 760nm and 880nm respectively. (Image courtesy of Soraghan (2010))

half maximum (FWHM), with 40mW ±10mW optical output power (note: this power incorporates all four 760nm die in the P-1894 package). The single 880nm die is also ±10nm with a 80nm FWHM, but with an optical output power of 13mW ±1mW. Figure 5.5 shows spectrometer recordings of both LEDS, where the wavelength spread of each LED can be observed. The shoulder to the right of the central peak in the 880 recordings is from limitations in the manufacturing process and has been observed in other optical sources from the same company (Soraghan, 2010).

5.5 Light Detection

5.5.1 Specification

As discussed in Chapter 3 there is significant attenuation (7–9 orders of magnitude) of the optical power by the tissue traversed. With this in mind, the choice of optical detector is limited to highly sensitive devices. It must also be capable of detecting optical energy in the NIR range and have appropriate response characteristics in line

with a CWNIRS system.

The choices in this area are varied (Strangman *et al.*, 2002a) but can be narrowed according to sensitivity, operating voltages, active area, optical coupling, size, etc. A high-sensitive, low noise, avalanche photodiode (APD) detector was the solution of choice, as it is for many NIRS systems (Boas *et al.*, 2004).

5.5.2   Avalanche Photodiodes

The choice made for this experimental system was Avalanche photodiodes (APDs), specifically the Hamamatsu Photonics, C5460-01 module. This device has a wavelength range between 400nm and 1000nm, high sensitivity of $-1.5 \times 10^8 V/W$, and a 3mm diameter active area. This APD has a detection bandwidth from DC to 100kHz and can detect optical energy as low as 0.005nW.

This satisfies many of the conditions necessary for the optical detection in this NIRS system. This equipment was mounted in a die-case enclosure and coupled to a 610mm fiber-optic bundle using a custom-design connector to maximize light transport to the active area (Soraghan, 2010, Chapter 5). The fiber-optic bundles are then connected to a subject using a source-detector probe holder, which is described next.

5.6   Source-Detector Coupling & Configuration

5.6.1   Specification

The method of coupling the optical components to a subject presents a number of issues. Intuitive solutions like helmets or solid mounting systems do not provide the kind of versatility required for these experiments. The holders need to be easily movable and flexible to suit various head shapes. It is also necessary that they not cover too much area, which can make hair parting difficult. This is needed to expose sufficient naked scalp for the sources and detectors, since hair (and hair follicles) are a significant

absorber of NIR light.

5.6.2   Configurations

Each holder was created using brass tubing to hold LEDS and detector fibers semi-rigidly in place. These were soldered on to thin brass sheets which were cut to remove anything structurally unnecessary to maintain flexibility. This was then glued (hot-melt) into felt for the comfort of the subject.The final result is a semi-rigid structure with a soft underside that could deform sufficiently to suit various head shapes.
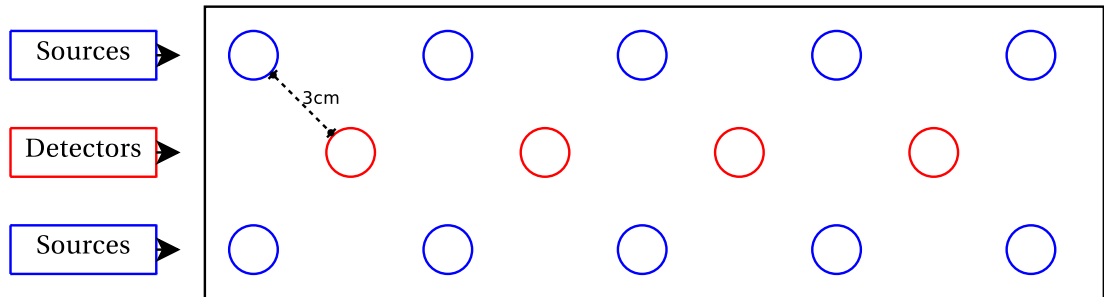
Figure 5.6: Optet Configuration for Frontal Studies

The configuration of the optode holders was dependent on the location of the recording on the head and the size of the area of scalp being investigated. Figure 5.6 shows the design of a holder typically used for investigating metabolic activity in the frontal cortex. It is narrow and long in order to fit the forehead comfortably.

Figure 5.7 depicts an early probe holder design used to cover semi-circular areas of motor cortex. It covers a small area but can facilitate up to seven light sources and a single detector.

The final design (shown in Figure 5.8) covers a large area and was designed to be used for interrogating the motor areas and is an excellent option when attempting to locate a metabolically active area. In this design, each detector can see four sources. Note: non-neighboring light sources (< 3cm apart) in this probe holder are deemed too distant to provide sufficient signal for this detection system, due to the high scattering
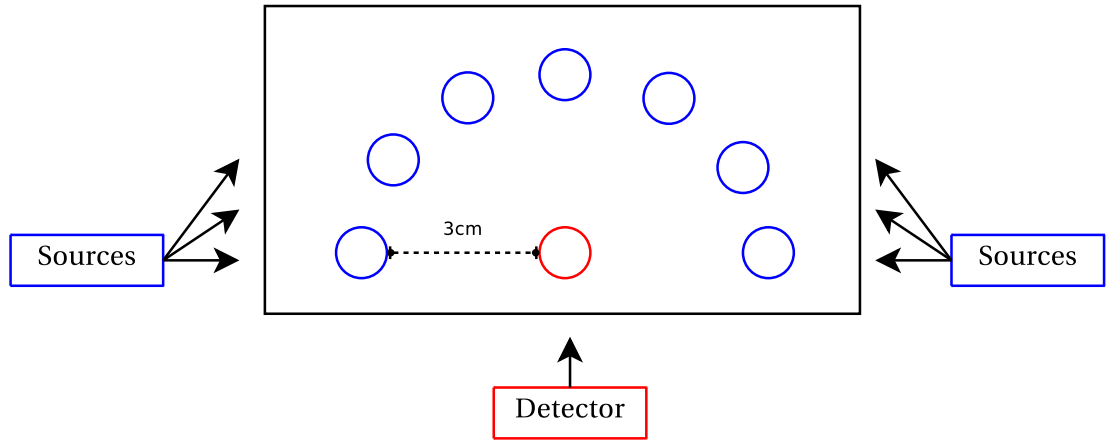
Figure 5.7: Optet configuration for small area searches
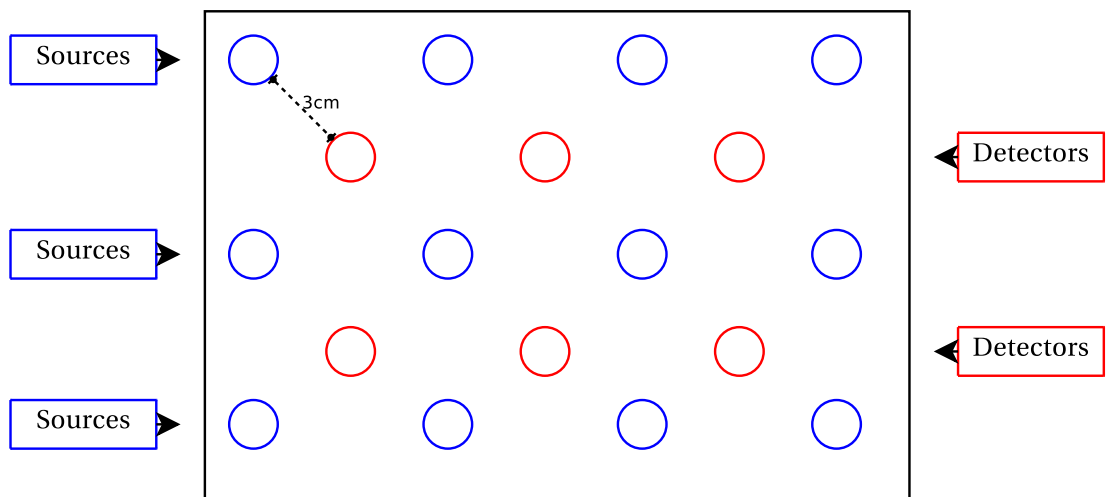
Figure 5.8: Optet configuration for large area motor studies

nature of the underlying tissue (Elwell *et al.*, 1999).

5.7 Chapter Summary

This chapter has outline the construction of a flexible and versatile NIRS-BCI system. This hardware was designed and constructed in conjunction with the Soraghan (2010) dissertation. This hardware is a multi-channel extension of the work of Coyle (2005) and is specifically designed and optimized for BCI experiments. The following chapter introduces versatile software systems to run on this device as well as improvements to the optical multiplexing systems originally designed.

Chapter 6

Reconfigurable NIRS Software Systems

In this chapter we shall discuss the implementation of a reconfigurable software platform for the hardware systems in the preceding chapter. Chapter 3 has outlined the necessity for customizable and robust software control systems. As well as supplying user interaction and experimental design functions, these systems should also be formulated to improve approaches to the interrogatory signal synthesis problem described in Section 3.2.1. To fully realize advances in fNRIS-BCI we must have control over optical signal generation and acquisition.

In creating a platform of this type it is necessary to define the requirements for achieving all the goals predicated by the experiments. The next section will deal with other software platforms of this type and compare them according to the specific requirements of the NIRS modality.

6.1 Software Design Considerations

We must outline the software chain needed to create a versatile and robust system. The aim of this work was to create a single software platform to control all aspects of the research thus making it unnecessary to continuously switch between hardware, software and programing languages. It was also designed to reduce the workload on the researcher when creating new approaches to data analysis. These new approaches should also be applicable offline and on real-time data.

6.1.1 Software Requirements

An fNIRS-BCI requires a range of functionality within its control system. Initially three essential requirements were specified.

- Uncomplicated hardware control and interfacing

- Software modulation / demodulation to replace a cumbersome hardware system

- The ability to rapidly implement and test real-time DSP and classification methods

Secondary requirements included integrated diagnostic capability, convenient raw data storage for offline analysis, experimental design control and aural subject cues. Before looking into the implementation of the requirements, we must examine the hardware system being controlled. Figure 6.1 shows the conceptual flow diagram of the intended system.

6.1.1.1 Hardware Cofigurability

A clear advantage of any software system is its ability to integrate any type of hardware. In order to implement any fNIRS-BCI control the final aim is a device that can process data in real-time. The basic usage of these systems should be accessible to researchers
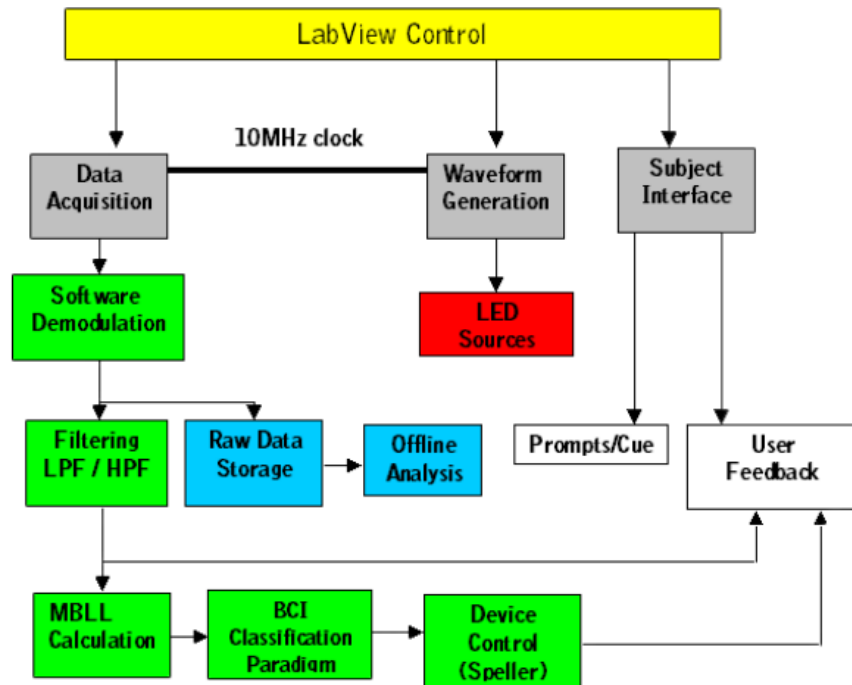
Figure 6.1: Software block diagram illustrating the main elements of control needed within this fNIRS-BCI.

other than computer scientists and engineers. Hardware integration and control must be implemented so it can remain opaque to the end user. This was one of the foremost considerations when choices were made in the design of this system.

6.1.1.2   Experimental Design Implementation

Subject cues are highly variable depending of the interrogated region and there are numerous feedback types possible. All this variation should be invisible to the subjects and easily configurable for the researcher. The main requirements for the experimental design will involve timings, cues, feedback options and trial randomization.

6.1.1.3 Novel Method Prototyping

Although any BCI software system should have some basic options for data processing it is necessary that novel methods be implemented to test their validity. The mechanism by which these methods are implemented must be simple yet comprehensive enough to allow maximum flexibility. NIRS as a BCI modality still requires significant research into data processing routines and noise removal techniques.

The next section is an exposition of a software system that implements these requirements and is followed by an description of a novel software controlled demodulation scheme.

6.2 Integrated Software Systems

We will expand upon the software system described by Matthews *et al.* (2008b). This system is designed to integrate seamlessly with the National Instruments hardware specified in Chapter 5. The software provides the researcher with the ability to control all aspects of of the experimental process. Modules are provided to control the following:

- Hardware interactions.

- Signal modulation / demodulation.

- Experimental paradigm control.

- Data visualization.

- User interaction.

- Physiological noise removal.

- Feature extraction & classification.

.

6.2.1 Software Development

To increase the efficiency in design and development, both hardware and software were based on products supplied by National Instruments (NI). As well as providing a wide choice of signal generation and acquisition hardware all NI equipment can be controlled via a single software development platform LABVIEW.

LABVIEW provides an integrated development environment for graphical or data flow programming language, sometimes referred to as "G". It marries the code development with the user interface design using the Front Panel (user interface) and the block Diagram (source code). Subroutines and functions are referred to as Virtual Instruments (VIs). Each VI contains both a front panel and block diagram. The execution flow of a program is determined by the left to right position of the VI blocks.
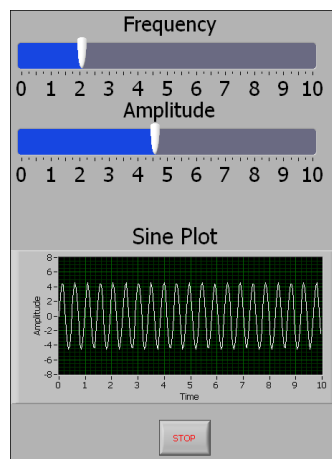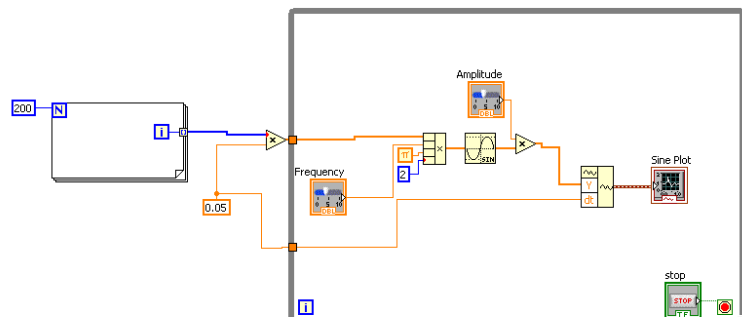
(a) The Front Panel   (b) The Block Diagram

Figure 6.2: Example of a simple virtual instrument. The front panel has user controlled sliders to specify frequency and amplitude. The graph displays a sine wave with those attributes. The block diagram generates an array of numbers and using the frequency and amplitude from the front panel calculates the sine function.

Figure 6.2 is an example of a VI that calculates and plots a sine wave given the user input of frequency and amplitude. The front panel (Figure 6.2a) has sliders for setting the frequency and amplitude and a graph to contain the plot. The block diagram (Figure 6.2b) is equivalent to the source code. A "For" loop generates an array of numbers. Those number are scaled to the equivalent of 10 seconds of data sampled at 20Hz. That data, plus the frequency and amplitude inputs from the front panel, are used to calculate the sine data. That calculation itself is in a loop so the graph can be changed interactively by the user.

6.2.2 User Interfaces

Designing an interface to any software platform is an important part of any development process. In this section we break the systems user interfaces into two categories. The first is control interfaces, which allow the researcher to set up new experiments and control the hardware interaction. VIs have been written to configure source detector pairings, acquisition and generation speeds and LED output powers.

The second, subject interfaces, are customizable by the researcher to present various cues and feedback to subjects during an experiment.

6.2.2.1 Control Interfaces

The control interfaces were designed to allow maximum flexibility to a researcher with the least difficulty setting up an experiment. Figure 6.3 is the main experimental control screen.

From this screen it is possible to supply user cues and associated audio cue files if desired (Fig. 6.3-B). The researcher can pick the number of cues to use as well as how often each may be repeated and timing information (Fig. 6.3-A). The background function of the system automatically takes the rest period time and randomizes it between the time supplied and twice that time for each trial. The order in which
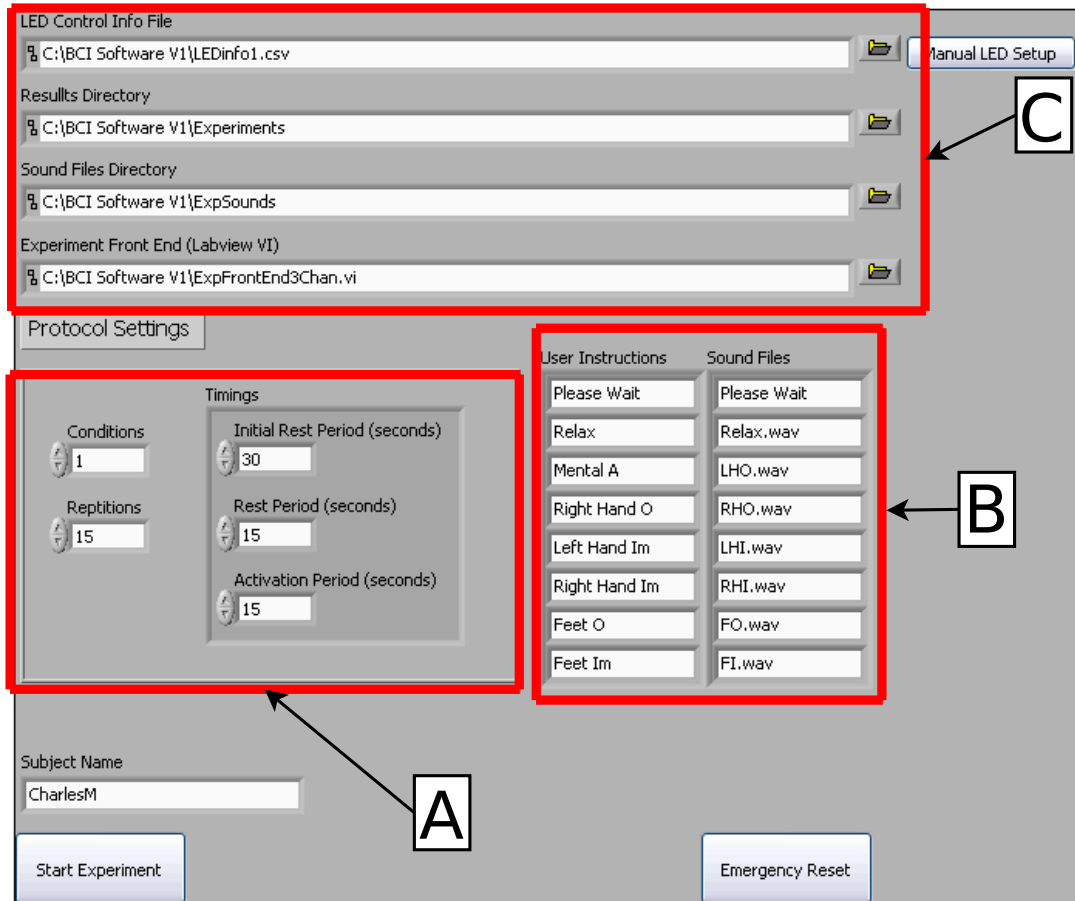
Figure 6.3

the cues are presented is also randomized. The file input boxes (Fig. 6.3-C) allow customization of LED setup info, the directory for results storage, the directory for audio cues and finally a link to the subject view front end.

6.2.2.2   Subject Interfaces

There are a number of subject views depending on the specifics of the experiments. Figure 6.4 is a selection of cues from a non-feedback experiment. A subject would only ever see one of these at a time during an experiment.

Figure 6.4-A & B are simple motor cortex cues, "O" for overt and "Im" for imagi-

A	Right Hand O

B	Left Hand Im

C	Continually subtract 17 From 2130
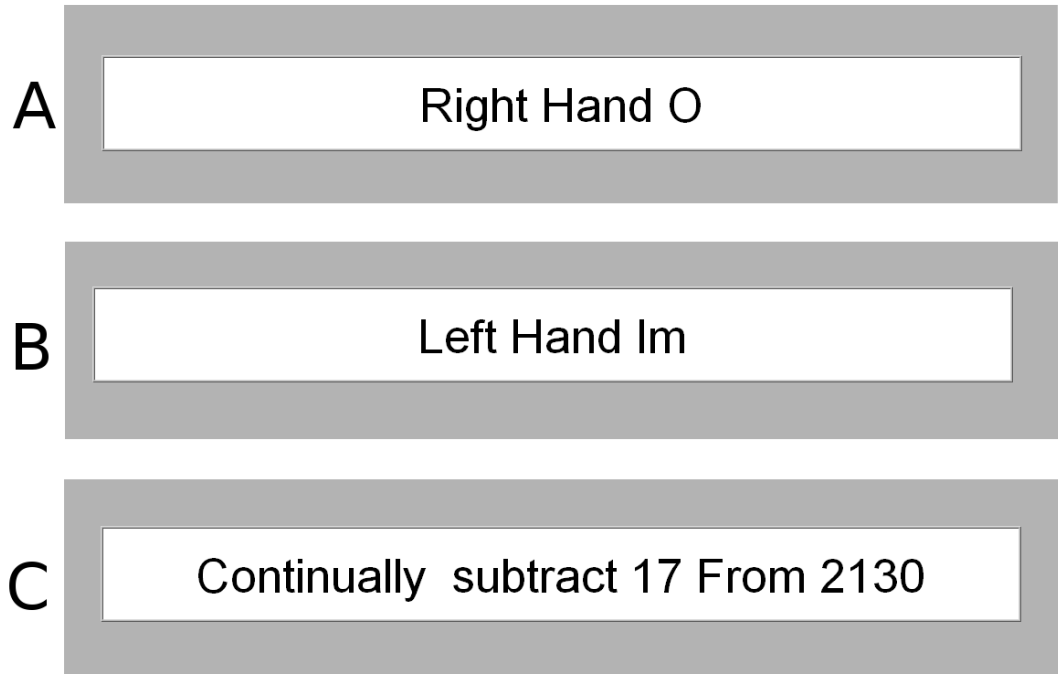
Figure 6.4: Three examples of visual cues supplied to a subject during an experiment

nary. Figure 6.4-C is a mental arithmetic task. The numbers presented are randomly generated during the course of the experiment.

Figure 6.5 is an experimental view that gives the subject an indication of the fluctuations in ΔHbR and ΔHbO_2 during an experiment. The particular version shown in Figure 6.5 indications activity along the motor strip. Each indicator is labeled with the location of the optode according to 10-20 system (Fig. 6.5-B). Subject cues are supplied at the top of the screen (Fig. 6.5-A).

Basic knowledge of LABVIEW allows a researcher to alter existing subject interfaces or design entirely new VIs and insert them into the data processing chain.

6.2.3 Hardware Control

A significant advantage of basing this software on the LABVIEW platform is it's dedicated hardware compatibility. Data acquisition and generation is performed with Na-
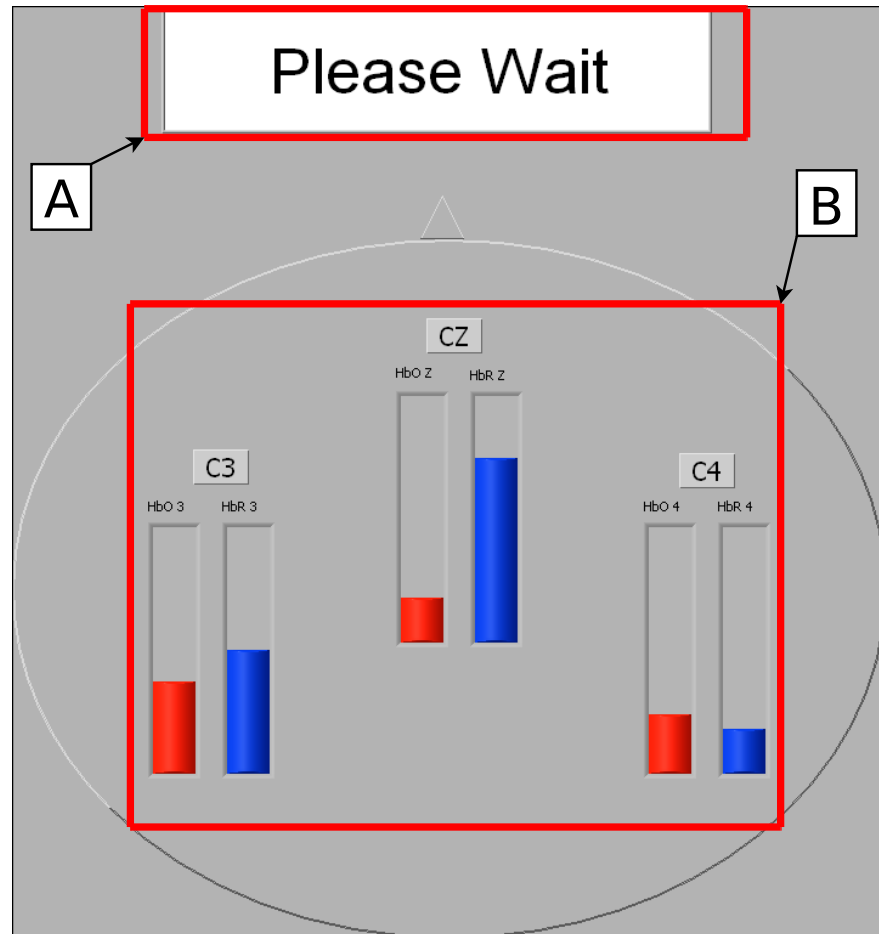
Figure 6.5: A view of hemodynamic feedback supplied to the subject with cues supplied along the top of the screen

tional Instruments (NI) equipment and Labview is designed to integrate easily with their hardware. Labview is also designed for general-purpose hardware interaction, allowing the ability to introduce more acquisition and generation systems if the need arises.

Labview through the PXI chassis, allows for micro-second synchronization between the acquisition and generation cards. Generation and acquisition rates are all controlled through a single VI. This VI sets up the coordination between generation and acquisition cards. The clock signal from one of the acquisition cards is routed to
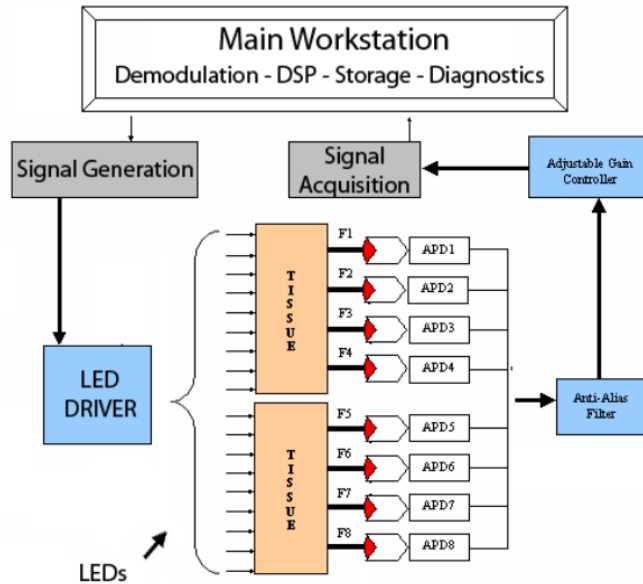
Figure 6.6: Hardware Block

one of the RTSI lines. All the other cards on the system use this signal for synchro-
nization. With the current hardware sampling can be taken from up to 8 APDs and
generation allows up to 16 LEDs (32 generation channels, 2 wavelength per LED).

6.2.4 Data Processing & Classification

The software was designed specifically to allow simple integration of data processing and
classification routines. As discussed in Chapter 3 a typical fNIRS signal is saturated
with different types of physiological noise. Problems also arise when using a high
number of channels and with the application of processing routines simultaneously to
all channels. Potential loss of data and compromised hardware timing can result.

This system was designed to allow easy integration of the standard LABVIEW filter
functions into the signal processing chain. User defined signal processing functions in
C or C++ can be integrated via a DLL or such functions can be written directly in
LABVIEW and included in the processing chain. Most processing functions have been

optimized for real-time operation. The system also enables the display of the timings for each process, leaving the researcher capable of calculating a time-budget allowed for each processing stage.
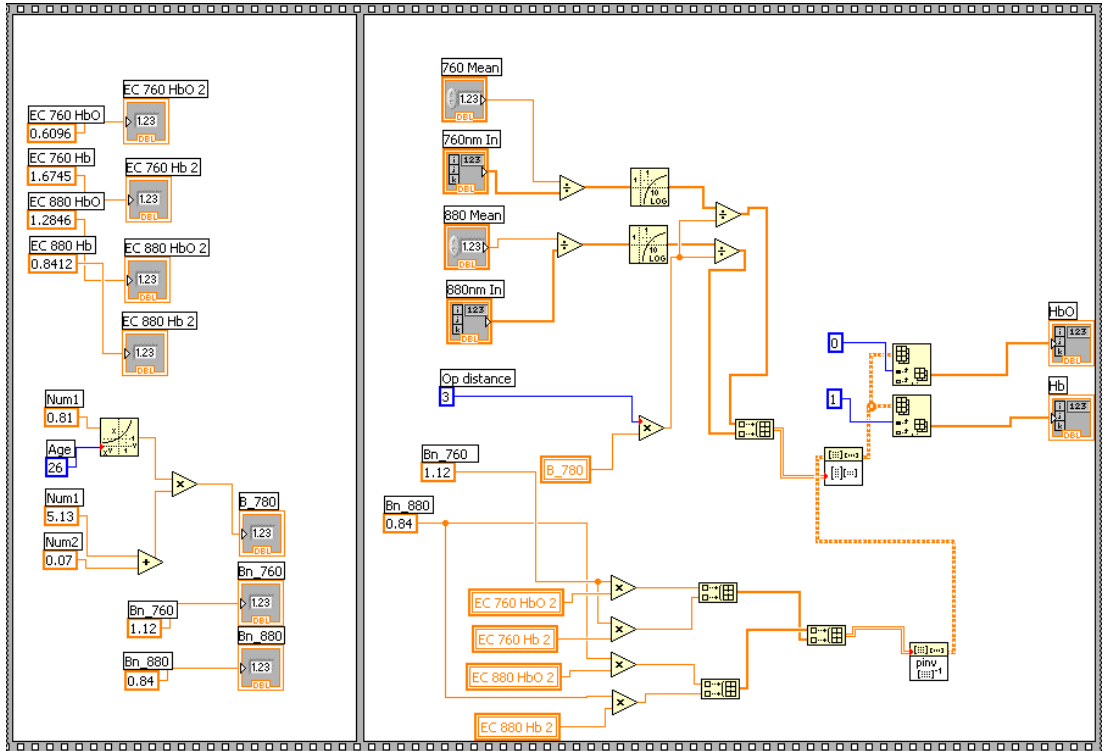
Figure 6.7: Block Diagram for the calculation of the Modified Beer-Lambert law

As with the flexibility of the signal processing functions, it is also possible to select from a number of different classification routines. Creating and including new classification schemes can be done using MATLAB, DLLs or LABVIEW code. A standard LABVIEW library includes a function allowing MATLAB source code files to be directly inserted into the control chain. This minimizes development and test times, giving the researcher a quicker insight as to whether a function can perform adequately in real-time.

An example is Figure 6.7. This is the block diagram for calculating the Beer-Lambert sample by sample. The function takes in a single sample for 760nm, a single
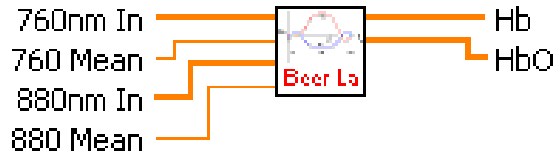
Figure 6.8: Icon for the Beer-Lambert Calculation

sample for 880nm and a running updated mean value for both. These values are used in conjunction with some constants (per experiment, these can also be configured elsewhere) like subject age, inter-optode distance to calculates the relative concentrations of ΔHbR and ΔHbO_2. Once a function has been completed it can be saved as a standalone VI and included in a larger program. Figure 6.8 is how the Beer-Lambert function appears in another program. To "call" this function it is simply a matter of connecting the correct inputs and outputs.

6.2.5 Test Systems

The ability to analyze hardware and software performance and troubleshoot any problems that may arise is important for any software of this type. Included within this system is a diagnostic section that allows the researcher to inspect the raw signals coming from the system in real-time. It is possible to cycle through each data input channel and view the performance of LEDs and APDs. This tool is also used to check if source-detector positioning is appropriate and all channels are responding correctly before an experiment.

Figure 6.9 is an example of a testing interface for experiment preparation. The researcher uses this VI to ensure all LEDs are transmitting and being detected with sufficiently high resolution. It is possible to examine the spectrum of the data from each APD connected to the system as well as the demodulated values from each wavelength.

Another useful test system allows the replay of pre-recorded data for testing data processing routines. This system requests the location of the raw optical data file saved
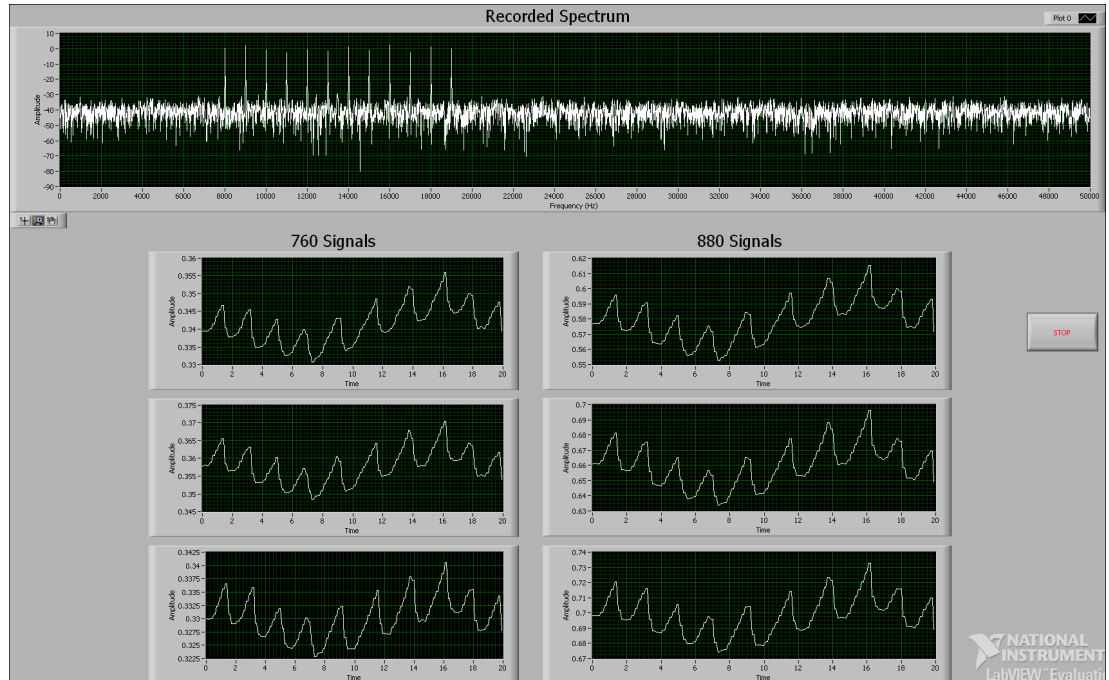
Figure 6.9: Front panel for the signal testing system. This can be run by the researcher to test the strength of the signal from each APD and each individual wave-length.

from a previous experiment. Once a file is selected the system uses hardware timing clocks to serve out the samples at their original sampling rates. This allows simulated real time testing of novel methods.

6.2.5.1 Data Storage

At the end of each experiment the raw light intensity data is stored in a file for additional offline analysis. This data is also formatted as a file for use with the HomER NIRS analysis tool (Huppert, 2006). All data is timestamped with millisecond values from the hardware timing clock as well as a stimulus marker to differentiate rest and active regions for each sample in offline analysis.

6.2.6 Conclusion

We have described a robust and customizable software system for design and control of fNIRS-BCI experiments. The next section uses this system in conjunction with the hardware from Chapter 5 to implement and test a new approach to the signal synthesis problem.

6.3 Software Controlled Signal Synthesis

As discussed in section 3.2 there are avenues for improvement to be found in investigating the interrogatory signal synthesis issues. This section outlines the approach to the multiplexing of the optical signal required within this interrogatory signal synthesis problem. The methods implemented here are specifically designed to reduce the overhead in equipment and cost for a NIRS-BCI while reducing communications channel interference. Using the theory of spread spectrum communication it is possible to remove complex signal conditioning hardware for LED current generation and reduce acquisition and generation equipment specifications. These spread spectrum techniques also offer less narrow band channel crosstalk, multi-path fading and higher noise immunity than their frequency based counterparts (Dixon, 1994). This approach also allows for lower computational overhead, lower hardware costs for simplified NIRS-BCI and incorporates all the signal advantages of using a spread spectrum system.

6.3.1 Current Demodulation Strategies

A key reason for designing a new software system was the ability to discard a costly and bulky hardware demodulation system. A difficulty of NIRS measurement is that the optical intensity is attenuated by about 10^{-8} during tissue interrogation. To allow the signals to be recovered, each wavelength is modulated by a carrier signal. In previous systems, separate hardware lock-in amplifiers were used to demodulate the signals

(Coyle, 2005). This new system removes the need for expensive and cumbersome lock-in amplifiers and moves all demodulation into software (Everdell *et al.*, 2005). Where previously the system was constrained by the requirement of these amplifiers, this new software alternative allows for more scalable and cost effective multichannel design. It also allows for investigation of as yet untested demodulation strategies.

Using the original demodulation scheme NIR light interrogates the region of interest from multiple LED sources. This light is then detected by a single APD. The APDs output is digitized by the data acquisition card and placed in the acquisition buffer for processing. This data, retrieved in windowed blocks, is processed with a Hanning-windowed FFT, producing a complex spectrum. This spectrum is passed to the frequency search function. The specific search frequencies are specified either in a text file or can be adjusted in the software prior to the experiment. The function also takes a search window for each frequency specified as a percentage of the sampling frequency. This approximates an amplitude modulation strategy similar to that of AM radio.

This process can be repeated for any number of input channels constrained only by the processing time and physical hardware channels. The hardware of this system has eight usable input channels. Experiments have been conducted using seven input channels with usually 4–6 dual-wavelength LEDs visible per APD.

Here we will examine a new approach to the demodulation system using the theories of spread spectrum communication. We will outline the basics of multi-user communication, the theory behind spread spectrum communication and the implementation and implications for NIRS. We will also compare this new approach to other multiplexing methods and present the results of experiments.

6.3.2 Multi-user Communication

To acquire ΔHbR & ΔHbO_2 concentrations in a single source-detector NIRS system two wavelengths or light must be transmitted through the same medium. These signals must in some way be separable from each other. In communications theory the solution to these problems are referred to as multiple access methods. These solutions are used when multiple signals wish to share the same communication channel. In this case the physical channel is tissue in the region of interest.

With a multichannel NIRS systems (Multi-source, single detector) the problem remains the same except the overhead in channel allocation, detection and demodulation is increased. Multiple access methods are all based around sub-dividing the bandwidth in some way so as to avoid interference between simultaneously communicating channels.
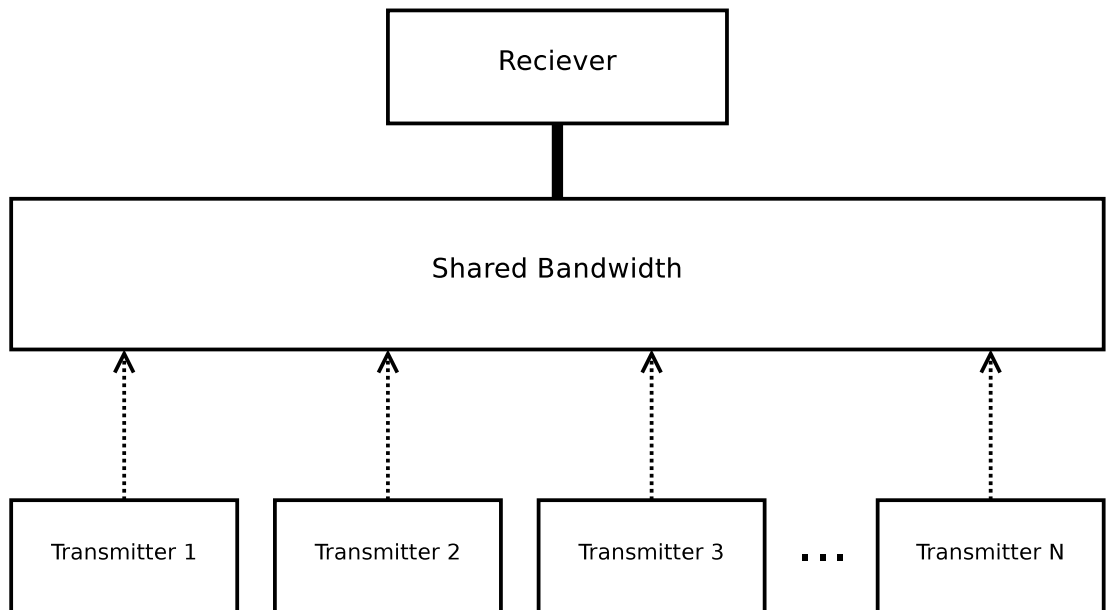
Figure 6.10: Multi-user communication.

6.3.2.1 Common Multiple Access Methods

There are several multiple-access methods available within communications theory. Commonly these approaches are broken down into four categories: space, time, frequency and code division. Different NIRS systems use different implementations of multiple access methods from these categories. An advantage in NIRS from a communications perspective is the central control of transmission and detection. Many multiple-access methods are designed to accept un-synchronized communications or have to implement extra methods establishing synchronization.

Space-division multiplexing (SDM) is the term for transmitting from a location where no other signal is present to interfere. A common example would be CB radios with low transmission range. They all transmit on the same frequency but will only relay information from other radios within range. This category would equate in NIRS to setting distances between source-detector groups large enough so they don't interfere with each other.

A time division system relies on a frame duration T being subdivided into N different non-overlapping slots where N is the number of transmitters. Each transmitter is then assigned a time slot for transmission. This method, known as Time Division Multiple Access (TDMA), avoids interference by prohibiting simultaneous transmission (Proakis & Salehi, 1995). The OMM-1000 (Shimadzu Corporation) used by Ranganatha *et al.* (2004, 2007) for NIRS-BCI investigations synchronizes the timing between its sources and the PMT detectors. The optical detection is cycled one wavelength at a time.

Frequency division systems or frequency division multiple access (FDMA) subdivides the frequency bandwidth into N non-overlapping channels (Weinstein & Ebert, 1971). Each transmitter is assigned a sub-channel band over which to transmit. An example is amplitude modulation (AM) where each transmitter is assigned a carrier frequency and modulates the amplitude of that frequency to transmit information. Another is frequency modulation (FM) where the carrier frequency itself is shifted within

the sub-channel band to convey the information (Proakis & Salehi, 1995). NIRS systems using FDMA are common (Coyle, 2005; Everdell *et al.*, 2005). The hardware systems outlined in Chapter 5 were initially specified to use FDMA as its main form of communications (Soraghan, 2010).

Finally we will examine in detail the theory behind code division multiple access (CDMA). The background of this multi-user access method is based on spread spectrum communication theory. In this method the transmissions are spread across the available bandwidth.

A pseudo-random noise (PN) sequence is assigned to each transmitter. For demodulation to be possible the chosen sequences must be orthogonal to each other. Without this constraint information would leak across channels. Each bit of information to be transmitted is modulated using these an entire sequence. The receiver is aware of each sequence used for each transmitter. After synchronizing with the transmitter it can demodulate the information transmitted. In section 6.3.3 we will examine, in detail, the theory behind developing a CDMA communications system.

6.3.2.2 Space Division Multiplexing and NIRS

Using a multi-channel NIRS system to detect multiple activation types introduces the problem of possible cross talk between areas. Using the fMRI data from Chapter 4 and Monte-Carlo models of photon transmission (Humphreys, 2007) we can reliably state that this cross talk is negligible outside a certain distance.

Figure 6.11 shows a 2D area plot from a Monte-Carlo model of photon migration through tissue (Humphreys, 2007). Figure 6.12 indicates three areas of activation from an fMRI scan.

In the Monte-Carlo model, the radiative flux density more than 2cm away from the injection point is quite low. Generally, in NIRS experiments, a source-detector distance of 3cm is used, which exhibits a 10^{-7}–10^{-9} level of attenuation in flux density
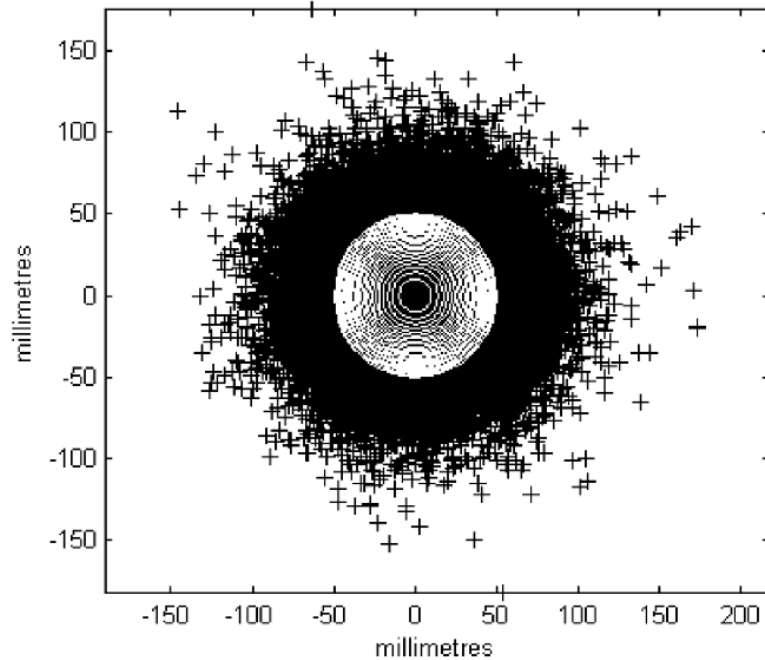
Figure 6.11: Plot of the density of reflected photons from a Monte-carlo model (Humphreys, 2007). Photons are inserted at (0,0) and model shows the reduction in the quantity of photons emerging from the tissue in relation to the distance from the insertion point.

(Soraghan, 2010). With distances beyond 3cm the variation in the signal begins to fall below the 0.005nW sensitivity of the detector. From the discussion in Section 3 we can show that source-detector distances above 6cm yield negligible information due to the extremely low flux density. This indicates that sets of optodes placed greater than this distance apart will have negligible cross-talk.

In Figure 6.12 it is possible to observe the hemodynamic plume in functional areas as detected through fMRI. Spatial measurements between these active areas mapped to the scalp show that the distances between is so far apart as to eliminate crosstalk.
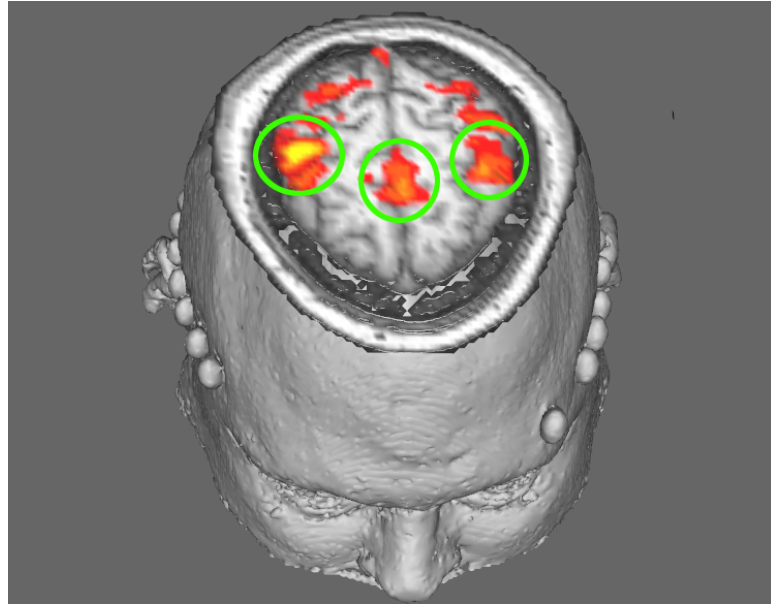
Figure 6.12: 3D mapping of motor cortex activation regions. Spatial measurement performed on these regions implies little interference or crosstalk could occur during a simultaneous NIRS investigation of theses sites.

6.3.3 Spread Spectrum Communication

Spread-spectrum (SS) communications uses wide-band noise-like signals to transmit information. The result of this are transmissions that are spread in the frequency domain. These techniques have a higher narrow-band noise immunity, are less susceptible to eaves-dropping and other sources of interference like multi-path fading (Viterbi *et al.*, 1995).

The system uses pseudo random binary sequences to modulate communication sources. Receivers detect transmissions and use linear algebraic methods to demodulate the signals. Similarly this research investigates the application of this to the interrogatory signal synthesis problem. Using SS techniques to modulate and demodulate optical signals in a NIRS negates the need for analog signal generation and reduces harmonic and narrow-band interference inherent in FDMA systems.

6.3.3.1 Pseudo Random Binary Sequences

Pseudo-random binary sequences or pseudo-noise (PN) sequences are required in cryptography and spread spectrum communication. They are "pseudo" random because after a generated sequence reaches its length of N bits or "chips" it will start to repeat itself (Helleseth & Kumar, 1999). This differentiates it from true random sequences like those generated from white noise or radioactive decay. Commonly, these sequences are generated using hardware or software implementations of Linear feedback shift registers.

6.3.3.2 Linear Feedback Shift Registers

Linear feedback shift registers are required to generate pseudo-random bit sequences necessary for applications in SS communications and cryptography (Golomb, 1981). A shift register is a type of digital logic circuit. In hardware, a chain of flip-flops would store a single bit state each. According to a common clock, each flip flop would pass its state on to the next in the chain. In Figure 6.13 the initial state of the register is passed along the chain and a new input is in place in the next cycle.
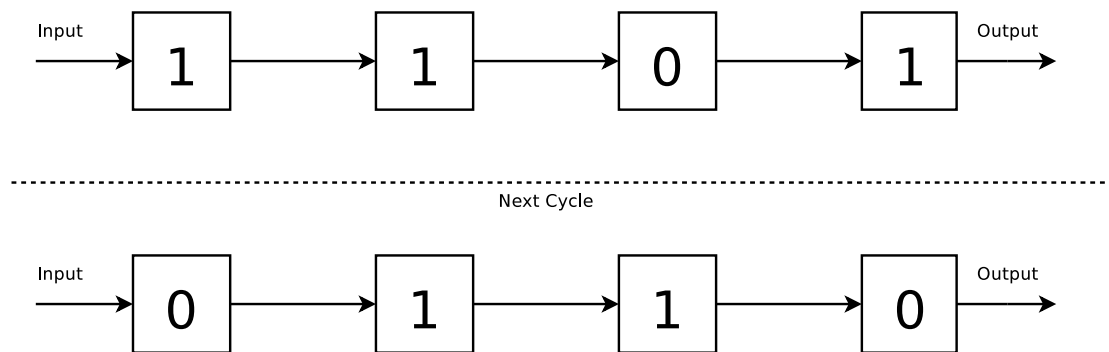
Figure 6.13: A four bit digital shift register. Each unit in the chain stores a bit state and that state is shifted through the chain.

Within linear feedback shift registers (LFSRs) the input to the register is a linear combination of its previous state. The only linear bit wise operations are XOR and

inverse XOR so some or all of the bits in the current state are XOR-ed to create the new input.

There are two common implementations of LFSRs, Fibonacci and Galois. Figure 6.14 shows a Fibonacci implementation. In this implementation the input is an XOR-ed combination of some or all of the bit sequence. Specifically, Figure 6.14 shows a LFSR where all the bits in the sequence are used to generate the new input. In most cases certain elements or taps are chosen to give an output sequence with specific properties. Galois LFSR performs the XORs during the shifts so internal bits to the registers are altered in a cycle. The Galois provide faster operation when implemented in hardware but both types are mathematically equivalent (Sklar, 1988).
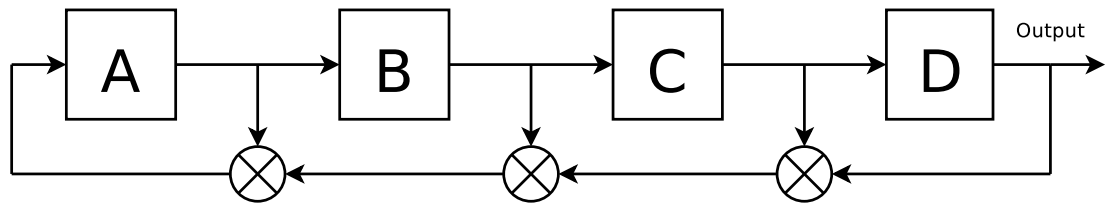
Figure 6.14: Fibonacci Linear Feedback Shift Registers

Both methods will produce equivalent outputs in the correct circumstances. While Fibonacci implementation is the conventional representation of LFSRs, in hardware, the Galois performs its XORs in parallel giving it an advantage in performance.

In hardware LFSRs can be used as binary counters and the sequences they produce can be considered valid binary number systems. In this dissertation however we are concerned with their ability to produce pseudo-random binary sequences. As mentioned in the start of this section LFSRs are used to generate PRBSs for use in communications and cryptography.

Careful choice of the placement of the XOR-ed bits or taps allows sequences to be produced which have a number of properties essential to these applications. With the correct tap selection a register N bits in length will create a pseudo-random sequence $2^n - 1$ bits in length before repeating. These sequences are called Maximal Length
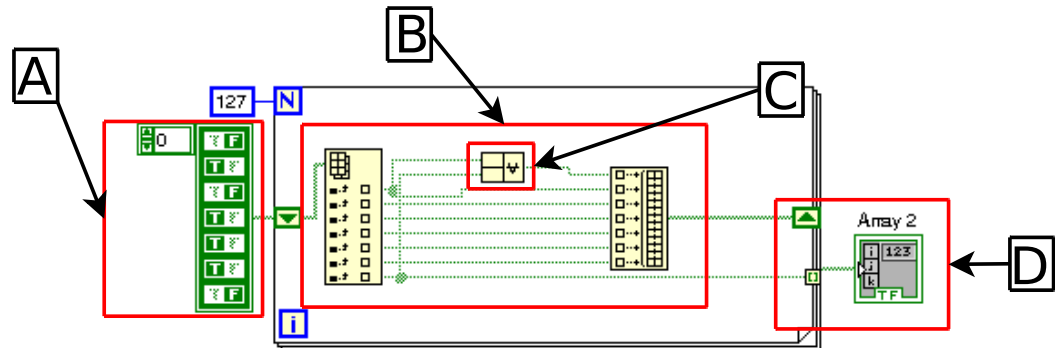
Figure 6.15: Linear Feedback Shift Register implemented in Labview. This example will generate an M-Sequence (Section 6.3.3.3) 127bits long. A: the seed values. B: The array of binary values is broken out and shifted, C: Specific taps are XORed. D: The output is a binary array 127 ($2^n - 1$, N = 7) in length.

Sequences (M-Sequence) (Dinan & Jabbari, 1998). Figure 6.15 is the block diagram from a labview implementation of a LFSR that generates an M-sequence 127 bits in length.

6.3.3.3 Maximal Length Sequences

Maximal length sequences (M-sequences) are of particularly importance to this implementation. A single sequence can provide the codes for multiple transmitters while also being trivial to generate. M-sequences are defined as binary sequences with the following properties:

Balance Property There is only one more '1' than '0' in the sequence.

Run Property Runs of 1s or 0s are in specific quantities. eg half of the runs are length 1, one quarter are length 2, an eighth are length 3, etc...

Auto-correlation Property The auto-correlation of the sequence is only significant at 0 or multiples of N.

The auto-correlation property is especially important for this implementation. An M-sequence that has been shifted is orthogonal to the original unshifted sequence. For SS communication to be effective the sequence must be orthogonal and hence a single M-sequence can provide PN codes to multiple transmitters. M-sequences are no longer commonly used in telecommunications. They are trivial to predict and hence communications using them are susceptible to interception. Many telecommunication implementations like cellular networks and GPS use alternative PN sequences like Gold or Kasami codes. Most other PN codes are generated using combinations of M-Sequences. Since a NIRS implementation does not require protection from interception, M-Sequences provide the simplest solution to assigning codes to transmitters.

6.3.3.4 CDMA formulation

Using M-sequences, we wish to be able to decode the information recorded by the APDs when the LEDs are modulated with SS techniques. Hence, the problem can be re framed as such:

We are looking for a least squares solution to $Mz = c$ where M and c are a known matrix and column vector respectively,

The solution is:

$$z = \underset{y}{\operatorname{argmin}} \|My - c\| = M^+ c$$

where M^+ is the Moore-Penrose generalized inverse of M.

Applying this to the the NIRS communication problem:,

$x(t)$ is a vector of the M-sequence used to modulate the LEDs.

$y(t)$ is the recorded data from the APD.

A is the matrix of attenuation caused by traversing the tissue which is the unknown.

t is a time constant over which we assume no change in A.

This problem equates to the following. Given the column vectors $x(t_0), ..., x(t_k)$ and values for $y(t_0), ..., y(t_k)$ find A such that,

$$\sum_{i=0}^{k} (Ax(t_i) - y(t_i))^2$$

is minimized.

This then is equivalent to minimizing,

$$\left\| X^T A^T - Y^T \right\|$$

where $X = [x(t_0), ..., x(t_k)]$ and $Y = [y(t_0), ..., y(t_k)]$ and hence, as stated above, the solution to this is,

$$A^T = (X^T)^+ Y^T$$

The properties of the Moore-Penrose inverse gives us $(X^T)^+ = (X^+)^T$, which makes

$$A = YX^+$$

However, it would be extrordiniarily ineffecent to compute the matrix X^+. Instead standard methods are used to directly solve for A given X and Y.

6.3.4   System Implementation

A Matlab function was used to supply the predefined taps and generate the m-sequence. An effective sampling rate for the system was set at 10Hz to match the FDMA system already in place. A register length of 7 bits was chosen which resulted in a sequence

length of $2^n - 1$ or 127 chips. Shorter sequences showed significant crosstalk between channels. Each LED would then be modulated using 127 chips every 0.1s.

6.3.5 Signal Generation & Source Modulation

During experimental setup using the functions described in Section 6.1.1.2 a graphical interface provides the researcher the ability to configure the source-detector settings. These settings specify the number of detectors and the sources each one can detect. The software uses this configuration to calculate the number of shifted signals required to adequately multiplex the correct sources for each detector. Correspondingly, a matrix is produced for each detector which maps each source to a particular shifted sequence.

These shifted sequences are then converted to a digital waveform for the generation process. This waveform is the length in time of a single period desired for detection, in this case 100ms. At the end of each waveform a period is allowed where all the sources are off (approximately 5% of sequence time). This is included to provide a synchronization point so the detector can phase lock its version of the transmitted sequences.

Once all the necessary waveforms have been generated this is passed to the NI signal generation card. The generation voltage is chosen using methods derived from Chapter 5 to allow maximum source brightness while controlling the LED die temperature.

6.3.6 Signal Acquisition and Demodulation

The APD outputs are sampled at 16kHz. This rate was chosen as it allow 12 samples to be averaged per chip followed by 76 samples where all LED are off. This rate is significantly lower that the sampling rates of about 100kHz used in the FDMA implementation. The last 76 samples allow the system to detect the end of the sequence and synchronize for demodulation.

This signal is then passed in software to the demodulation function. This function

is a Labview implementation of the CDMA formulation presented in section 6.3.3.4. The output of this function is the detected light intensities for each LED assigned to that APD for that time period.

6.3.7 Comparative Analysis Experiment

An experiment was performed where the CDMA method of modulation is performed on an optical phantom with different levels of optical absorber. Two more systems, time and frequency division, were used as a comparison .

6.3.7.1 Motivation

This experiment will demonstrate that a CDMA based modulation scheme can be used within an NIRS-BCI at lower generation and sampling rates than other modulation methods while still being capable of resolving signal details. During this experiment data was recorded using two other modulation schemes, time division and frequency division. These will enable comparative results to be produced.

6.3.7.2 Time Division System

A square wave was generated for each LED and supplied to the generation system. These waves allowed only one active source at a time. Upon acquisition, the data collected and samples timed against each LED were averaged to a single value. The cycle time of all the LEDs was set to 100ms hence the effective sampling rate was 10Hz.

6.3.7.3 Frequency Division System

Using the same software configurable frequency division multiplexing system outlined in Chapter 5 the system, still sampling at an effective rate of 10Hz, collected data from each level of absorber.

6.3.7.4   Experimental Protocol

This experiment aims to demonstrate the validity of using a CDMA system with lower sampling and generation rates to provide demodulation for a NIRS-BCI. Using the hardware outlined in Chapter 5 optodes were attached to an optical phantom. Four LED units were used (760nm & 880nm) in each, eight signals modulated). The phantom was a cylindrical container filled with water. During the course of the experiment liquid parachlorometaxylenol (PCMX) was diluted in this water to act as an absorber. Inside the phantom a controlled agitation was introduced. This agitation could be altered at a varying rate to simulate a pulsatile signal.
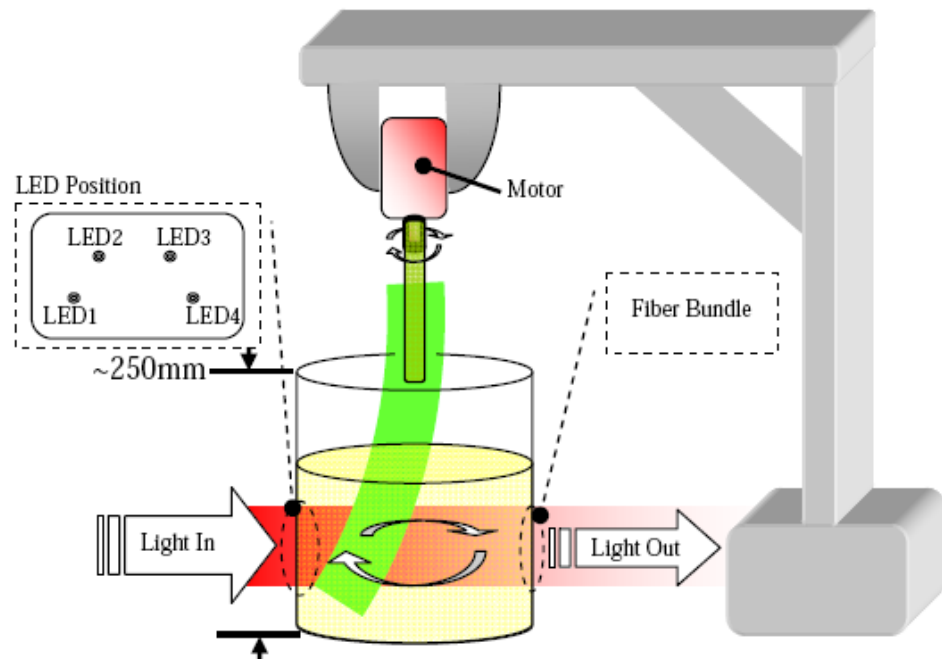
Figure 6.16: Illustration of an optical phantom designed to emulate physiological signals. Figure reproduced from Soraghan (2010)

Figure 6.16 illustrates the phantom used in this experiment. The arm connected to the motor introduces agitation in the absorber as well deflecting the optical signal periodically generating the desired pulsatile output.

With no absorber diluted in the transmission medium, the detectors saturated,

producing no output. The starting point was to include enough PCMX to reduce the detector saturation. Each modulation/demodulation method was run in turn and the result recorded. This first recording was used as a baseline or best-possible result. Next, the level of absorber was increased and each modulation process was repeated. This process was continued until the pulsatile signal was visibly almost undetectable. In all, absorber was increased eleven times and recording were made for each method.

The signal recorded with the least absorber from the frequency division system was considered the best result. In post processing the signal was correlated to all the rest of the signals to compare their degradation.

Finally a signal was recorded using all three methods where the LEDs remained unpowered. This gave a measure of the noise contained within the system and was used to calculate signal to noise ratios (SNR).

Figure 6.17 shows a selection of demodulated signals from one channel for each method. The reduction in the quality of the signal is obvious for all methods by the final absorber level. The TDM method performs poorly throughout.
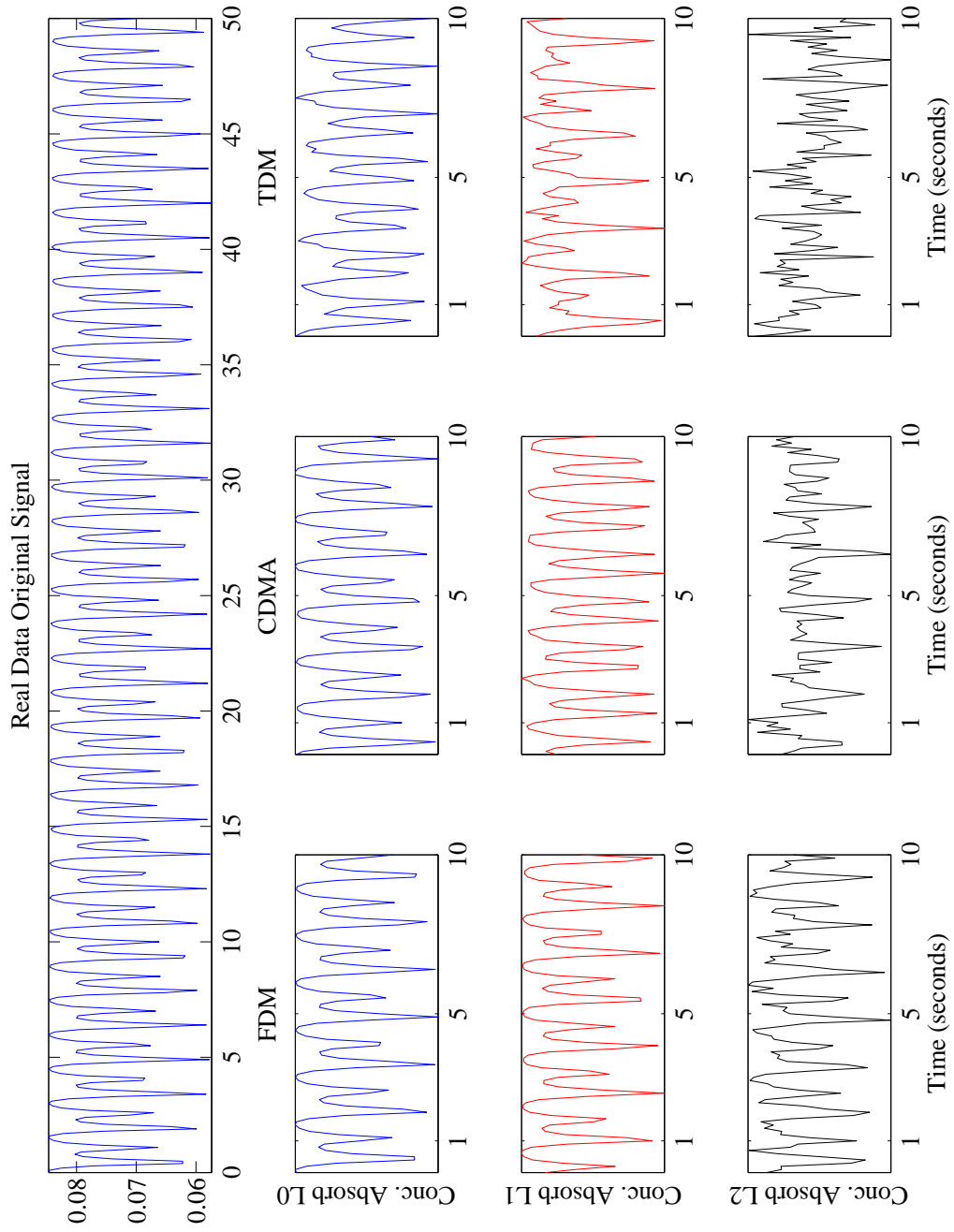
Figure 6.17: Comparison of the effects of different absorber levels on each process. Each method and the plot of the signal at three different levels of absorber, L0 (absorber negligible) L1 and L2.

6.3.8 Results

The aim of the experiment was to show that a SS method preforming with lower specification can adequately resolve details in the optical signal. To achieve this the recordings from each level of absorber are correlated to an ideal signal to give a measure of degradation.

6.3.8.1 Resolving Signal Detail
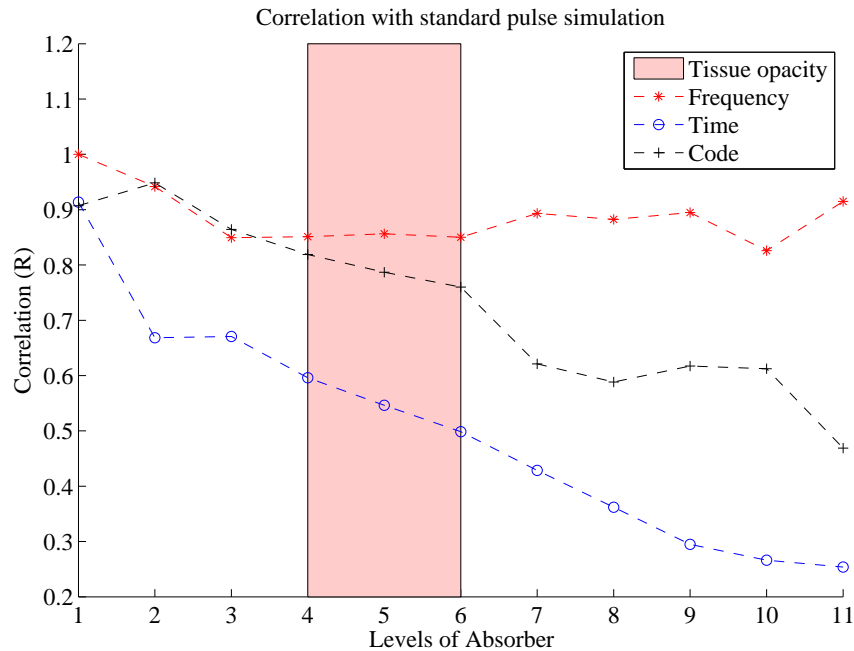
Figure 6.18: The results for each method at every absorber concentration level is normalized and correlated with the standard. This presents the Pearsons R value of correlation at all absorber levels.

Figure 6.18 shows the CDMA approach compared to frequency and time methods. Even with the large discrepancy between sampling and generation rates in the frequency method, the CDMA method was capable of resolving the signal detail through most of the experiment.

Another comparative measure was to calculate the root mean squared (RMS) power

of real data over a number of experiments and compare that to the RMS of the frequency demodulation approach. Using this data it was possible to determine the range of signal attenuation common in real experiments. This allows an assessment of the level of absorber *vs* the general opacity of tissue.

This analysis lead to the assumption that the opacity of the phantom was comparable to that of human tissue between the 4th and 6th absorber level. Given this measure it is possible to assume that if the method performs well within this region it is suitable for use within a NIRS-BCI modality.

Within this region the CDMA approach only deviates slightly from the frequency system. Time division performs very poorly at resolving the necessary detail within the signal.

6.3.8.2 Signal to Noise Ratio

In calculating the signal to noise ratio the difference in data collection techniques becomes more apparent. Figure 6.19 is a plot of the SNRs for all method versus the levels of absorber in the system. The frequency demodulation method maintains a significantly higher SNR throughout. This highlights the drawback of using a lower resoloution CDMA over FDMA however the CDMA system still maintains a suitable SNR within the regions of tissue opacity to resolve necesary signal detail.

6.3.9 System Implications

The implementation of this system in a next generation NIRS-BCI would allow a reduction in the complexity of the data generation and modulation systems. This particular implementation reduces the harmonic interference created using frequency systems thus allowing the running of these systems at a much lower generation and acquisition rates. Another advantage of this system is the removal of analog signal generation allowing implementation with an entirely digital system. This also allows simpler LED driver
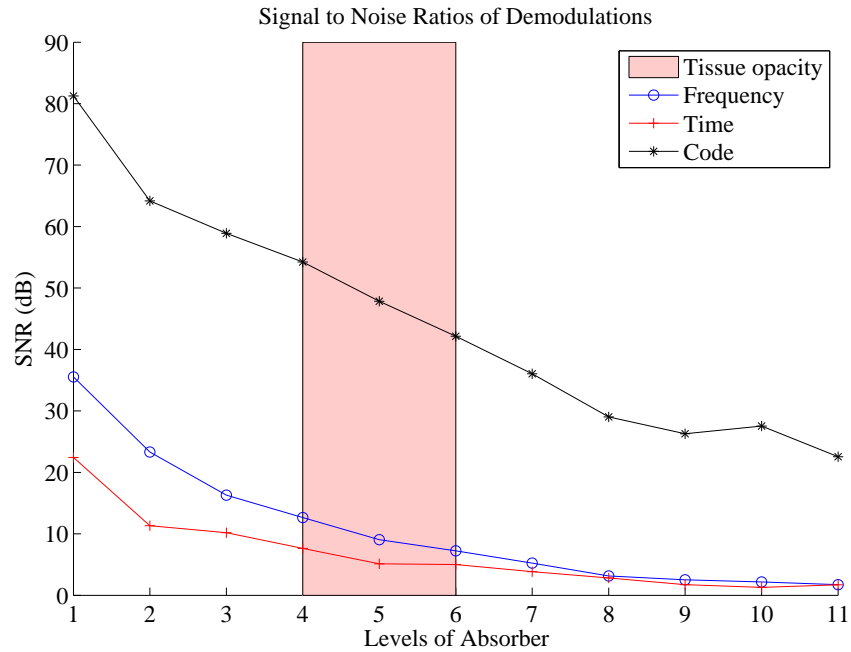
Figure 6.19: Signal to Noise analysis of methods. FDMA is understandably higher due to higher sampling rates.

electronics.

6.4 Chapter Conclusion

This chapter outlined a robust customizable software system designed specifically for fNIRS-BCI applications. By employing this software and the hardware systems described in Chapter 5 it was possible to develop a novel approach to the interrogatory signal synthesis problem.

We have shown the advantages of a highly configurable software system to investigate the area of research in BCIs. The importance of the software designed around any system of this type has been highlighted. The ability to have software configurable demodulation systems allows significant reduction in hardware cost and complexity.

Chapter 7

Signal Processing and Analysis Methods

As discussed in Chapter 3 there is a large quantity of physiological interference to understand in search of activation data in NIRS. The following chapter examines Empirical Mode Decomposition as a method of signal analysis and removal of physiological interference. We will also investigate methods of optimizing the approach to real time signal processing. This is achieved by defining systems to select sources of most relevance to a particular experiment. Finally we will examine a number of simple real-time classification methods that can be applied.

7.1   Empirical Mode Decomposition

Empirical Mode Decomposition (EMD) was developed by Huang *et al.* (1998a) as an analysis method for non-linear and non-stationary signals. The basic method decomposes a time-series into intrinsic mode functions (IMFs). IMFs can be described as simple oscillatory modes as a counterpart to the simple harmonic functions although instead of constant amplitude and frequency,an IMF can have variable amplitude and

frequency along the time axis.

Formally, IMFs are defined as signals with

- equal numbers of extrema as zero-crossings

- approximately zero-mean, as defined by the stopping criterion.

While extracting IMFs from the original signal the process iterates or sifts each IMF till it meets the stopping criterion. This process is detailed in the next section.

7.1.1   EMD Process

The algorithm behind EMD is as follows (Rilling *et al.*, 2003):

1. Extract all extrema locations from signal $x(t)$.

2. Interpolate between minima to create lower envelope $e_{min}(t)$ then again between maxima for higher $e_{max}(t)$.

3. Calculate mean signal between envelopes, $m(t) = (e_{min}(t) + e_{max}(t))/2$.

4. Subtract this signal from original $d(t)_1 = x(t) - m(t)$

5. Repeat steps 1–4 upon $d(t)_1$ until result matches stopping criterion (sifting process). If performed k times the first IMF is $d(t)_k$.

6. Subtract $d(t)_k$ from $x(t)$ and repeat again until final residual is monotonic.

Once the process is complete the IMFs produced are the constituent non-linear, non-stationary signal components of the original.

7.1.1.1   Sifting process

After the calculation of the mean from the upper and lower envelopes and its subtraction from the data this output should technically be an IMF. This process however

may generate new extrema indicating new modes lost in the the first iteration. To incorporate these new modes the sifting process goes over the data repeatedly until some stopping criteria is met.

7.1.1.2 Stopping Criteria

There are two methods of determining when to stop the sifting process. The first proposes determining a sum of differences between sifting states $d(t)_k$ and $d(t)_{k-1}$.

$$S_k = \frac{\sum_{t=0}^{T} |d(t)_k - d(t)_{k-1}|^2}{\sum_{t=0}^{T} d(t)_{k-1}^2} \tag{7.1}$$

For the sifting to complete S_k must fall below a pre-selected threshold. The second stopping criterion suggests the sifting should complete if the number of extrema doesn't change over the course of a set number of sifts.

7.1.2 Hilbert-Huang Transform

The Hilbert-Huang transform is a combination of EMD and the Hilbert transform to provide view of the instantaneous frequencies contained in the signal. It allows a much clearer time-frequency analysis for signals composed of non-linear and non-stationary components (Huang *et al.*, 1998a).

The Hilbert transform is defined as a linear operator that creates a complex function whose real part corresponds with the original signal while the imaginary part is a progressive function of the original, *i.e.* its signal strength is zero for all frequencies less than zero.

The IMFs produced by EMD are very well behaved under the Hilbert transform making this an effective analysis method.In the next section we examine an example of a signal with stationary and non stationary components to outline the advantages of this type of analysis.

7.1.3 EMD Example

Below is a common example to test the effectiveness of EMD to remove non-stationary and nonlinear signals. First, a signal composed of a single sine wave is combined with a second sweep signal or 'Chirp'. These signals and their combination can be seen in Figure 7.1 (Rilling *et al.*, 2003).
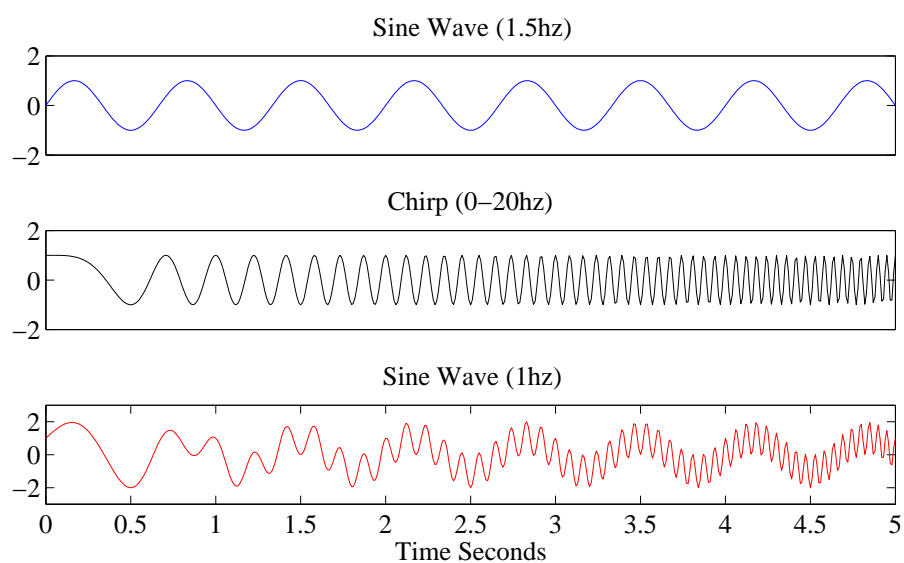
Figure 7.1: Two signals are combined to investigate the effectiveness of EMD. A simple sine wave and a chirp signal

This is a basic example of the type of signal separation EMD was designed for. Unlike many other signal decomposition methods the intrinsic mode functions tend to represent actual physical signals contained in the original.
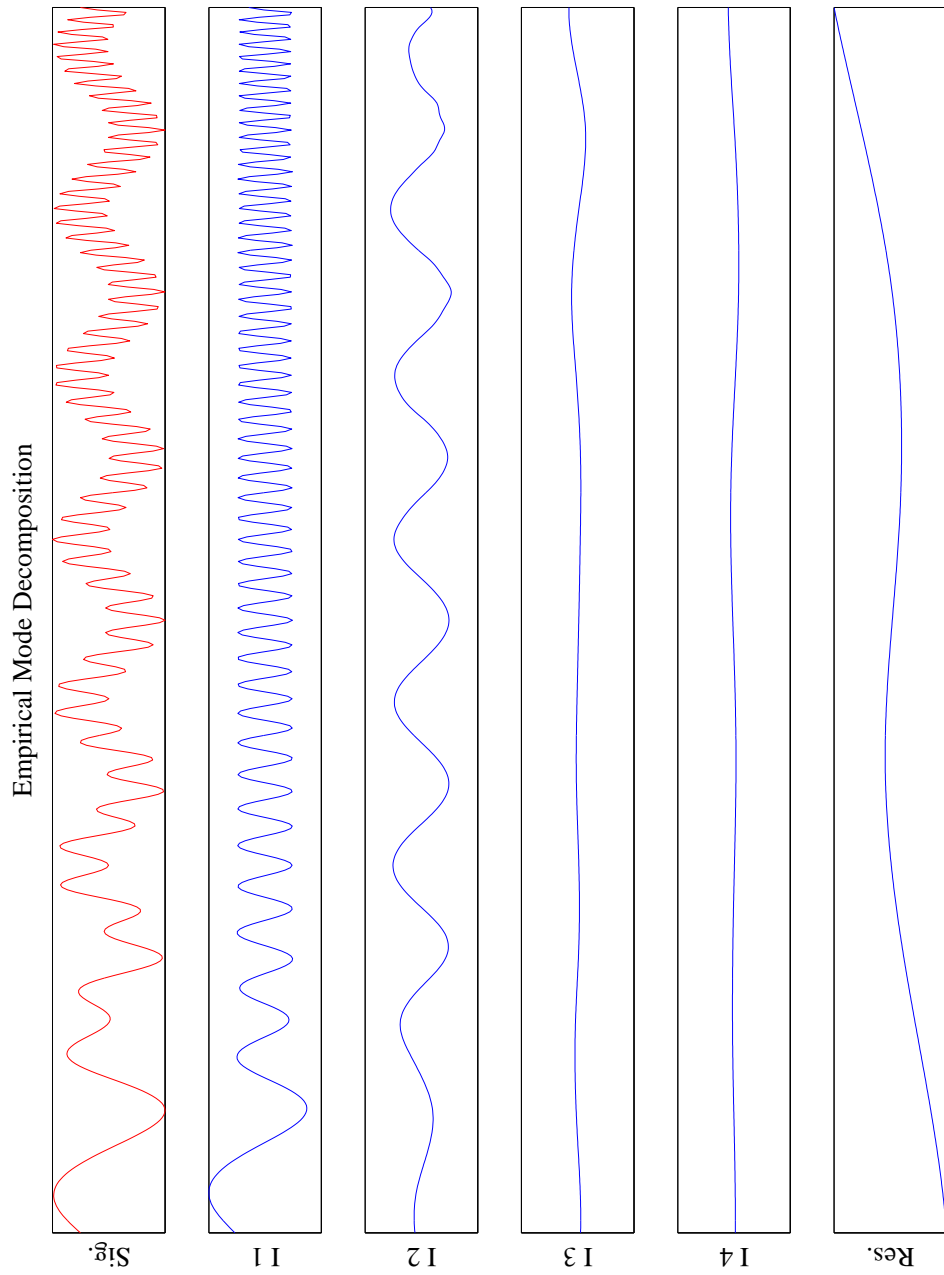
Figure 7.2: Collection of intrinsic mode functions generated from the EMD process. Analysis of the first two IMFs show the extracted original signals

(a) Short Time Fourier Transform

(b) Hilbert-Haung Transform
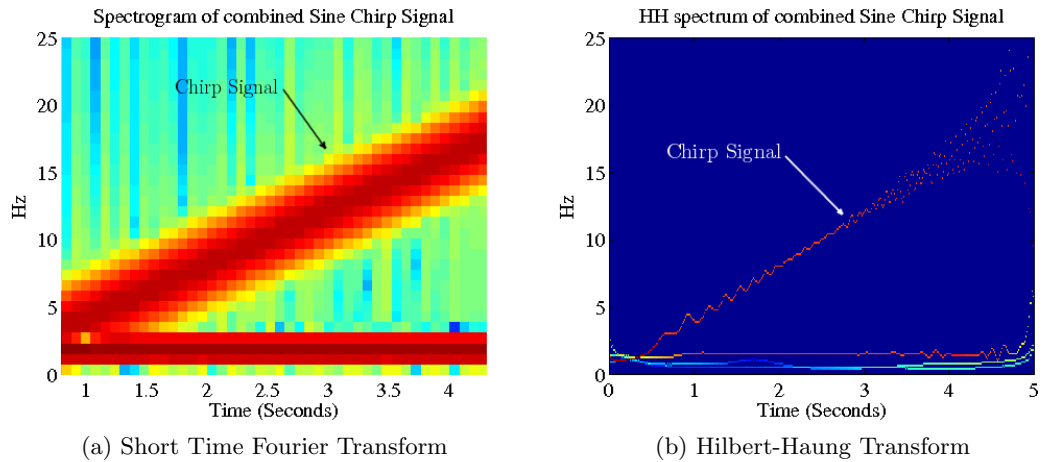
Figure 7.3: A good example of the power of EMD and Hilbert analysis. The Hilbert Huang spectrum provides a much narrower and clearer view of the time frequency components.

Figure 7.3 takes this example to it's final destination. After EMD is performed on a signal the IMFs are well behaved under the Hilbert transform. Using this property it is possible to build the time-frequency plot in Figure 7.3b. The same signal has been transformed and plotted using the short-time Fourier transform (STFT). Although it is still possible to pick out both signals from this spectrum plot they are 'smeared' in both frequency and time.

7.1.4 EMD applied to NIRS

As discussed in Chapter 3 most of the major sources of physiological interference are both non-linear and non-stationary. Although standard filtering and adaptive filtering are adequate for the removal the higher frequency components, the low frequency oscillations or Mayer waves are spectrally too close to the activation frequency for these approaches to be effective.

EMD presents a possible solution to this problem. Previous studies have been performed to examine blood pressure variations measured with an implantable catheter

in rats where EMD was an invaluable tool (Huang *et al.*, 1998b). From this point we can see the application of EMD to NIRS has two advantages. Firstly, it allows us to decompose a signal and investigate the components. The investigation can lead to a better understanding of the low frequency components. Secondly, for the application of a NIRS BCI we can use the IMFs to remove these high and low frequency components with little or no impact on the functional signal.
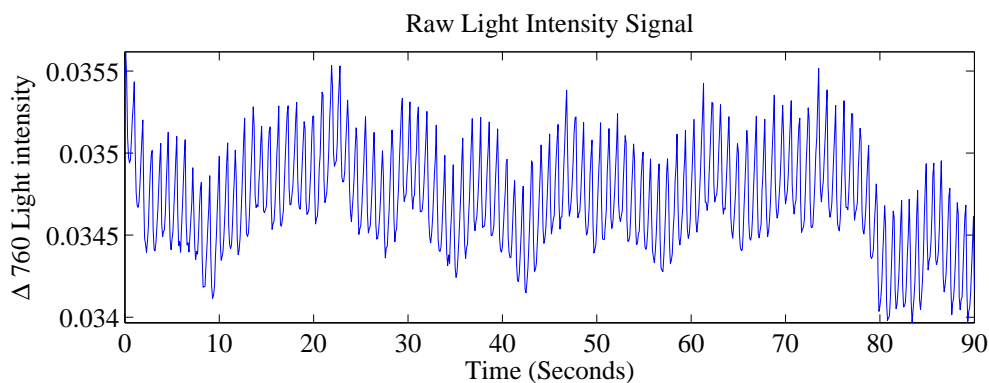
Figure 7.4: A raw light intensity gathered from under the motor area. This particular recoding is the raw 760nm optical intensity recorded from that region.

7.1.4.1 Signal Decomposition

EMD provides a comprehensive analysis tool for NIRS signals. As an example we will examine a signal of unprocessed data collected from the NIRS equipment. It is a 90 second excerpt from a initial rest-period of an experiment. From this data, presented in Figure 7.4, it is possible to discern signals like heart-beat and lower frequency oscillations.

We will first examine the information we can gather using EMD and Hilbert spectral analysis. Figure 7.5 shows the original signal, its intrinsic mode functions and the Hilbert spectrum derived from the IMFs. With this information it is possible to make a more comprehensive analysis of these lower frequency components. It may also be possible to use this approach to monitor these oscillations in real-time.
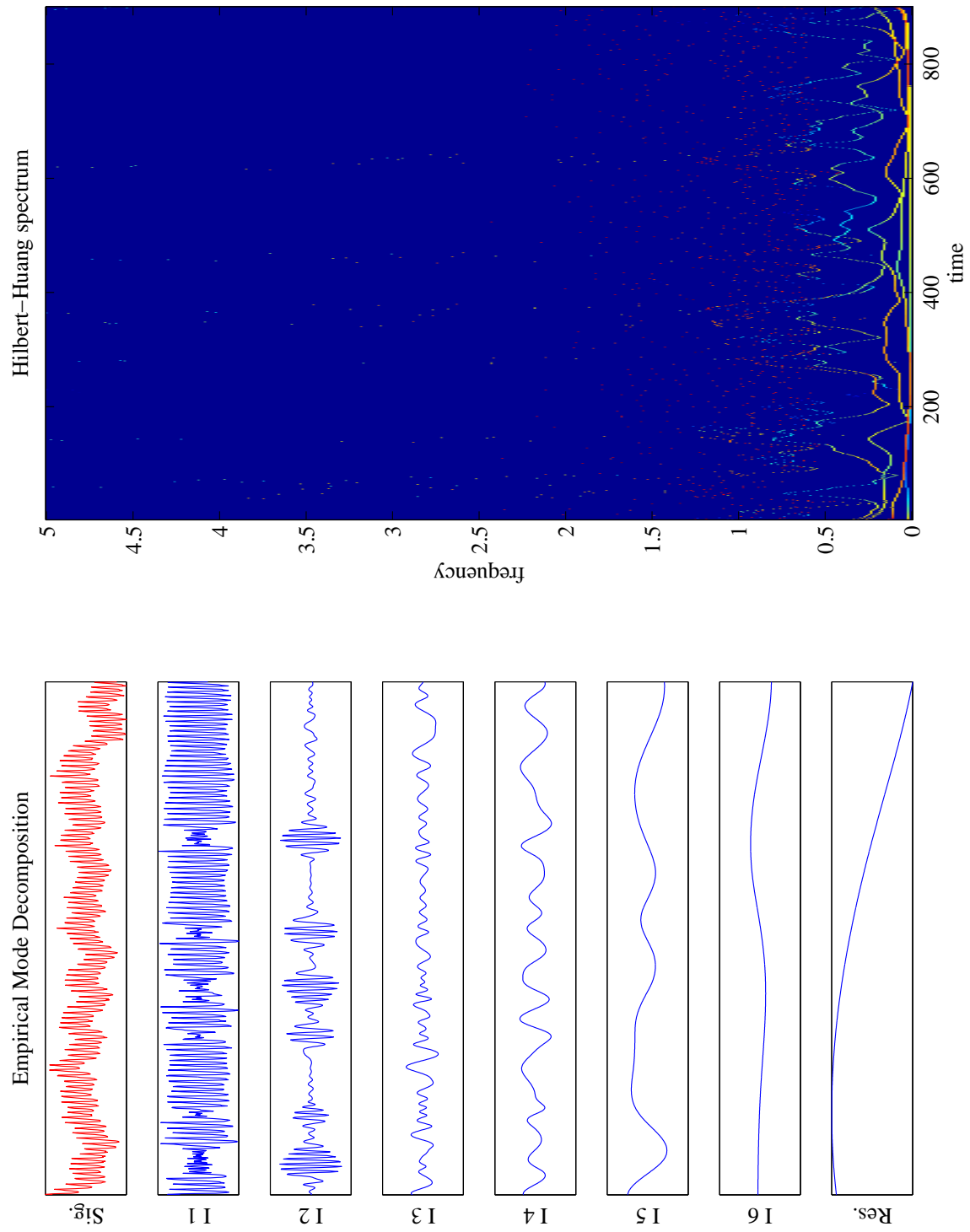
Figure 7.5: This figure displays the original signal (top Left) and its decomposed intrinsic mode functions. The plot on the left represents the instantaneous frequencies calculated using the Hilbert transforms of the IMFs.

7.1.4.2 Interference Reduction

Standard filtering for the Mayer-waves will introduce a serious attenuation to the activation signal of interest. One approach of using EMD to curtail this problem is to perform a frequency analysis of each IMF. The EMD process is tuned to remove oscillation throughout the signal. It has been shown that the IMFs containing the higher and lower frequencies unimportant to the experiment can be simply subtracted.

In this implementation an FFT is performed on each IMF. A frequency window is defined ranging from 0.1Hz to 0.8Hz. Any IMF with more that half its entire power residing within this window is kept. The rest are discarded. The results of this processing ensures that only unnecessary signals are removed.
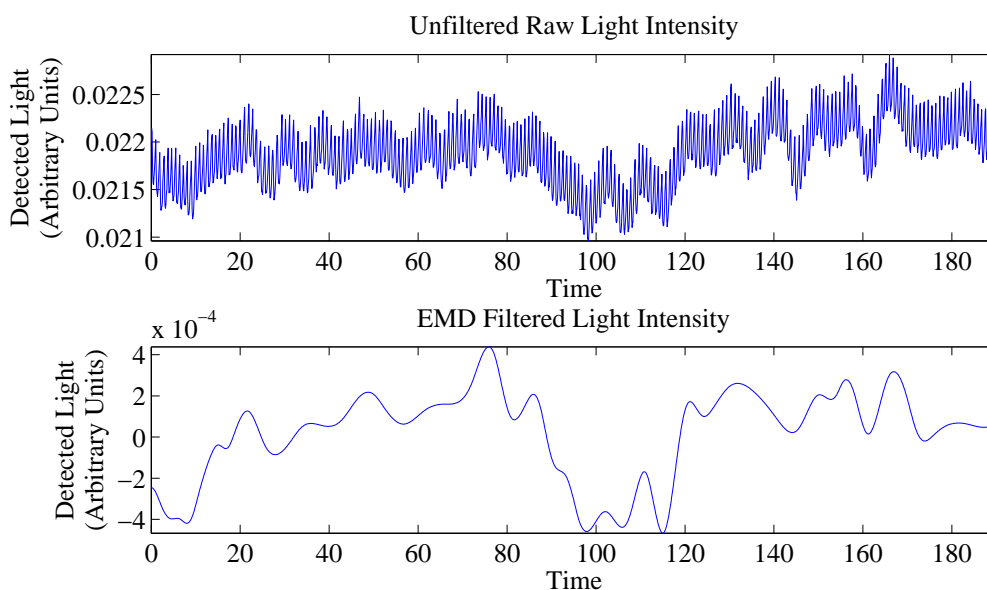
Figure 7.6: A single Raw Light channel filtered using emperical mode decomposition.

Figure 7.6 is an example of a raw NIRS signal decomposed using EMD and recombined excluding the IMFs outside the frequency band of interest.Given that EMD decomposes signals based on discernable and realistic fluctations of the raw signal the IMFs chosen to form this filtered signal more likey represent the physiological fluctions

130

induced by mental activation.
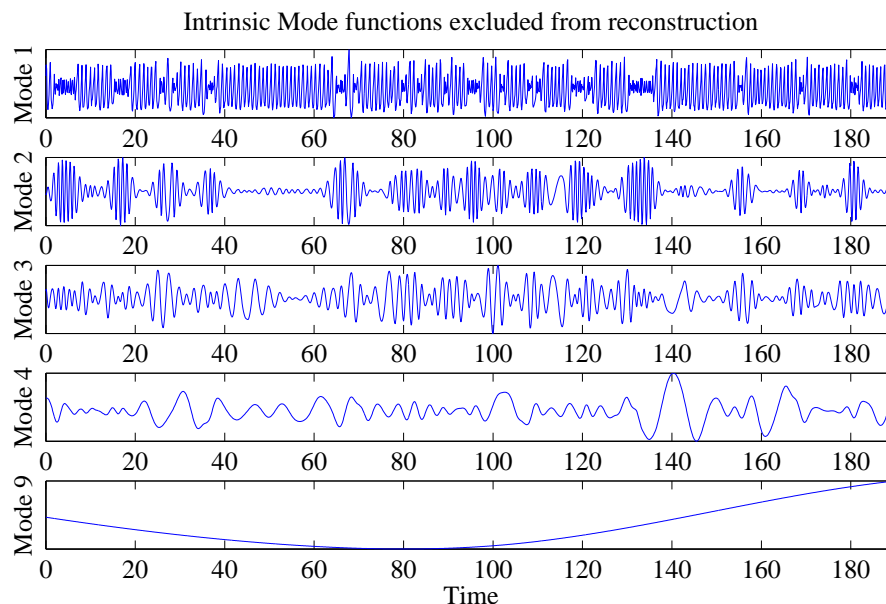
Figure 7.7: Modes exculded from reconstruction. In this example modes 1-4 are the higher frequency components while mode 9 is the a low frequency trend.

In post processing it is possible to examine those modes included and excluded from the final signal. Figure 7.7 is a plot of thos modes excluded. It is possible to discern specific singals, like heart beat (Mode 1 & 2), from these. This allows a closer a examination and analysis of the actual physiological processes involved in this interference.

7.1.4.3   Application to Single Trial Experiments

Extending the technique used in Section 7.1.4.2 it is possible to use EMD during real-time experiments. This method involves dealing locally with each activation and applying the above technique. Upon completion of a particular mental task, the raw data collected during the activation is processed using the Beer-lambert to obtain Absorber concentrations. Following this each channel is decomposed using EMD over the activation window. The signals are reconstructed excluding the IMFs outside the frequencies

of interest.
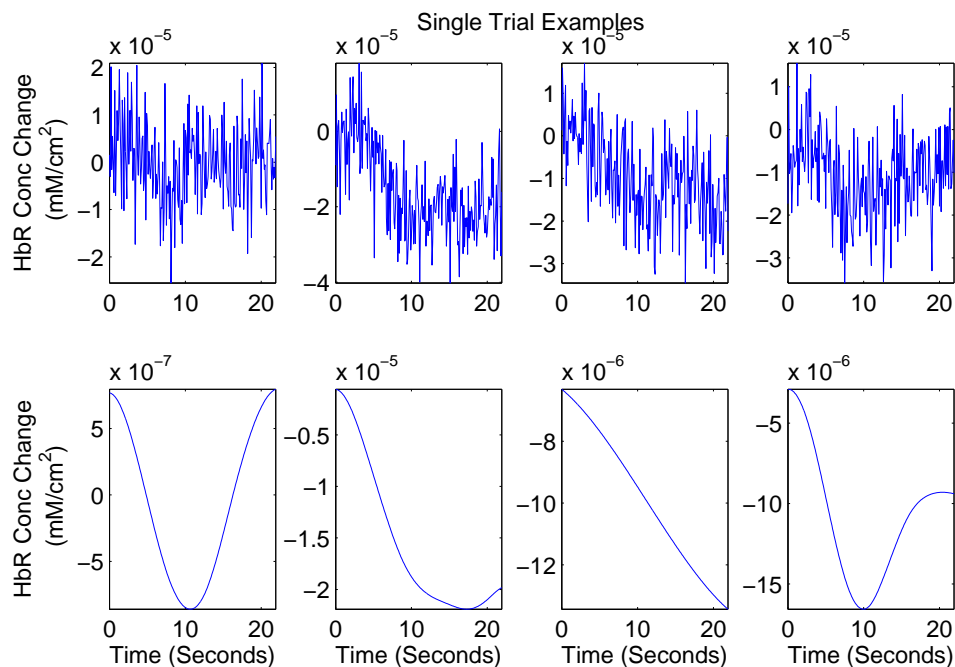
Figure 7.8: Processed HbR examples of single Trial activations. Each activation shows a distinctive reduction is HbR.

After processing these signals can then be passed to a classification system for analysis. Section 7.2 deals with this important component of the NIRS-BCI data analysis chain.

7.1.4.4 Implications

EMD offers a wide range of options in NIRS analysis. The ability to decompose the NIRS signal in a way which best represents underlying physiological processes allows significant advancment. Real-time processing using this technique for noise reduction produces the signals most closely correlated with those of interest. Further use of this technique will also bring better understanding not only to the nature of the heamodynamic activity but the sources of physiological interference as well.

7.2 Model Based signal Analysis

7.2.1 Model Creation

Mathematical models are useful in many areas of system analysis. They can be described as:

> *"A representation of the essential aspects of an existing system (or a system to be constructed) which presents knowledge of that system in usable form."* (Eykhoff, 1974).

These models are common in natural sciences, engineering and social sciences. Creating a model that attempts to simulate a particular process can help a researcher to gain further insight into how that process operates. Generally these models are designed to allow systems to be controlled, optimized or predicted. They are also used in the area of system identification. In the empirical data collected from some black box process or system is compared against a model with the aim of learning more about the underlying function of the process.

In this section we aim to create a model that simulates the expected hemodynamic activity and compare detected data from NIRS. To create a model that simulates this expected behavior it is first necessary to define the expected behavior. In the same way as fMRI analysis in Chapter 4 we must decide upon a basis for a modeled Hemodynamic response function (HRF).

After a decision is made concerning the HRF it can be convolved with a point process defined by the stimulus onset timings. Figure 7.9 is an example generated from an experiment

7.2.1.1 Response Function Comparison

The probability density function (PDF) from a Gamma distribution was used in the same manner for fMRI processing but the PDF for the normal distribution is common

Point process of stimulus onsets
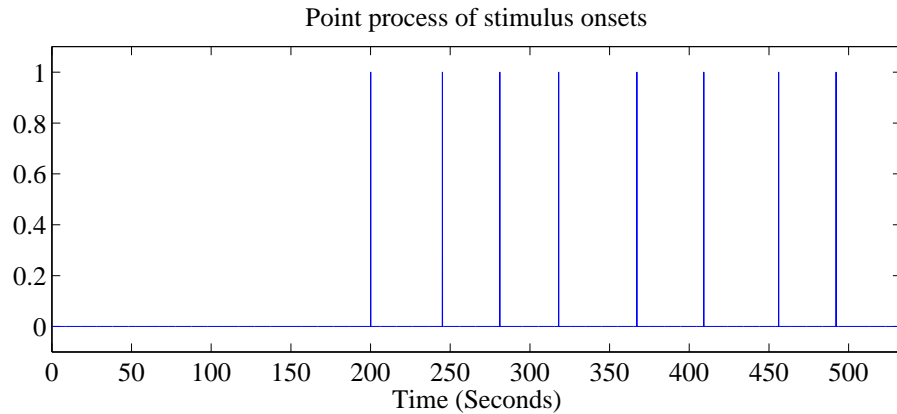
Figure 7.9: Point process created using the timings gathered from stimulus onsets. This can be convolved with a HRF kernel to simulate the data.

also.

Inverted Normal Distrubution as HRF   Inverted Gamma Distrubution as HRF
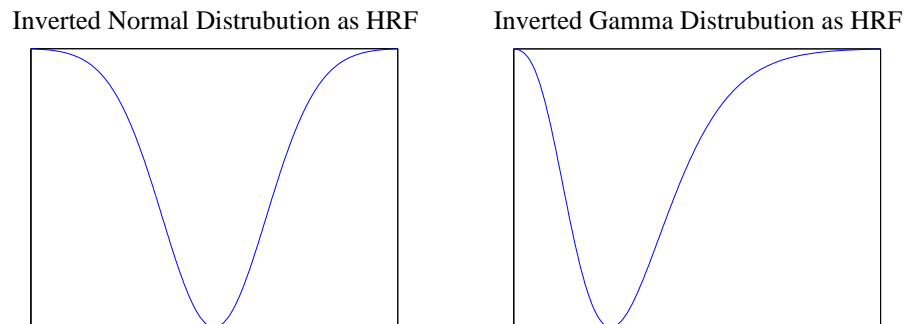
Figure 7.10: Modeled Hemodynamic Response function options. Normal distribution on right and gamma distribution on the left.

Using experimental data it is possible to validate the best choice of HRF. The experiment described here involved sixteen trials, eight overt left hand and eight right hand movement on a single subject. Optode groups were placed over the right and left hemisphere. Using the timing records of the experiment three stimulus trains were produced. The first contained a spike for all activations.

The next two were stimulus trains that contained only right hand activation (Activation 1) and left hand activation (Activation 2). Activation models representing the

134

Event related stimulus train generated with a gamma curve

Event related stimulus train generated with a normal curve

Time (seconds)
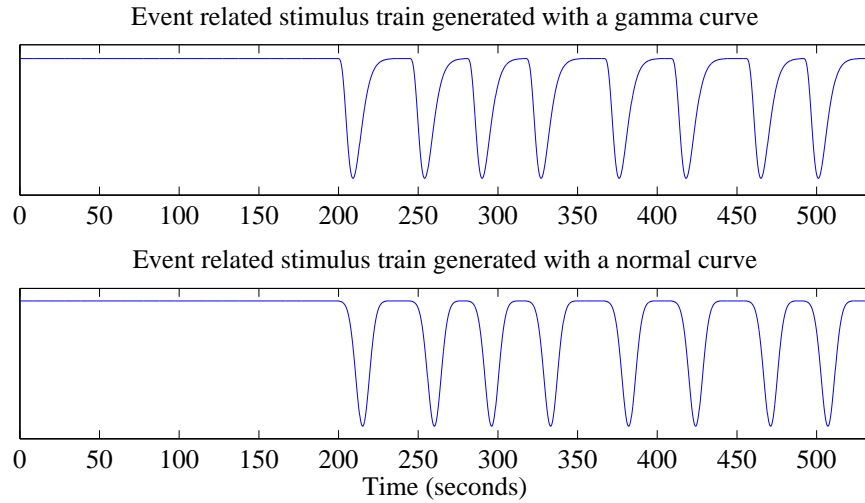
Figure 7.11: Point process derived from the timing onsets withing the experiment.

Chan	HS	Norm All	Gam All	Norm A1	Gam A1	Norm A2	GamA2
1	L	0.5266	0.5714	0.3077	0.3923	0.3053	0.3647
2	L	0.4445	0.4503	0.3928	0.3975	0.1661	0.2289
3	L	0.3852	0.4024	0.4570	0.4974	-0.0003	0.0673
4	L	0.3162	0.3411	0.2958	0.3142	0.1047	0.1605
5	R	0.2058	0.1426	0.0458	-0.0945	0.2675	0.3529
6	R	0.3641	0.3350	0.1752	0.0551	0.3425	0.4470
7	R	0.3709	0.3596	0.0510	-0.0346	0.4456	0.5466
8	R	0.3162	0.3485	0.0393	0.0127	0.3768	0.4292
9	R	0.2510	0.2798	0.0201	0.0081	0.2761	0.3470
10	R	0.0294	0.0933	-0.1346	-0.0624	0.0552	0.1410
11	R	-0.0093	-0.0095	0.0018	0.0111	-0.0247	-0.0128

Table 7.1: Results of a normalized cross-correlation between models and filtered data. HS indicates over which hemisphere channel was located. A1 is activation 1 or an Overt right hand activation. A2 is overt Left hand. Norm or Gam represent a normal or gamma based HRF

experimental data were produced when these trains were convolved with both our HRF candidates.

In the next section we shall investigate how this process can be used for optimizing the signals.
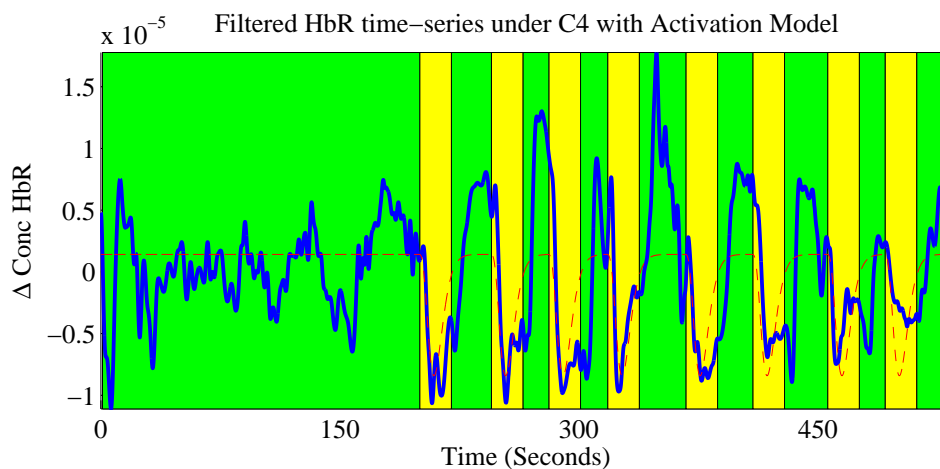
Figure 7.12: Activation model overlayed onto NIRS time-series data.

7.2.2 Optimum Source Selection

Many applications in the area use multi-variate signal analysis to achieve classification. Given correct placement of optodes and satisfactory signal detection then it is possible to use only one channel to perform this same classification. This approach significantly reduces processing overheads in comparison to multi-variate approaches

A multi-channel NIRS-BCI allows an experiment to be conducted over a much broader area of the cortex. This, as discussed in Chapter 5, helps reduce the uncertainty about optode placement and inter-subject variability in active areas. Once it's ascertained that an active area has been located then it should be possible to automatically detect the channel with the best signal. For this purpose the system implemented takes its cues from fMRI.

Using the basic model of the hemodynamic activity described above we correlate this with our recorded data. We use the Pearson product-moment correlation coefficient or Pearson's R to analyze each channel compared to the model.

Figure 7.13 is an example of this method applied to an experiment on a single subject. Optodes holders were placed over C3 and C4. Channel 1-4 are recordings from around C3 and 5-11 surround C4. From this data Channel 1 shows the strongest

Model Correlation with recorded data (* indicate p < 0.05)
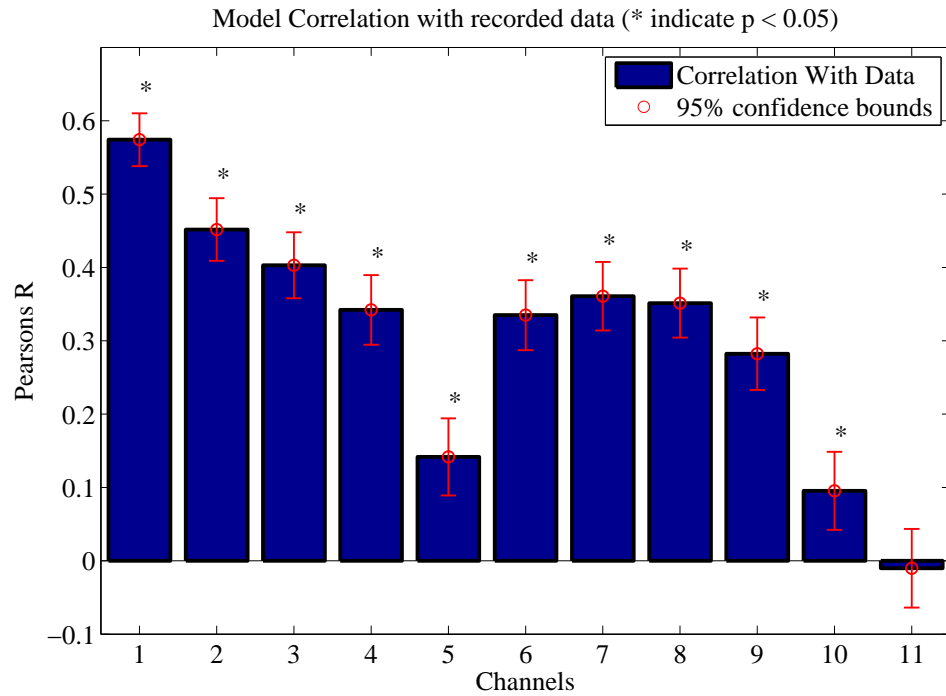
Figure 7.13: 11 Channel experiment correlated with gamma activation model. Channel 1-4 are grouped around C3 while 5-11 are around C4.

correlation to the model. For a single type of activation i.e. left hand, this method will indicate the channel with the best response.

7.2.3 Source selection & Multiple Activations

Using this same approach but applying it to a multiple activation type experiment.This has many advantages. If using a large area optet it is possible to identify relevant source-detector channels independently of knowing where exactly they are placed. Another advantage is the ability to locate the best areas for separating bi-lateralized activations.
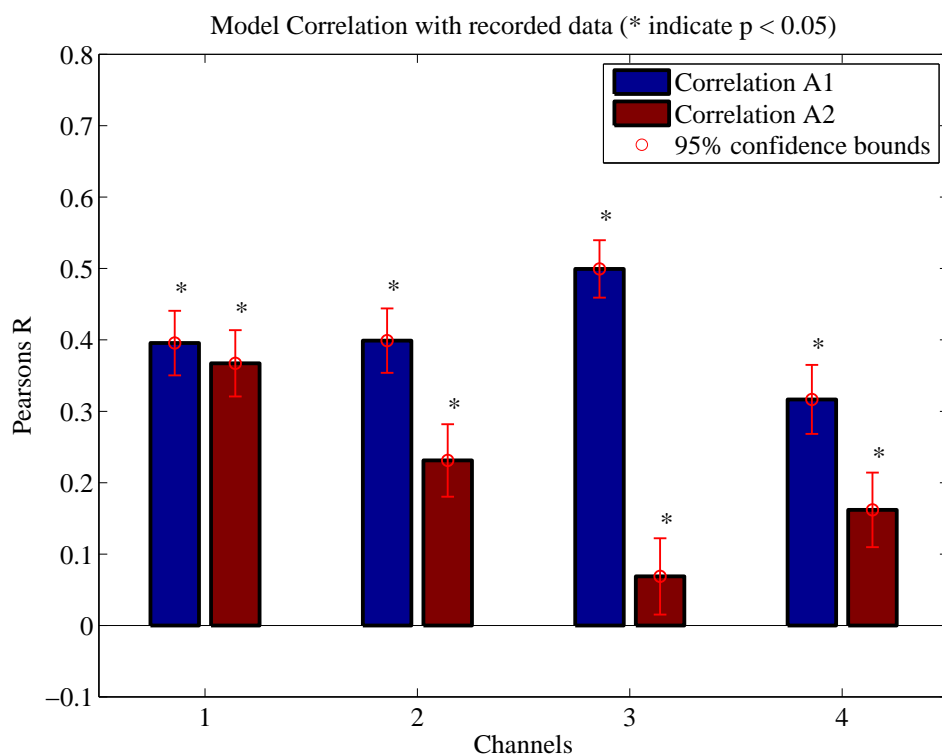
Figure 7.14: Right(A1) and Left (A2) hand activations correlated with NIRS time-series from C3

As discussed in Chapter 3 using right and left hands as separate stimulus type can prove difficult. It is certainly more difficult when the stimulus type involves the dominant hand as the both hemispheres tend to respond strongly. Using the multi-channel optodes and these multi-model approaches it is possible to identify the channels most effective at separating right from right.

Figure 7.14 is a good example. This data was recorded on the left hemisphere in

the area of C3. As the subject in this case is right-handed this is the recording from the dominant side. Channel 1 shows this bi-lateral activation as it correlates nearly equally well with both activation types. Channel 3 however shows activation 1 (Right Hand) to dominate significantly. Figure 7.16 displays the time series plots from these channels and it is possible to see the dips of activations matching the model results.
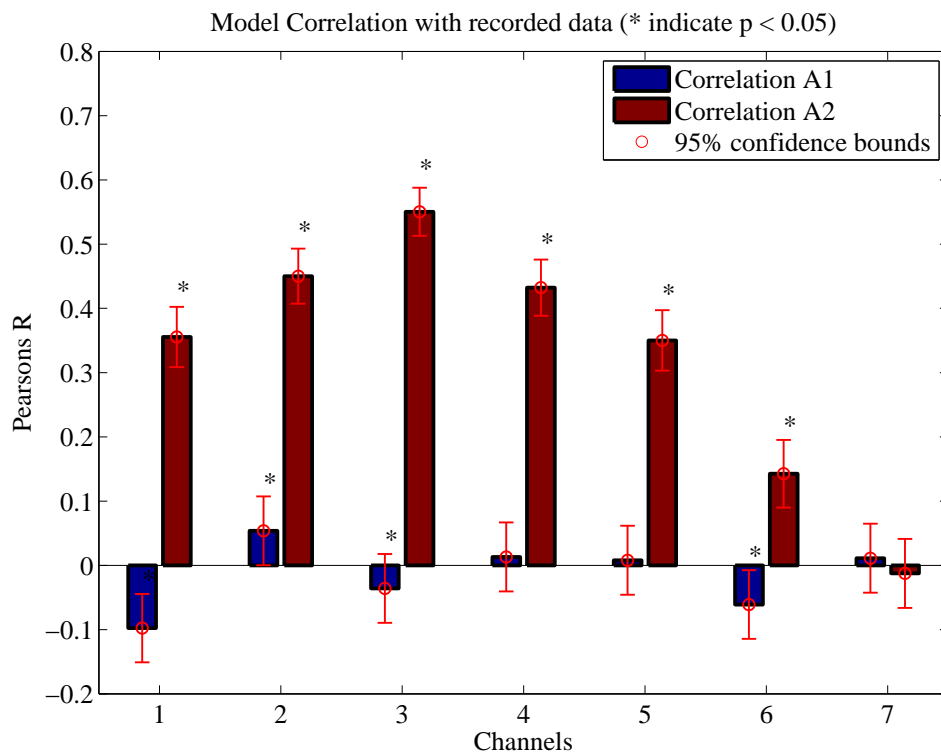
Figure 7.15: Right(A1) and Left (A2) hand activations correlated with NIRS time-series from C4

On the opposite hemisphere Figure 7.15 is more obviously dominated by left hand activation.
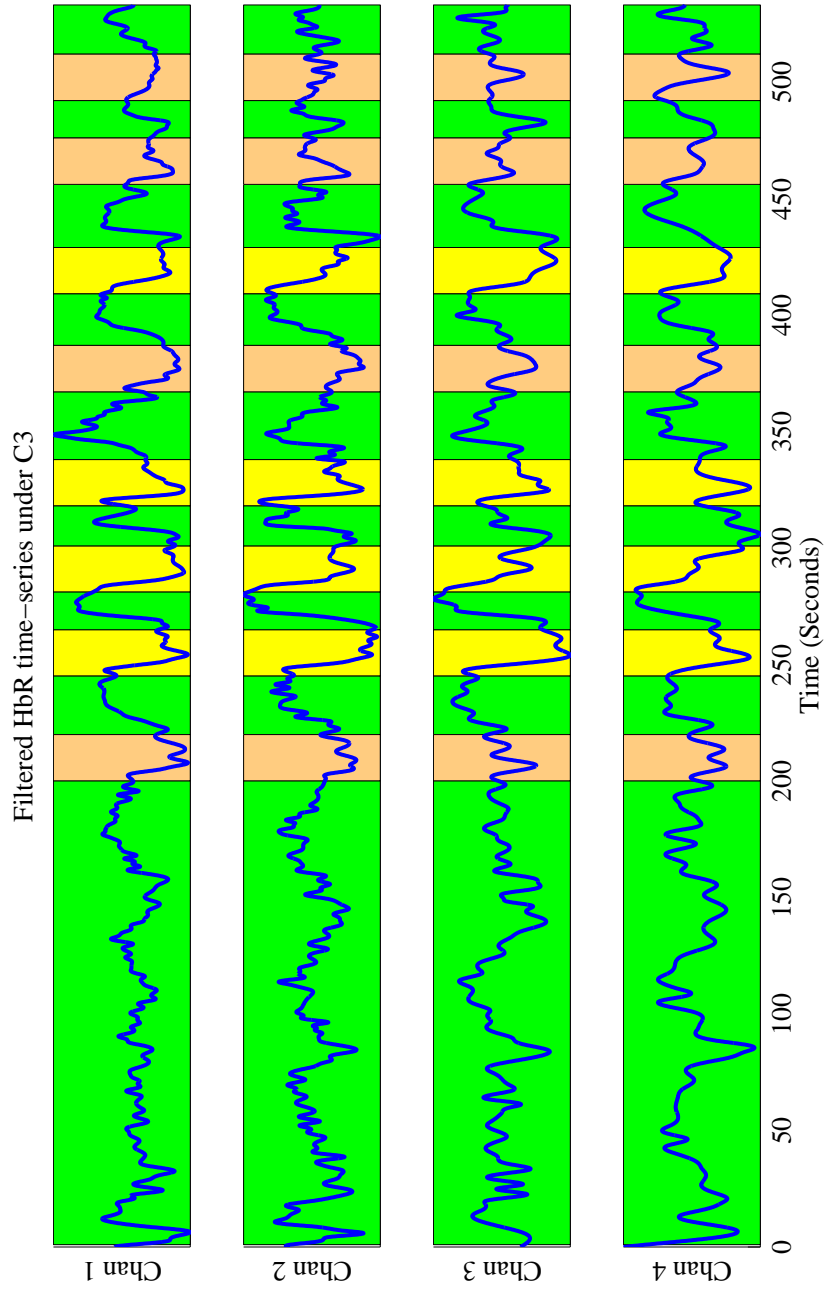
Figure 7.16: C3 time-series data. Green represents rest periods, pink represents left hand active periods and yellow is right hand active periods.

7.3 Single-Trial Classification

Having reduced the complexity of the classification problem to a single channel, it is possible to use very simple approaches in real-time. Here we will discuss and compare three methods for single trial classification.

In most cases, as discussed in detail previously, when looking at the motor strip, an activation results in in a decrease in ΔHbR. Also detected activations in ΔHbR are more highly localized that ΔHbO_2. The following section we will deal exclusively with ΔHbR activation in the motor strip but these methods are versatile enough to be applied in other locations and classification using ΔHbO_2.

7.3.1 Classification Methods

7.3.1.1 Simple Thresholding

The first approach tested is that of applying simple thresholds to the HbR concentration data. At the start of an experiment a long initial rest period is first recorded before the stimuli begin. This is to allow the subject to relax and establish a baseline of non-active readings.

In this classification method the mean and standard deviation of this long rest period are recorded. These values are then used to define the thresholds. Figure 7.17 shows an example of this classification. The samples highlighted in red are samples that fall below some threshold. This threshold is some multiple of the standard deviation below the mean. The same classification was performed on rest periods to ascertain rates of false positives.

7.3.1.2 Data Slope Analysis

An investigation of the most obvious activations identified by eye implies that during an activation ΔHbR reduces at a much higher rate than it varies during rest. It also
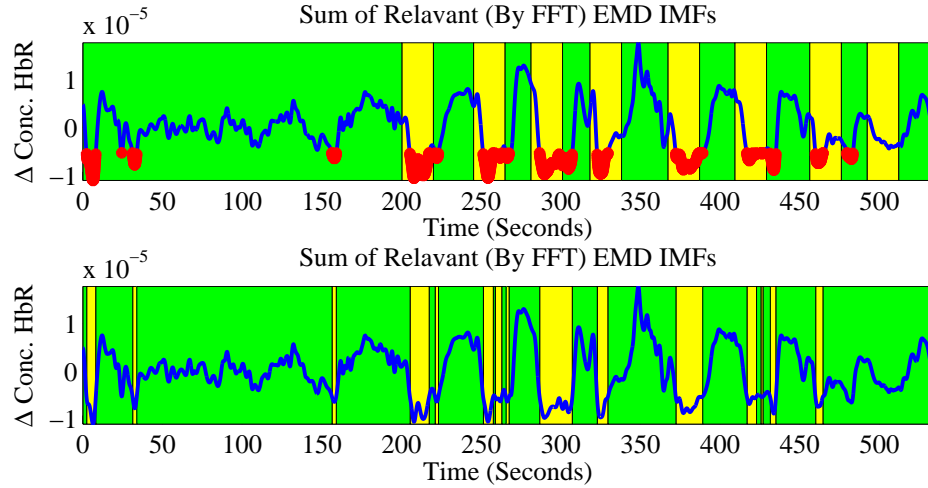
Figure 7.17: Simple threshold applied to processed data. The yellow segments of the top plot represent actual activation periods. On the bottom the yellow represents activation periods detected by the classifier.

drops for a longer period of time than its standard variation. In an attempt to take advantage of this characteristic we make an analysis of the slope of the data.

Instead of finding the empirical derivative of the whole data set we concentrate on three second windows. Three seconds is chosen because it corresponds generally with time of steepest descent at the beginning of an activation. Across this window a line is fitted using a simple LMS operation. The slope of this line is recorded. The window is moved by a single sample and the process is repeated.

After this processing is done a threshold is applied to the activation periods. Similarly to the simple thresholding, mean and standard deviation of the slope data across the rest period is recorded and thresholds are defined as multiples of the standard deviation. The same classification was performed on rest periods to ascertain rates of false positives.

7.3.1.3   Single Trial Gamma Correlation

Given the results presented in Section 7.2 an approach was developed to replicate the results in a single trial setting. Each active period was extracted and correlated with a single gamma curve. In this way it was possible to use Pearson's R value to set a threshold to classify each activation.

7.3.2   Method Comparison

7.3.2.1   Receiver Operator Characteristic Analysis
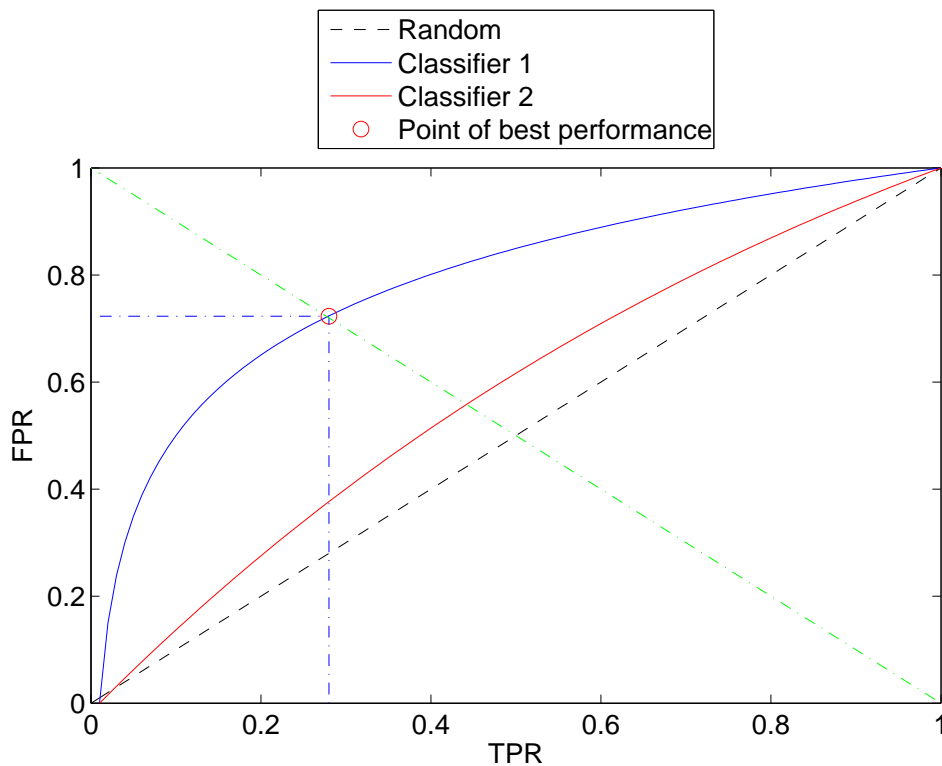
Figure 7.18: An example of ROC analysis. Classifier 1 performs better than Classifier 2. Threshold of best performance is indicated for classifier 1.

Receiver Operator Characteristic (ROC) Curves are used in signal detection theory.

They are defined as a plot of the binary classifiers sensitivity versus its specificity (1-specificity) as the specified threshold is varied (Egan, 1975; Fawcett, 2006). They have also been extended to analysing the behavoiur of medical diagnostic systems (Swets, 1988). An equivalent depiction of a ROC curve is to plot the true positive rate (TPR) against the false positive rate (FPR).

The first two advantages allow the choice of threshold of best performance and an intuitive classifier comparison. The first is achieved by finding the threshold that gives the best trade off between TPR and FPR. If a line is drawn from the top left corner of the graph to the bottom right the point where that line intersects with the curve is the threshold of best performance.

7.3.2.2   Results
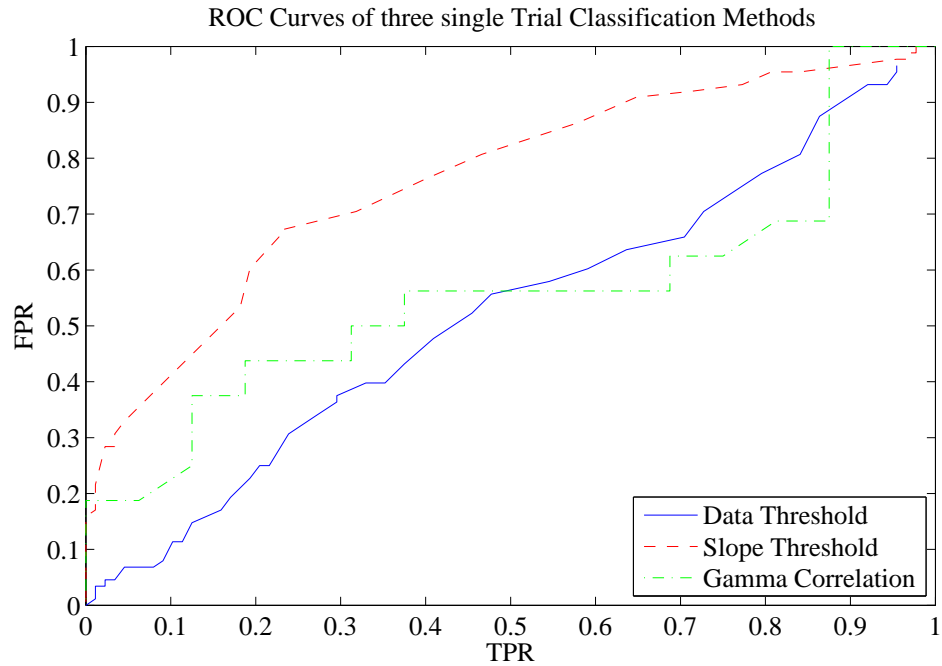
Figure 7.19: ROC curves for three classifiers

Figure 7.19 show the ROC analysis of all three methods. The results presented show that the slope analysis performed best out of the three methods.

	n	p			n	p			n	p	
p'	0.71	0.29	P'	p'	0.56	0.44	P'	p'	0.52	0.48	P'
n'	0.29	0.71	N'	n'	0.37	0.63	N'	n'	0.45	0.55	N'
	N	P			N	P			N	P	
	(a) Slope				(b) Gamma				(c) Simple Threshold		

Table 7.2

7.4   Chapter Conclusions

This chapter has examined signal processing approaches to improve system performance after demodulation. Empirical mode decomposition has provided a new foundation for

NIRS signal analysis as well as a method for the attenuation of physiological interference. It does so in a way so as to preserve the underlying sources of this interference.

Model based analysis has given the researcher in NIRS-BCI the ability to easily select optimum sources and ascertain which channels are more sensitive to different stimulus with less reference to optode placement and biological knowledge.

Finally three simple classification methods were examined for their ability to consistently identify activations in real-time.

Chapter 8

Conclusions and Future Work

This chapter reviews the contributions presented in this dissertation and suggests the directions for future research in this area.

8.1 Objectives and Contributions

8.1.1 Objectives

The objectives of this research were:

1. Evaluate current NIRS-BCI assumptions using comparable functional scanning modality.

2. Propose and implement improvements to the signal analysis and processing methods of NIRS-BCI.

8.1.2 Contributions

This dissertation detailed advances in the area of NIRS-BCI signal processing and analysis. The contributions are as follows:

1. Implementation of a robust and versatile software system to assist the research in terms of hardware control, signal acquisition, and user feedback.

2. Development and implementation of a spread spectrum communications technique that maintains sufficient signal quality for NIRS-BCI research while reducing hardware requirements.

3. Application and validation of a signal decomposition method known as empirical mode decomposition to NIRS signals to reduce homeostatic physiological interference and also aid signal analysis.

4. Adaptation of a model based analysis technique from functional magnetic resonance imaging to allow optimum channel selection and improve separation of right hand and left hand functional activity in motor cortex structures.

5. The application of novel real-time feature classification methods to the selected optimum channels.

8.2 Conclusions

The aim of this work was to re-evaluate the processes behind NIRS-BCI from first principals and establish methodologies to advance this research. This section will review the contributions outlined above in the context of the research area as a whole.

8.2.1 Problem Analysis

The initial two chapters examine the motivation and background behind this research. Specifically, Chapter 2 dealt with the physical, biological and physiological systems involved in establishing a multi-channel NIRS-BCI and its surrounding structures. The generalize model of a BCI as communication tool for severely disabled subjects was also established.

Chapter 3 outlined the current research in NIRS-BCI examining mental activation strategies, hemodynamic response to functional activation and activation locations. The importance of hardware and software systems is also highlighted as well as approaches to physiological interference reduction.

Given the information acquired in Chapter 2 and 3, Chapter 4 presents a small scale fMRI study to confirm the assumptions within the NIRS-BCI research community. This study emphasised the necessity of multi-channel approaches given the high level of inter-subject variability. The study also validated which mental activation strategies best suited NIRS-BCI.

8.2.2 Core System Development

Chapter 5 outlined the construction of a flexible and versatile NIRS-BCI system. This bespoke, multi-channel, system was designed specifically to tackle the challenges of NIRS-BCI experiments. Multi channel systems not only allow the examination of multiple functional areas but provide a better ability to select the locations of optimal response for a given activation. This approach does requires automated systems to identify optimal sources which are outlined in Section 7.2.3.

Following this, Chapter 6, outlines a robust, customizable software system designed specifically for NIRS-BCI applications. The development of a spread spectrum modulation – demodulation technique demonstrates the advantage of using such a highly configurable system. This demodulation technique aims to reduce the cost and complexity for future NIRS-BCI hardware. Results obtained in Chapter 7 in relation to source selection and classification were also highly dependant on the validity of these systems.

8.2.3 Signals Analysis and Processing

Chapter 7 presents signal processing approaches to improve post-demodulation analysis and classification systems. The non-linear and non-stationary nature of the hemo-

dynamic signals require new analysis methods to further advance this research. Empirical mode decomposition is used to both analyse and filter hemodynamic signals. It does so in a way so as to preserve the underlying sources of this interference.

The processing of the fMRI study in Chapter 4 inspired the use of similar classification methods to be applied to NIRS data. The model based analysis allows automated identification of optimum sources.

This system is also employed in discrimination between left and right hand activation. These experiments show that bi-lateral activation can interfere with this discrimination but multiple sources and optimal channel selection significantly reduces this interference.

Finally three simple classification methods were examined for their ability to consistently identify activations in real-time. Using ROC analysis it is shown that an examination of the slope of the signal during activation periods out-performs the other methods as a classifier.

8.3 Future Work

8.3.1 Clinical Evaluations

Evaluation of Motor Imagery within BCI paradigms

In section 3.1.3.2 the use of motor imagery is discussed in its relation to BCI paradigms. It has been used extensively in BCI modalities such as EEG (Beisteiner *et al.*, 1995; Neuper *et al.*, 1999), fMRI (Yoo *et al.*, 2004), and NIRS (Coyle *et al.*, 2007; Ranganatha *et al.*, 2007). Debate still surrounds the functional areas activated during motor imagery (Decety *et al.*, 1994; Roth *et al.*, 1996) but the author recommends an extensive study into its value within a BCI paradigm. Studies have shown that overt motor action in able-bodied subjects is more comfortable, keeps the subject more alert, and has higher detection rates than imagined action (van de Laar, 2009). A study

consisting of both able-bodied and disabled subjects should be used to understand if there is value in instructing able-bodied subjects to perform covert motor action.

Extension of Advances to Stroke Rehabilitation Therapies

A pilot study (Ward *et al.*, 2007) outlined the use of NIRS in conjunction with constraint induced movement therapy combined with NIRS-BCI paradigms in relation to stroke rehabilitation. This successful study highlights another possible avenue of application for the system outlined in this dissertation. The advancements outlined in this dissertation have the potential to improve the functionality of this application. There should also be an extended study of these methods with the aim of moving the research into clinical use.

8.3.2 Direct Extension of Research

Development of lower cost, dedicated NIRS-BCI systems

Section 6.3.3 outlines the use of spread-spectrum communications techniques for the purpose of optical multiplexing. The results showed that it is possible to develop NIRS-BCI systems with lower equipment specifications. This implementation would reduce costs and allow increased use in research and clinical settings.

The Use of EMD to Further Evaluate Localized Low-pressure Trends

Section 7.1 proposed and implemented EMD as a new approach to signal processing and analysis within NIRS-BCI. This decomposition method produces non-linear and non-stationary components directly linked to physiological processes. Further analysis

of these components may allow a deeper understanding of the biological processes behind the low-frequency oscillations observed in the NIRS signal.

8.4   Concluding Remarks

This dissertation describes the development of techniques for NIRS-BCI signal processing and analysis. The re-examination of the cognitive process and assumptions behind NIRS-BCI have allowed the reporting on marked differences in overt and imagined motor movement, separable functional areas, and identifying lateralized activations. The implementation of customized, versatile hardware and software systems enable the examination of new techniques that aid in standardizing NIRS-BCI paradigms.

References

ALLISON, B., WOLPAW, E. & WOLPAW, J. (2007). Braincomputer interface systems: progress and prospects. *Expert review of medical devices*, **4**, 463–474. 33

ALLISON, J., MEADOR, K., LORING, D., FIGUEROA, R. & WRIGHT, J. (2000). Functional MRI cerebral activation and deactivation during finger movement. *Neurology*, **54**, 135. 41, 57

ATTWELL, D. & IADECOLA, C. (2002). The neural basis of functional brain imaging signals. *TRENDS in Neurosciences*, **25**, 621–625. 20

BANDETTINI, P., WONG, E., HINKS, R., TIKOFSKY, R. & HYDE, J. (1992). Time course EPI of human brain function during task activation. *Magnetic Resonance in Medicine*, **25**, 390–397. 56

BAUERNFEIND, G., LEEB, R., WRIESSNEGGER, S. & PFURTSCHELLER, G. (2008). Development, set-up and first results for a one-channel near-infrared spectroscopy system. *Biomedizinische Technik*, **53**, 36–43. 45, 47, 51

BEISTEINER, R., HÖLLINGER, P., LINDINGER, G., LANG, W. & BERTHOZ, A. (1995). Mental representations of movements. brain potentials associated with imagination of hand movements. *Electroencephalogr. Clin. Neurophysiol.*, **96**, 183–93. 150

BERGER, H. (1929). Uber das elektrenkephalogramm des menschen. *Arch Psychiatr Nervenkr*, **87**, 527–570. 34

BERNE, R. & LEVY, M. (1996). *Principles of physiology*. Mosby Elsevier Health Science. 16, 18

BIGGER, J., JR, FLEISS, J., STEINMAN, R., ROLNITZKY, L., KLEIGER, R. & ROTTMAN, J. (1992). Frequency domain measures of heart period variability and mortality after myocardial infarction. *Circulation*, **85**, 164. 51

BILLINGSLEY, P. (2008). *Probability and measure*. Wiley India Pvt. Ltd. 63

BOAS, D.A., CHEN, K., GREBERT, D. & FRANCESCHINI, M.A. (2004). Improving the diffuse optical imaging spatial resolution of the cerebral hemodynamic response to brain activation in humans. *Opt Lett*, **29**, 1506–8. 85

BOSO, M., POLITI, P., BARALE, F. & ENZO, E. (2006). Neurophysiology and neurobiology of the musical experience. *Functional neurology*, **21**, 187. 38

BOZKURT, A. & ONARAL, B. (2004). Safety assessment of near infrared light emitting diodes for diffuse optical measurements. *Biomed Eng Online*, **3**, 9. 81

BRODMANN, K. (1994). Localisation in the cerebral cortex. *Smith-Gordon, London*. 64

BUSHBERG, J., SEIBERT, J., LEIDHOLDT JR, E. & BOONE, J. (2002). *The essential physics of medical imaging*. Williams & Wilkins. 21

CAO, Y., D'OLHABERRIAGUE, L., VIKINGSTAD, E., LEVINE, S. & WELCH, K. (1998). Pilot study of functional MRI to assess cerebral activation of motor function after poststroke hemiparesis. *Stroke*, **29**, 112. 57

CHAPPELL, M. (1985). Effects of ambient temperature and altitude on ventilation and gas exchange in deer mice (Peromyscus maniculatus). *Journal of Comparative Physiology B: Biochemical, Systemic, and Environmental Physiology*, **155**, 751–758. 15

CIUCIU, P., POLINE, J., MARRELEC, G., IDIER, J., PALLIER, C. & BENALI, H. (2003). Unsupervised robust non-parametric estimation of the hemodynamic response function for any fMRI experiment. *IEEE Transactions on medical imaging*, **22**, 1235–1251. 62

CLARK, S.A. (1997). *Design of pulse oximeters*, chap. 1. Taylor & Francis. 15

COHEN, M., KOSSLYN, S., BREITER, H., DIGIROLAMO, G., THOMPSON, W., ANDERSON, A., BOOKHEIMER, S., ROSEN, B. & BELLIVEAU, J. (1996). Changes in cortical activity during mental rotation A mapping study using functional MRI. *Brain*, **119**, 89. 44

COOLEY, R.L., MONTANO, N., COGLIATI, C., VAN DE BORNE, P., RICHENBACHER, W., OREN, R. & SOMERS, V.K. (1998). Evidence for a central origin of the low-frequency oscillation in RR-interval variability. *Circulation*, **98**, 556–61. 52

COPE, M. (1991). *The application of Near Infrared Spectroscopy to noninvasive monitering of cerebral oxygenation in the newborn infant*. Ph.D. thesis, Univerestiy College London, London, England. 27, 29

COYLE, S. (2005). *Near-Infrared Spectroscopy for Brain Computer Interfacing*. Ph.D. thesis, National University of Ireland, Maynooth. 29, 31, 32, 38, 39, 40, 41, 43, 47, 56, 71, 72, 75, 76, 82, 83, 88, 103, 106

COYLE, S., WARD, T. & MARKHAM, C. (2004a). Physiological noise in near-infrared spectroscopy: Implications for optical brain computer interfacing. In *The 26th Annual International Conference of the IEEE Engineering in Medicine and Biology Society*, San Francisco, CA. 42, 53, 76, 77, 78

COYLE, S., WARD, T., MARKHAM, C. & MCDARBY, G. (2004b). On the suitability of near-infrared (NIR) systems for next-generation brain-computer interfaces. *Physiol. Meas.*, **25**, 815–22. 1, 2, 76

COYLE, S.M., WARD, T.E. & MARKHAM, C.M. (2007). Brain-computer interface using a simplified functional near-infrared spectroscopy system. *Journal of Neural Engineering*, **4**, 219–226. 52, 53, 76, 150

CRAMER, S., FINKLESTEIN, S., SCHAECHTER, J., BUSH, G. & ROSEN, B. (1999). Activation of distinct motor cortex regions during ipsilateral and contralateral finger movements. *Journal of neurophysiology*, **81**, 383. 42, 68

CURTIS, H. & BARNES, N. (1989). Biology (5th edn). *Worth, New York*. 15

DALE, A. (1999). Optimal experimental design for event-related fMRI. *Human brain mapping*, **8**, 109–114. 59

DAMADIAN, R., GOLDSMITH, M. & MINKOFF, L. (1977). NMR in cancer: XVI. FONAR image of the live human body. *Physiological chemistry and physics*, **9**, 97. 20

DE VILLOTA, E., CARMONA, M., RUBIO, J. & DE ANDRÉS, S. (1981). Equality of the in vivo and vitro in oxygen-binding capacity of haemoglobin of patients with severe respiratory disease. *British Journal of Anaesthesia*, **53**, 1325. 15

DECETY, J., PERANI, D., JEANNEROD, M., BETTINARDI, V., TADARY, B., WOODS, R., MAZZIOTTA, J. & FAZIO, F. (1994). Mapping motor representations with positron emission tomography. 44, 150

DEVOR, A., TIAN, P., NISHIMURA, N., TENG, I., HILLMAN, E., NARAYANAN, S., ULBERT, I., BOAS, D., KLEINFELD, D. & DALE, A. (2007). Suppressed neuronal activity and concurrent arteriolar vasoconstriction may explain negative blood oxygenation level-dependent signal. *Journal of Neuroscience*, **27**, 4452. 40

DICKERSON, R. & GEIS, I. (1983). *Hemoglobin: structure, function, evolution, and pathology*. Benjamin-Cummings Publishing Company. 15

DINAN, E. & JABBARI, B. (1998). Spreading codes for direct sequence CDMA and wideband CDMA cellular networks. *IEEE communications magazine*, **36**, 48–54. 111

DIXON, R. (1994). *Spread spectrum systems: with commercial applications*. John Wiley & Sons, Inc. New York, NY, USA. 102

DUNCAN, A., MEEK, J.H., CLEMENCE, M., ELWELL, C.E., TYSZCZUK, L., COPE, M. & DELPY, D. (1995). Optical pathlength measurements on adult head, calf and forearm and the head of the newborn infant using phase resolved optical spectroscopy. *Physics in Medicine and Biology*, **40**, 295–304. 30

EDVINSSON, L., MACKENZIE, E. & MCCULLOCH, J. (2002). *Cerebral blood flow and metabolism*. Lippincott Williams & Wilkins Philadelphia, PA. 31

EGAN, J. (1975). Signal detection theory and {ROC} analysis. 144

ELWELL, C.E., SPRINGETT, R., HILLMAN, E. & DELPY, D.T. (1999). Oscillations in cerebral haemodynamics: Implications for functional activation studies. *Adv Exp Med Biol*, **471**, 57–65. 52, 87

ERSLAND, L., ROSÉN, G., LUNDERVOLD, A., SMIEVOLL, A., TILLUNG, T. & SUNDBERG, H. (1996). Phantom limb imaginary fingertapping causes primary motor cortex activation: an fMRI study. *Neuroreport*, **8**, 207. 57

EVERDELL, N.L., GIBSON, A.P., TULLIS, I.D.C., VAITHIANATHAN, T., HEBDEN, J.C. & DELPY, D.T. (2005). A frequency multiplexed near-infrared topography system for imaging functional activation in the brain. *Review of Scientific Instruments*, **76**, 093705. 78, 103, 106

EYKHOFF, P. (1974). System identification: parameter and state estimation. *Chichester, England*. 133

FAWCETT, T. (2006). An introduction to ROC analysis. *Pattern recognition letters*, **27**, 861–874. 144

FRIEDLAND, R. & IADECOLA, C. (1991). Roy and Sherrington (1890): a centennial reexamination of "On the regulation of the blood-supply of the brain". *Neurology*, **41**, 10–4. 20

FRISTON, K., HOLMES, A., WORSLEY, K., POLINE, J., FRITH, C., FRACKOWIAK, R. *et al.* (1995). Statistical parametric maps in functional imaging: a general linear approach. *Hum Brain Mapp*, **2**, 189–210. 61

GELLER, A., SCHLEIFER, I., SEDERBERG, P., JACOBS, J. & KAHANA, M. (2007). PyEPL: A cross-platform experiment-programming library. *Behavior Research Methods*, **39**, 950. 58

GOLOMB, S. (1981). *Shift register sequences*. Aegean Park Press Laguna Hills, CA, USA. 109

GRATTON, G. & CORBALLIS, P.M. (1995). Removing the heart from the brain: Compensation for the pulse artifact in the photon migration signal. *Psychophysiology*, **32**, 292–9. 52

GRAY, H. (1918). *Anatomy of the Human Body*. Lea & Febiger. 8, 9, 10

GUGER, C., SCHLÖGL, A., NEUPER, C., WALTERSPACHER, D., STREIN, T. & PFURTSCHELLER, G. (2001). Rapid prototyping of an EEG-based brain-computer interface (BCI). *IEEE Transations On Neural Systems And Rehabilitation Engineering*, **9**, 49–58. 33

HAIHONG, Z. & CUNTAI, G. (2006). A kernel-based signal localization method for nirs brain-computer interfaces. In *ICPR '06: Proceedings of the 18th International Con-*

ference on Pattern Recognition, 1158–1161, IEEE Computer Society, Washington, DC, USA. 74

HAMEL, E. (2004). Cholinergic modulation of the cortical microvascular bed. *Progress in Brain Research*, **145**, 171–178. 20

HARDER, D., ALKAYED, N., LANGE, A., GEBREMEDHIN, D. & ROMAN, R. (1998). Functional hyperemia in the brain: hypothesis for astrocyte-derived vasodilator metabolites. *Stroke*, **29**, 229. 20

HELLESETH, T. & KUMAR, P. (1999). Pseudonoise sequences. *The Mobile Communications Handbook*. 109

HILL, N.J., LAL, T.N., SCHRODER, M., HINTERBERGER, T., WILHELM, B., NIJBOER, F., MOCHTY, U., WIDMAN, G., ELGER, C., SCHOLKOPF, B., KUBLER, A. & BIRBAUMER, N. (2006). Classifying EEG and ECoG signals without subject training for fast BCI implementation: comparison of nonparalyzed and completely paralyzed subjects. *IEEE Trans Neural Syst Rehabil Eng*, **14**, 183–186, comparative Study. 33

HINTERBERGER, T., WEISKOPF, N., VEIT, R., WILHELM, B., BETTA, E. & BIRBAUMER, N. (2004). An EEG-driven brain-computer interface combined with functional magnetic resonance imaging(fMRI). *IEEE Transactions on Biomedical Engineering*, **51**, 971–974. 48

HIRTH, C., OBRIG, H., VILLRINGER, K., THIEL, A., BERNARDING, J., MUHLNICKEL, W., FLOR, H., DIRNAGL, U. & VILLRINGER, A. (1996). Non-invasive functional mapping of the human motor cortex using near-infrared spectroscopy. *Neuroreport*, **7**, 1977. 83

HOMAN, R.W., HERMAN, J. & PURDY, P. (1987). Cerebral location of international 10-20 system electrode placement. *Electroencephalogr Clin Neurophysiol*, **66**, 376–82. 40, 42

HUANG, N., SHEN, Z., LONG, S., WU, M., SHIH, H., ZHENG, Q., YEN, N., TUNG, C. & LIU, H. (1998a). The empirical mode decomposition and the Hilbert spectrum for nonlinear and non-stationary time series analysis. *Proceedings: Mathematical, Physical and Engineering Sciences*, **454**, 903–995. 122, 124

HUANG, W., SHEN, Z., HUANG, N. & FUNG, Y. (1998b). Engineering analysis of biological variables: an example of blood pressure over 1 day. *Proceedings of the National Academy of Sciences*, **95**, 4816. 128

HUMPHREYS, K. (2007). *An investigation of remote non-contact photoplethysmography and pulse oximetry*. Ph.D. thesis, National University of Ireland, Maynooth, IRL. 28, 106, 107

HUPPERT, T. (2006). HomER nirs analysis software. This is an electronic document. Date retrieved: May 28, 2007. 48, 49, 52, 54, 101

HUPPERT, T., HOGE, R., DIAMOND, S., FRANCESCHINI, M. & BOAS, D. (2006). A temporal comparison of BOLD, ASL, and NIRS hemodynamic responses to motor stimuli in adult humans. *Neuroimage*, **29**, 368–382. 47

HWANG, H., KWON, K. & IM, C. (2009). Neurofeedback-based motor imagery training for brain–computer interface (BCI). *Journal of Neuroscience Methods*, **179**, 150–156. 40

INOUYE, T., SHINOSAKI, K., IYAMA, A. & MATSUMOTO, Y. (1993). Localization of activated areas and directional eeg patterns during mental arithmetic. *Electroencephalography and Clinical Neurophysiology*, **86**, 224 – 230. 38

IZZETOGLU, M., DEVARAJ, A., BUNCE, S. & ONARAL, B. (2005). Motion artifact cancellation in nir spectroscopy using wiener filtering. *Biomedical Engineering, IEEE Transactions on*, **52**, 934– 938. 54

JALONEN, J. (1981). Oxygen transportation in the blood. *Annals of clinical research*, **13**, 39. 13

JASPER, H. (1983). The ten-twenty electrode system of the International Federation. *Recommendations for the Practice of Clinical Neurophysiology*, 3. 34, 40

JEANNEROD, M. (1995). Mental imagery in the motor context. *Neuropsychologia*, **33**, 1419–1432. 44

JOBSIS, F.F. (1977). Noninvasive infrared monitoring of cerebral and myocardial oxygen sufficiency and circulatory parameters. *Science*, **198**, 1264–7. 1, 27

KANDEL, E., SCHWARTZ, J., JESSELL, T., MACK, S. & DODD, J. (1991). *Principles of neural science*. Elsevier New York. 11, 13

KANDEL, E., SCHWARTZ, J. & JESSELL, T. (2000). Principals of neural science. 10

KATO, T. (2004). Principle and technique of nirs-imaging for human brain force: fast-oxygen response in capillary event. *International Congress Series*, 85–90. 40

KIM, S., ASHE, J., HENDRICH, K., ELLERMANN, J., MERKLE, H., UGURBIL, K. & GEORGOPOULOS, A. (1993). Functional magnetic resonance imaging of motor cortex: hemispheric asymmetry and handedness. *Science*, **261**, 615–617. 67, 69

KRUSIENSKI, D., SCHALK, G., MCFARLAND, D. & WOLPAW, J. (2007). A-Rhythm Matched Filter for Continuous Control of a Brain-Computer Interface. *IEEE Transactions on Biomedical Engineering*, **54**, 273. 48

LAUTERBUR, P. (1973). Image formation by induced local interactions: examples employing nuclear magnetic resonance. *Nature*, **242**, 190–191. 20

LEUTHARDT, E., MILLER, K., SCHALK, G., RAO, R. & OJEMANN, J. (2006). Electrocorticography-based brain computer interface-the Seattle experience. *IEEE Transactions on Neural Systems and Rehabilitation Engineering*, **14**, 194. 48

LOGOTHETIS, N. (2003). MR imaging in the non-human primate: studies of function and of dynamic connectivity. *Current opinion in neurobiology*, **13**, 630–642. 35

MACDONELL, R.A.L., JACKSON, G.D., CURATOLO, J.M., ABBOTT, D.F., BERKOVIC, S.F., CAREY, L.M., SYNGENIOTIN, A., FABINYI, G.C. & SCHEFFER, I.E. (1999). Motor cortex localization using functional MRI and transcranial magnetic stimulation. *Neurology*, **53**, 1462–. 64

MARDIA, K., KENT, J., BIBBY, J. *et al.* (1979). *Multivariate analysis*. Academic press London. 61

MARIEB, E. (2003). *Essentials of human anatomy & physiology*. Benjamin Cummings. 11

MARTIN, G. (2006). *Human neuropsychology*. Prentice Hall. 10

MASON, S., BASHASHATI, A., FATOURECHI, M., NAVARRO, K. & BIRCH, G. (2007). A comprehensive survey of brain interface technology designs. *Annals of Biomedical Engineering*, **35**, 137–169. 33

MATTHEWS, F., PEARLMUTTER, B., WARD, T., SORAGHAN, C. & MARKHAM, C. (2008a). Hemodynamics for brain-computer interfaces. *Signal Processing Magazine, IEEE*, **25**, 87–94. 2

MATTHEWS, F., SORAGHAN, C., WARD, T., MARKHAM, C. & PEARLMUTTER, B. (2008b). Software platform for rapid prototyping of NIRS brain computer interfacing techniques. In *Conference proceedings:... Annual International Conference of the*

IEEE Engineering in Medicine and Biology Society. IEEE Engineering in Medicine and Biology Society. Conference, vol. 1, 4840. 2, 49, 92

MAYHEW, J.E.W. (2003). Neuroscience: A Measured Look at Neuronal Oxygen Consumption. *Science*, **299**, 1023–1024. 39

MAZZIOTTA, J.C., TOGA, A.W., EVANS, A., FOX, P. & LANCASTER, J. (1995). A probabilistic atlas of the human brain: Theory and rationale for its development : The international consortium for brain mapping (icbm). *NeuroImage*, **2**, 89 – 101. 64

MISULIS, K. & SPEHLMANN, R. (1994). *Spehlmann's evoked potential primer: visual, auditory, and somatosensory evoked potentials in clinical diagnosis*. Butterworth-Heinemann Medical. 35

MIYAI, I., TANABE, H., SASE, I., EDA, H., ODA, I., KONISHI, I., TSUNAZAWA, Y., SUZUKI, T., YANAGIDA, T. & KUBOTA, K. (2001). Cortical mapping of gait in humans: a near-infrared spectroscopic topography study. *Neuroimage*, **14**, 1186–1192. 47

NAITO, M., MICHIOKA, Y., OZAWA, K., ITO, Y., KIGUCHI, M. & KANAZAWA, T. (2007). A communication means for totally locked-in ALS patients based on changes in cerebral blood volume measured with near-infrared light. *IEICE TRANSACTIONS on Information and Systems*, **90**, 1028–1037. 38, 45

NEUPER, C., SCHLÖGL, A. & PFURTSCHELLER, G. (1999). Enhancement of left-right sensorimotor EEG differences during feedback-regulated motor imagery. *J. Clin. Neurophysio*, **16**, 373–82. 150

NICHOLLS, J., MARTIN, A., WALLACE, B. & KUFFLER, S. (1992). *From neuron to brain: a cellular and molecular approach to the function of the nervous system*. Sinauer Associates. 12, 13

OGAWA, S. & LEE, T. (1990). Magnetic resonance imaging of blood vessels at high fields: in vivo and in vitro measurements and image simulation. *Magnetic Resonance in Medicine*, **16**, 9–18. 26, 56

OGAWA, S., LEE, T., NAYAK, A. & GLYNN, P. (1990). Oxygenation-sensitive contrast in magnetic resonance image of rodent brain at high magnetic fields. *Magn Reson Med*, **14**, 68–78. 26

OKADA, E. & DELPY, D. (2003). Near-infrared light propagation in an adult head model. I. Modeling of low-level scattering in the cerebrospinal fluid layer. *Applied optics*, **42**, 2906–2914. 28, 71

OKADA, E., FIRBANK, M., SCHWEIGER, M., ARRIDGE, S., COPE, M. & DELPY, D. (1997). Theoretical and experimental investigation of near-infrared light propagation in a model of the adult head. *Applied optics*, **36**, 21–31. 28

OKUI, N. & OKADA, E. (2005). Wavelength dependence of crosstalk in dual-wavelength measurement of oxy-and deoxy-hemoglobin. *Journal of Biomedical Optics*, **10**, 011015. 81

OLDFIELD, R. (1971). The assessment and analysis of handedness: the Edinburgh inventory. *Neuropsychologia*, **9**, 97–113. 58

PASLEY, B.N. & FREEMAN, R.D. (2008). Neurovascular coupling. *Scholarpedia*, **3**, 5340. 19

PFURTSCHELLER, G., LEEB, R., KEINRATH, C., FRIEDMAN, D., NEUPER, C., GUGER, C. & SLATER, M. (2006). Walking from thought. *Brain Research*, **1071**, 145–52. 33

POOLEY, R.A. (2005). Fundamental Physics of MR Imaging. *Radiographics*, **25**, 1087–1099. 25

PORRO, C.A., FRANCESCATO, M.P., CETTOLO, V., DIAMOND, M.E., BARALDI, P., ZUIANI, C., BAZZOCCHI, M. & DI PRAMPERO1, P.E. (1996). Primary Motor and Sensory Cortex Activation during Motor Performance and Motor Imagery: A Functional Magnetic Resonance Imaging Study. *J. Neurosci.*, **16**, 7688–7698. 38

PROAKIS, J. & SALEHI, M. (1995). *Digital communications*. McGraw-hill New York. 105, 106

RAJAPAKSE, J., KRUGGEL, F., MAISOG, J. & VON CRAMON, D. (1998). Modeling hemodynamic response for analysis of functional MRI time-series. *Human Brain Mapping*, **6**, 283–300. 62

RANGANATHA, S., HOSHI, Y. & ET AL. (2004). Near infrared spectroscopy based brain-computer interface. In *3rd International conference on Experimental Mechanics and 3rd conference of the Asian Committee on Experimental Mechanics*, Singapore. 105

RANGANATHA, S., ZHANG, H., GUAN, C., THULASIDAS, M., HOSHI, Y., ISHIKAWA, A., SHIMIZU, K. & BIRBAUMER, N. (2007). Temporal classification of multichannel near-infrared spectroscopy signals of motor imagery for developing a brain-computer interface. *NeuroImage*, **34**, 1416–1427. 38, 40, 41, 43, 47, 52, 54, 56, 74, 105, 150

RAO, S., BINDER, J., BANDETTINI, P., HAMMEKE, T., YETKIN, F., JESMANOWICZ, A., LISK, L., MORRIS, G., MUELLER, W., ESTKOWSKI, L. *et al.* (1993). Functional magnetic resonance imaging of complex human movements. *Neurology*, **43**, 2311–8. 66

RILLING, G., FLANDRIN, P. & GONÇALVÈS, P. (2003). On empirical mode decomposition and its algorithms. In *IEEEEURASIP Workshop on Nonlinear Signal and Image Processing NSIP-03, Grado (I)*. 123, 125

ROTH, M., DECETY, J., RAYBAUDI, M., MASSARELLI, R., DELON-MARTIN, C., SEGEBARTH, C., MORAND, S., GEMIGNANI, A., DÉCORPS, M. & JEANNEROD, M. (1996). Possible involvement of primary motor cortex in mentally simulated movement: a functional magnetic resonance imaging study. *Neuroreport*, **7**, 1280. 44, 150

ROY, C. & SHERRINGTON, C. (1890). On the regulation of the blood-supply of the brain. *The Journal of Physiology*, **11**, 85. 19

SATO, H., KIGUCHI, M., KAWAGUCHI, F. & MAKI, A. (2004). Practicality of wavelength selection to improve signal-to-noise ratio in near-infrared spectroscopy. *NeuroImage*, **21**, 1554–1562. 81

SCHALK, G., MCFARLAND, D., HINTERBERGER, T., BIRBAUMER, N. & WOLPAW, J. (June 2004). BCI2000: a general-purpose brain-computer interface (BCI) system. *Biomedical Engineering, IEEE Transactions on*, **51**, 1034–1043. 48

SEYDNEJAD, S. & KITNEY, R. (2001). Modeling of Mayer waves generation mechanisms. *IEEE Engineering in Medicine and Biology Magazine*, **20**, 92–100. 52, 53

SHANNON, C. (1949). Communication in the presence of noise. *Proceedings of the IRE*, **37**, 10–21. 78

SHIBASAKI, H., SADATO, N., LYSHKOW, H., YONEKURA, Y., HONDA, M., NAGAMINE, T., SUWAZONO, S., MAGATA, Y., IKEDA, A., MIYAZAKI, M. *et al.* (1993). Both primary motor cortex and supplementary motor area play an important role in complex finger movement. *Brain*, **116**, 1387. 42

SHIRYAEV, A. (1996). Probability, volume 95 of. *Graduate texts in mathematics*. 51

SKLAR, B. (1988). Digital communications: fundamentals and applications. 110

SLINEY, D. & WOLBARSHT, M. (1980). *Safety with lasers and other optical sources:a comprehensive handbook*. New York: Plenum Press, New York, 1st edn. 81

SMITH, S., JENKINSON, M., WOOLRICH, M., BECKMANN, C., BEHRENS, T., JOHANSEN-BERG, H., BANNISTER, P., DE LUCA, M., DROBNJAK, I., FLITNEY, D. *et al.* (2004). Advances in functional and structural MR image analysis and implementation as FSL. *Neuroimage*, **23**, 208–219. 61

SORAGHAN, C., MATTHEWS, F., KELLY, D., WARD, T., MARKHAM, C., PEARLMUT-TER, B. & O'NEILL, R. (2006). A dual-channel optical brain-computer interface in a gaming envrioment. In *Proceedings of the 9th International Conference on Computer Games: AI, Animation, Mobile, Educational and Serious Games*, Dublin Institute of Technology, Ireland. 52, 76

SORAGHAN, C., MATTHEWS, F., MARKHAM, C., PEARLMUTTER, B., ONEILL, R. & WARD, T. (2008a). A 12-Channel, real-time near-infrared spectroscopy instrument for brain-computer interface applications. In *Conference proceedings:... Annual International Conference of the IEEE Engineering in Medicine and Biology Society. IEEE Engineering in Medicine and Biology Society. Conference*, vol. 1, 5648. 2, 48

SORAGHAN, C., CHARLES, M., MATTHEWS, F. & WARD, T. (2009a). Overview of optical bci research at nui maynooth. In *The Association of Physical Scientists in Medicine Annual Scientific Meeting (APSM ASM) 2009*, NUIM. 51

SORAGHAN, C., MARKHAM, C., MATTHEWS, F. & WARD, T. (2009b). Triple wavelength led driver for optical brain–computer interfaces. *Electronics Letters*, **45**, 392–394. 2, 81, 83

SORAGHAN, C., MATTHEWS, F., MARKHAM, C., PEARLMUTTER, B.A. & WARD, T. (2010). A versatile, multichannel continuous wave near-infrared spectroscopy (cwnirs)

instrument for optical brain-computer interface (obci) applications. *Journal of Neural Engineering (Under Review)*. 48, 75

SORAGHAN, C.J. (2010). *Development of A Versatile Multichannel CWNIRS Instrument for Optical Brain-Computer Interface Applications*. Ph.D. thesis, National University of Ireland, Maynooth, IRL. iv, 2, 33, 40, 41, 44, 45, 56, 58, 77, 83, 84, 85, 88, 106, 107, 116

SORAGHAN, C.J., WARD, T.E., MATTHEWS, F. & MARKHAM, C. (2008b). Optical safety assessment of a near-infrared brain-computer interface. In *Signals and Systems Conference, 208. (ISSC 2008). IET Irish*, 174–179. 81

SORENSEN, A., COPEN, W., ØSTERGAARD, L., BUONANNO, F., GONZALEZ, R., RORDORF, G., ROSEN, B., SCHWAMM, L., WEISSKOFF, R. & KOROSHETZ, W. (1999). Hyperacute stroke: simultaneous measurement of relative cerebral blood volume, relative cerebral blood flow, and mean tissue transit time. *Radiology*, **210**, 519. 38

SPINNEY, L. (2003). Hear my voice. *New Scientist*, **22**, 36–9. 40

STEVENS, C. (1979). The Neuron. *Scientific American*, **241**, 55–65. 11

STRANGMAN, G., BOAS, D. & SUTTON, J. (2002a). Non-invasive neuroimaging using near-infrared light. *Biological Psychiatry*, **52**, 679–693. 77, 81, 85

STRANGMAN, G., CULVER, J., THOMPSON, J. & BOAS, D. (2002b). A quantitative comparison of simultaneous BOLD fMRI and NIRS recordings during functional brain activation. *Neuroimage*, **17**, 719–731. 35, 57

STRICK, P. & PRESTON, J. (1982). Two representations of the hand in area 4 of a primate. I. Motor output organization. *J Neurophysiol*, **48**, 139–149. 67

SWETS, J. (1988). Measuring the accuracy of diagnostic systems. *Science*, **240**, 1285. 144

TAKANO, T., TIAN, G., PENG, W., LOU, N., LIBIONKA, W., HAN, X. & NEDERGAARD, M. (2006). Astrocyte-mediated control of cerebral blood flow. *Nature neuroscience*, **9**, 260–267. 20

TANJI, J. & SHIMA, K. (1994). Role for supplementary motor area cells in planning several movements ahead. *Nature*, **371**, 413–416. 42

THULBORN, K.R., WATERTON, J.C., MATTHEWS, P.M. & RADDA, G.K. (1982). Oxygenation dependence of the transverse relaxation time of water protons in whole blood at high field. *Biochimica et Biophysica Acta (BBA) - General Subjects*, **714**, 265 – 270. 27

TORONOV, V., WEBB, A., CHOI, J., WOLF, M., MICHALOS, A., GRATTON, E. & HUEBER, D. (2001). Investigation of human brain hemodynamics by simultaneous near-infrared spectroscopy and functional magnetic resonance imaging. *Medical Physics*, **28**, 521. 57

ULUDAG, K., STEINBRINK, J., VILLRINGER, A. & OBRIG, H. (2004). Separability and cross talk: optimizing dual wavelength combinations for near-infrared spectroscopy of the adult head. *NeuroImage*, **22**, 583–589. 29, 46, 81

VALLABHANENI, A., WANG, T. & HE, B. (2005). BrainComputer Interface. *Neural Engineering*, 85–121. 33

VAN DE LAAR, B. (2009). *Actual and Imagined Movement in BCI Gaming*. Master's thesis, University of Twente. 44, 150

VILLRINGER, A. & DIRNAGL, U. (1995). Coupling of brain activity and cerebral blood flow: basis of functional neuroimaging. *Cerebrovascular and brain metabolism reviews*, **7**, 240. 7

VILLRINGER, A., PLANCK, J., HOCK, C., SCHLEINKOFER, L. & DIRNAGL, U. (1993). Near infrared spectroscopy (NIRS): a new tool to study hemodynamic changes during activation of brain function in human adults. *Neurosci Lett*, **154**, 101–4. 1, 7, 38

VITERBI, A. *et al.* (1995). *CDMA: principles of spread spectrum communication*. Addison-Wesley Reading, MA. 108

WARD, T.E., SORAGHAN, C.J., MATTHEWS, F. & MARKHAM, C.M. (2007). A concept for extending the applicability of constraint induced movement therapy through motor cortex activity feedback using a neural prosthesis. *Computational Intelligence and Neuroscience*. 40, 41, 51, 56, 76, 151

WEINSTEIN, S. & EBERT, P. (1971). Data transmission by frequency-division multiplexing using the discrete fourier transform. *Communication Technology, IEEE Transactions on*, **19**, 628–634. 105

WEISKOPF, N., MATHIAK, K., BOCK, S.W., SCHARNOWSKI, F., VEIT, R., GRODD, W., GOEBEL, R. & BIRBAUMER, N. (2004). Principles of a brain-computer interface (BCI) based on real-time functional magnetic resonance imaging (fMRI). *IEEE Transactions on Biomedical Engineering*, **51**, 966–70. 33

WILSON, J., SCHALK, G., WALTON, L. *et al.* (2009). Using an EEG-Based Brain-Computer Interface for Virtual Cursor Movement with BCI2000. *Journal of Visualized Experiments*. 48

WOLF, M., FERRARI, M. & QUARESIMA, V. (2007). Progress of near-infrared spectroscopy and topography for brain and muscle clinical applications. *Journal of Biomedical Optics*, **12**, 062104. 76

WOLPAW, J., BIRBAUMER, N., HEETDERKS, W., MCFARLAND, D., PECKHAM, P., SCHALK, G., DONCHIN, E., QUATRANO, L., ROBINSON, C. & VAUGHAN, T. (2000). Brain-computer interface technology: a review of the first international meeting. *IEEE transactions on rehabilitation engineering*, **8**, 164–173. 33

WOOLRICH, M., JBABDI, S., PATENAUDE, B., CHAPPELL, M., MAKNI, S., BEHRENS, T., BECKMANN, C., JENKINSON, M. & SMITH, S. (2009). Bayesian analysis of neuroimaging data in FSL. *NeuroImage*, **45**, 173–186. 61

YAMAWAKI, N., WILKE, C., LIU, Z. & HE, B. (2005). An improvement of a time-frequency approach for an EEG-based brain-computer interface. *Int. J. of Bioelectromagnetism*, **7**, 289–291. 48

YOO, S.S., FAIRNENY, T., CHEN, N.K., CHOO, S.E., PANYCH, L.P., PARK, H., LEE, S.Y. & JOLESZ, F.A. (2004). Brain-computer interface using fMRI: Spatial navigation by thoughts. *Neuroreport*, **15**, 1591–5. 33, 150

ZHANG, Q., STRANGMAN, G.E. & GANIS, G. (2009). Adaptive filtering to reduce global interference in non-invasive nirs measures of brain activation: How well and when does it work? *NeuroImage*, **45**, 788 – 794. 52